



- Institute of Fundamental Technological Research
 - Polish Academy of Sciences
 - Warsaw • Poland
-
-

LECTURE NOTES

9

A. Dragon

D. Halm

Damage Mechanics

Some Modelling Challenges



Centre of Excellence for
Advanced Materials and Structures

WARSAW 2004

© Copyright by | Institute of Fundamental Technological Research
Polish Academy of Sciences

AMAS LECTURE NOTES

Series Editors:

Executive Committee of AMAS:

Zenon Mróz (*Scientific Coordinator*)

Krzysztof Doliński

Wojciech Nowacki

Henryk Petryk

Andrzej Siemaszko

Kazimierz Sobczyk

Executive Editor:

Józef Joachim Telega

*Production of this volume has been partially supported
by the European Commission*

Published and distributed by
Institute of Fundamental Technological Research
Świętokrzyska 21, 00-049 Warszawa, Poland

ISSN 1642-0578

Papier offset. kl. III, 70 g, B1
Ark. wyd.: 10,4; ark. druk.: 8,75
Skład w systemie L^AT_EX: T.G. Zieliński, K. Mróz
Oddano do druku i druk ukończono: II 2004
Druk i oprawa: Drukarnia Braci Grodzickich, Piaseczno, ul. Geodetów 47a

Contents

Preface	5
Notations concerning tensor algebra	7
1. Introduction and scope	9
2. Conceptual preview of damage mechanics via two elementary isotropic models	17
2.1. Isotropic ‘classroom’ damage model and its critical evaluation	18
2.2. Ductile fracture damage. An example of coupled damage-plasticity modelling (Rousselier, 1981 [35])	27
3. Anisotropic damage and normal unilateral effect: eigenvector approach for mesocracking damage	39
4. Mesocrack friction induced plasticity	49
4.1. Energy expression and affinities related to damage-and-friction response	50
4.2. Sliding criterion and evolution	54
5. Damage and frictional sliding interaction. Fully coupled model, its numerical implementation and applications (rock-like solids)	57
5.1. Generalized coupled model	57
5.2. Numerical integration of damage and sliding constitutive relations .	61
5.3. Identification of the material parameters	65
5.4. Applications: rock-like solids	68
6. Interaction of primary anisotropy with the damage-induced one (CMC’s)	75
6.1. Introduction	75
6.2. Initial anisotropy	76
6.2.1. Transverse isotropy	76
6.2.2. Extension to orthotropy	77
6.3. Anisotropic damage effects	80
6.3.1. Damage variable and thermodynamic potential	80
6.3.2. Damage evolution law	82
6.3.3. Example	83
6.4. Conclusion	86

7. Mesocrack interaction via morphology-based micromechanical approach	87
7.1. Microstructure schematization and local problem approach	89
7.2. Extension in presence of damage	92
7.3. A complementary localization-homogenization procedure	96
7.4. Discussion	98
8. Adiabatic shear banding in ductile metals via anisotropic damage modelling approach	101
8.1. The ASB-related damage variable and kinematic preliminaries	102
8.2. The constitutive model	106
8.3. Evaluation and application of the model	115
Remarks	127
Bibliography	129

Preface

The lecture notes presented in this volume fall within the scope of the course given by the first author in April–May 2002 as a part of the programme of the Centre of Excellence for Advanced Materials and Structures, Warsaw (Poland) under the auspices of the European Union. The lecturer is very indebted to the participants – young doctoral students and experienced researchers – for their comments, questions and remarks. Many of them are echoed in this text. It is divided into eight chapters attempting to cover significant ‘modelling challenges’ of contemporary nonlinear mechanics of solid materials related to progressive deterioration phenomena. The fields of quasi-brittle, dilatant engineering materials, of ceramic matrix composites and of high-strength metallic alloys are of primary focus. The small strain framework as well as the large deformation context are concerned (the second one limited to Chapter 8). The dissipative coupling of damage phenomena involved (microcracking, cavity growth and adiabatic shear banding) with different forms of plasticity and with some induced effects related to damage deactivation, is detailed. However the primary common denominator of the course is ANISOTROPIC DAMAGE and, in particular, damage-induced orthotropy eventually combined with initial (primary) anisotropy (as shown in Chapter 6).

What is at stake in the venture is a connection with salient mesomechanical deterioration mechanisms on the one hand and computational efficiency of the constitutive models and their identifiableness on the other. The methodology applied, exploiting the framework of internal variable formalism in a sometimes non-classical way (see pseudo-standard modelling, Chapters 3–6), is thus striving to keep simultaneously a strong link with micromechanical analyses and to put together the tools like multilinear elasticity, tensor functions representation theory and a large strain formulation coping with anisotropy effects and objectivity requirements combined. Of course, some

simplifying assumptions, regarding notably the damage description limited to the second-order tensorial one, have been inevitable.

The authors would like to express their thanks to the AMAS staff, notably to Professor Zenon Mróz, Scientific Coordinator, to Professors Krzysztof Doliński and Michał Basista and to Ms. Izabella Ślęczkowska for the kind assistance before and during lecture series and for their patience regarding the manuscript preparation.

Many thanks are due to Brigitte Vigner and Pascale Pouzin from the Mechanics & Physics of Materials Laboratory (CNRS and ENSMA) at Poitiers-Futuroscope for their excellent efforts in the efficient execution of the word processing of the manuscript. We express also our gratitude to colleagues from the team 'Modelling of Materials & Structures', especially to Carole Nadot-Martin and Patrice Longere for their assistance during the preparation of Chapters 7 and 8.

Notations concerning tensor algebra

Let **A** and **B** be two second-order tensors and **C** a fourth-order tensor. The Einstein convention (summation over repeated indices) is used. The following notations are used:

$$(\mathbf{A}\cdot\mathbf{B})_{ij} = A_{ik}B_{kj} \quad (\text{see the note below}),$$

$$\mathbf{A} : \mathbf{B} = A_{ij}B_{ji},$$

$$\text{tr } \mathbf{A} = A_{ii},$$

$$\text{tr}(\mathbf{A}\cdot\mathbf{B}) = A_{ik}B_{ki} = \mathbf{A} : \mathbf{B} \quad (\text{see the note below}),$$

$$(\mathbf{C} : \mathbf{A})_{ij} = C_{ijkl}A_{lk},$$

$$\mathbf{A} : \mathbf{C} : \mathbf{B} = C_{ijkl}A_{ji}B_{lk},$$

$$(A \otimes B)_{ijkl} = A_{ij}B_{kl},$$

$$(A \overline{\otimes} B)_{ijkl} = \frac{1}{2}(A_{ik}B_{jl} + A_{il}B_{jk}).$$

Note:

For simplicity reasons relative to finite strain context and relevant notation heaviness in Chapter 8, the dots representing the contraction with respect to one and/or two indices *are omitted*, i.e.:

$$(\mathbf{A}\mathbf{B})_{ij} = A_{ik}B_{kj} \quad (\text{instead of } \mathbf{A}\cdot\mathbf{B}),$$

$$\text{tr}(\mathbf{A}\mathbf{B}) = A_{ik}B_{ki} = \mathbf{A} : \mathbf{B} \quad (\text{instead of } \text{tr}(\mathbf{A}\cdot\mathbf{B})).$$

Chapter 1

Introduction and scope

The emergence and further development of Continuum Damage Mechanics (CDM) during the last forty years corresponded to evident needs of controlling material response in the presence of evolving micro- and meso-defects in order to meet structural reliability requirements in the context of engineering applications. Within the larger fields of Material Science and Technology and of Mechanics of Materials, the CDM itself has evolved, passed through different phases, upturns, doubts and some transformations. Its methodology – and, in particular, the scope of what is commonly termed 'continuum models' – has been gradually precised and its range restricted by scale, defect interaction and correlation, and statistical homogeneity related criteria and postulates. The exhaustive treatise by Krajcinovic [1] provides a rigorous, global survey in the matter corresponding to the mid-nineties state of the art. It presents the assets as well as the limits and some deficits of research at the time. The more recent article [2] by the same author attempting to assess “accomplishments, trends and needs” of Damage Mechanics (DM) pursues the deliberation and conclusions of the book [1]. It is stated, among others, that despite of much progress and the fertility of fields of actual and future research, there remains some reticence to employ the DM for purposeful industrial applications (see [2], p.274). Several reasons and postulates are elicited in this regard, related to damage modelling, sometimes focusing on “the *least* eventful and important part” of deformation regime, and to experimental research and identification problems related to damage control.

Among the issues of importance raised in the latter evaluation, Krajcinovic puts forward, in Section labelled 'Research needed' (cf. [2] p. 272), the problem of coupled dissipation for compression-dominated loading paths involving damage by microcracking accompanied by frictional sliding over the mating microcrack lips. Genuinely, the essential part of the present text is devoted to modelling of these phenomena for a broad class of quasi-brittle solids like rocks, concrete, ceramics, etc. More specifically, the actual lecture notes present a synthesis of the multi-segment model advanced recently by the present authors and coworkers, see e.g. [3, 4, 5]. The work at stake is attempting a unified, three-dimensional approach of the field concerned. The phenomena involved require reliable control of damage growth, handy mastery of opening/closure (and reverse) transition for any system of microcracks and a description of plasticity-like sliding evolution on closed crack set(s). These problems are approached here in the framework of rate-type constitutive theory with internal variables. The different model segments are strongly micromechanically motivated in their essential elements. Still, they are built to provide convenient tools for efficient structural analysis of engineering problems and, as such they constitute a continuum damage model coupled with a form of frictional sliding related plasticity. In order to deal with the complex issues like damage-induced anisotropy and continuity requirement for some macroscopic entities (energy, stress) – in spite of discontinuities involved in microcrack opening/closure phenomena – the methodology involved combines divers means of modelling not commonly put together in literature. Hence, the tensor functions representation theory, the multilinear functions framework applied to piecewise-linear elasticity (for a given damage configuration) are employed together with salient micromechanical results. Some interpenetration of an operational CDM viewpoint and corresponding capacities with micromechanical analyses and results may constitute a very efficient way of modelling. The recent work by Hild and coworkers [6, 7] provides an interesting illustration of such a combined methodology. Some micromechanical developments, based on a non-conventional approach starting from a specific geometrical and kinematical description of 'bonded aggregate'-like microstructures are given in the present text, attention being paid to nonlocal damage effects on the microscale.

A legitimate question arised some years ago concerning full understanding of the damage-related, inelastic response of quasi-brittle materials: what are the principal obstacles for an efficient control of the dissipative behaviour

involved? The question was legitimate with respect to a great number of papers focusing on damage by microcracking, and what is more, containing a large spectrum of investigations on several scale levels. It seems that three principal barriers intervening simultaneously were: (i) anisotropy linked to and evolving with multiple cracking, (ii) efficient control of opening/closure transition for a microcrack set(s), and (iii) three-dimensional character of effects involved. The second point is pivotal in the context of the present study.

The credit for identifying in the early eighties the problem of damage deactivation (due to closure of defects) and its consequences, termed sometimes 'unilateral effects', is due to Ladevèze and Lemaitre [8], see also Ladevèze [9], Lemaitre [10]. These authors attempted also modelling these effects starting from energy (thermodynamic potential) expressions. The recovery (total or partial) of the Young's modulus in the direction perpendicular to that of a closed crack set could be described. Further developments followed (Mazars [11], Simo and Ju [12], Yazdani and Schreyer [13]).

However, when adding anisotropy effects and three-dimensionality mentioned above, many difficulties arised and most of the models existing at the early nineties appeared unable to assure simultaneously energy and stress continuity and unilateral effects of damage deactivation. The stimulating critical review by Chaboche [14] has been an important step in thorough analysis of multiple aspects involved in and an advance for capturing the *full* extent of the problem to deal with.

In 1995, an interesting tentative of a global vision of the non-linear mechanics of materials has been proposed by Lubarda and Krajcinovic [15], including the classical rate theory of elastoplastic deformation of crystalline solids as well as the salient features concerning progressively mesofracturing solids. Indeed, as stated above, the complete dissipative picture for quasi-brittle material response comprises the continuum damage approach attempting to capture progressive degradation attributable to evolution of multiple defects coupled with the plasticity-like approach accounting for friction resistance and for irreversible frictional sliding over the internal crack surfaces. The extended framework of damage-elastoplastic constitutive modelling should allow for study of complex, cyclic and non-proportional loading paths, where coupled mesocrack growth and friction related dissipative mechanisms produce strong non-linearity, induced anisotropy, volumetric dilatancy and intricate hysteretic phenomena. The modelling to be synthesized

here may be considered in some respect as a specific constitutive formalism relevant to the aforesaid global framework postulated by Lubarda and Krajcinovic.

Regarding the above mentioned hysteretic behaviour for progressively mesofracturing solids, one may recall cyclic tests for some rocks, see for example Pecqueur [16]. Considering a compression-dominated loading cycle for microcracked sample one has some 'favourably' inclined crack-sets constrained to closure. The initial unloading process keeping compression-predominance – consider e.g. torsion cycles under superposed hydrostatic compression – is friction-locked, exhibiting a high apparent rigidity. Further unloading may be dissipative if reverse multistage frictional sliding over closed microcracks (reverse with respect to a loading branch) becomes active. The inelastic unloading is just one characteristic effect generated by microcracking-related damage. It is obvious that this effect cannot be managed within the framework of classical plasticity theory. It appeals for a more suitable, enlarged constitutive framework.

In fact, the modelling of friction resistance on cracks and of relative sliding effects with respect to hysteretic behaviour has received much attention in the past. An early, strong evidence in this sense, in the context of rock behaviour, can be found in Walsh [17]. Further analyses and models are due to Kachanov [18], Horii and Nemat-Nasser [19], Andrieux *et al.* [20], Nemat-Nasser and Obata [21], Ju [22], Krajcinovic *et al.* [23], Gambarotta and Lagomarsino [24], Fond and Berthaud [25], Lawn and Marshall [26]. This list is probably non-exhaustive. For the most part, the works adduced represent pertinent micromechanical studies leading, for some of them, to models capable to cover a *limited* range of stress-strain paths (one- and two-dimensional, axisymmetric, etc.). As stated before, one of the purposes of this review is to address, in a synthetic manner, basic hypotheses and issues of the 3D modelling proposed by Halm and Dragon [5, 27], employing a coherent internal variable formalism for the joint process of anisotropic damage by microcracking and frictional sliding at closed microcracks. The aim of this model is to provide an efficient, *macroscopic* – whereas strongly micromechanically motivated – approach suitable for boundary-value problems involving non-linear behaviour of quasi-brittle solids.

The approach presented is based on an earlier anisotropic damage model, the “basic version” proposed by Dragon *et al.* [3] and extended by Halm and Dragon [4] to include the unilateral effect concerning normal stiffness

recovery with respect to a mesocrack system constrained to closure. This extended version, summarized in Chapter 3, is then completed by the damage and frictional blocking/sliding model depicted above. This coupled model allows to treat simultaneously the both dissipative mechanisms involved for complex stress-strain paths including those implying the rotation of loading and damage axes. The corresponding developments are given in Chapters 4 and 5. An overview presented insists here and there on a modular structure of the model. The three corresponding segments, namely the basic version, the extended version (treated together in Chapter 3) and the coupled damage-and-friction complete version of Chapter 5 can be employed in order of growing complexity, according to engineering finality demanded. Further aim to set forth here is a more complete survey of a methodology concerning the numerical integration of the constitutive equations proposed and that relative to the identification of material constants involved. These issues are therefore developed in the second part of Chapter 5 where are furthermore presented selected examples illustrating damage and friction induced non-linear stress-strain behaviour incorporating hysteretic effect mentioned in the foregoing. A brief account is given of applications of the model for structural analyses. The problem of initial (primary) material anisotropy interfering eventually with a damage-induced (secondary) anisotropy is raised in Chapter 6.

The chapter is turned towards an enlarged class of quasi-brittle solids (for instance, ceramic matrix composites) compared to earlier Chapters 3-5 focusing mostly on rock-like materials. Another crucial problem concerning the microcrack interaction effect in relation with eventual nonlocal modelling is treated in Chapter 7 where a non-classical homogenization approach is developed including anisotropic damage behaviour for a class of engineering materials regarded as particulate composites [28]. Finally, in some methodological connection with the modelling of anisotropic damage by microcracking (Chapters 3-5), the problem of degradation by adiabatic shear banding (ASB) for a broad class of ductile metals under dynamic loading is outlined (Chapter 8). The latter problem involves large plastic deformation (associated with high strain rates). The model is presented for the ASB process viewed as an anisotropic damage mechanism coupled with thermo-elastic/viscoplastic deformation [29]. A structural application related to high velocity impact is illustrated.

The pivotal issue of the control of microcrack closure and opening phenomena is addressed through Chapters 3-5, where the stiffness recovery and

friction enter into consideration. The central simplifying hypothesis conveyed through the developments proposed, consists in reduction of any real microcrack-set configuration to an equivalent configuration of three mutually orthogonal systems of parallel cracks characterized by three eigenvectors ν^k ($k = 1, 2, 3$) and three non-negative eigenvalues D_k of the second-order damage tensor \mathbf{D} . In such a manner the damage-induced anisotropy is systematically limited to a form of orthotropy, see also [30].

The problem of transition from volume-distributed damage to surface-localized failure incipience has been amply debated at the end of the eighties and the beginning of the nineties, see for example [31–33]. The localization bifurcation in the presence of damage by microcracking inducing net anisotropy effects needs clearly a 3D treatment, two-dimensional projections misrepresenting mostly localization mechanisms (orientation and discontinuity mode). The computational procedure relative to 3D localization detection is given in [3], where some pertinent results obtained with the basic damage model are amply commented.

Covering the large spectrum of quasi brittle and ductile engineering materials and related deterioration mechanisms involving damage-induced anisotropy effects, this study attempts to reach a large audience from graduate and doctoral students to experienced scientists. In this spirit is proposed, for the students and engineers less familiarized with the damage mechanics formalism, an introductory chapter (Chapter 2) treating two fundamental damage mechanisms, namely microcracking and ductile cavity growth via two simple isotropic CDM models: Marigo [34], Rousselier [35]. Notwithstanding its introductory character, this chapter summarizes important local instability questions in particular the localization bifurcation viewed as a macroscopic fracture precursor (as mentioned above) and brings in premises of nonlocal modelling. In such a manner the present course ranging from the introductory chapter 2 via the microcracking related CDM modelling and related effects (unilateral phenomena and frictional sliding), further micromechanical insight, initial and induced anisotropy to specific ductile fracture damage modelling coupled with finite elastic viscoplastic deformation, attempts to put forward and to deal with some major “modelling challenges” in Damage Mechanics. The message advanced is that the challenges treated and other not covered in this book, should be possibly approached in a double and convergent way interconnecting efficient and operational CDM tools on the one hand together with micromechanical analyses and homogenization

methodology on the other. The different models discussed in the following – for microcracking elastic solids as well as for ductile elastic-plastic materials, both regarding anisotropic effects induced by deterioration mechanisms – exhibit some methodological unity in their setting assumptions and simplifications. In addition to their modular character they are three-dimensional and micromechanically motivated in most essential ingredients, a going concern consisting unceasingly in providing tools for efficient enhanced structural analysis.

Chapter 2

Conceptual preview of damage mechanics via two elementary isotropic models

This chapter contains a development of two isotropic, standard Continuum Damage Mechanics (CDM) models regarding respectively:

- deterioration of an elastic solid by progressive, randomly oriented microcracking,
- deterioration of an elastic-plastic material by multiple cavity growth.

Important appended notions related to damage models' licit application bounds are also recalled, notably the localization bifurcation. The purpose here is to give, via a short presentation of simple (albeit complete) damage models, the basic framework of modelling for engineering students lacking good familiarity and skills with internal variable based constitutive description of nonlinear (dissipative) material behaviour. Teaching practice has shown that such a gradual approach can be an asset to the less experienced student before going on to further, more advanced account of anisotropic damage and related effects in the following Chapters. Comprehension of essentials of the plasticity framework is only necessary for this introduction. Besides the introductory material, some prerequisites regarding nonlocal damage modelling are outlined at the end of this Chapter.

2.1. Isotropic ‘classroom’ damage model and its critical evaluation

Regarding nonlinear behaviour of quasi-brittle solids, the initiation and growth of multitude of microcracks is viewed as the predominant dissipative mechanism. As far as a scalar density of crack-like defects is considered as sufficient measure, i.e. when crack-field orientation is meaningless, the following entity is introduced for approximately penny-shaped microcracks (see, for instance, Walsh [17]):

$$\tilde{d} = r^c = \frac{\sum_i^N a_i^3}{V} \quad \text{or} \quad \tilde{d} = \frac{N a^3}{V}. \quad (2.1)$$

The summation above is done over microcracks indexed $i = 1, 2, 3, \dots, N$ of respective radii a_i within the volume V ; otherwise, in (2.1)₂ an average radius a is being introduced. Crack ‘saturation’ state can be envisioned as the one corresponding to $\tilde{d} = 1$ and constituting a hypothetical maximum for \tilde{d} . The admissible interval for d can thus be posed as $d \in [0, 1]$. The definition (2.1) stipulates particular geometry of crack-like defects. A more general dimensionless density related to *any microcrack*-induced decohesion can be introduced as (Kachanov [36]):

$$\hat{d} = \hat{d}(s) = \eta \frac{\sum_i^N s_i^{3/2}}{V} \quad (2.2)$$

where s_i is decohesion area related to an i -th crack and η is a dimensionless crack-form parameter. One can see that for $\eta = (\pi\sqrt{\pi})^{-1}$ exemplifying the penny-like (circular) microcracks, one obtains $\hat{d} \equiv \hat{d}(s) \equiv r^c$.

The density $\hat{d}(s)$ can be taken as a (general) micromechanical interpretation for the microcracking-related damage internal variable d . The latter, together with the components of the small strain tensor $\boldsymbol{\varepsilon}$ (external variable), constitutes a set of state variables governing a specific free-energy (thermodynamic potential) expression $\psi(\boldsymbol{\varepsilon}; d)$ for elastic-damage isothermal model of the material subjected to progressive crack-induced deterioration. If the expression $\psi(\boldsymbol{\varepsilon}; d)$ is limited to a homogeneous quadratic one in terms of ε_{ij} as follows (we denote by ρ the mass density):

$$\rho \psi(\boldsymbol{\varepsilon}; d) = w(\boldsymbol{\varepsilon}; d) = \frac{1}{2} \boldsymbol{\varepsilon} : \mathbf{C}(d) : \boldsymbol{\varepsilon}, \quad (2.3)$$

the model describes degradation of elastic moduli, via the elastic rigidity tensor \mathbf{C} -dependence on d , with no residual strains which could be eventually induced by defects (see Chapter 3). Note that an alternative expression of the damage dependent strain energy $w(\boldsymbol{\varepsilon}; d) = A(d) + \mathbf{B}(d) : \boldsymbol{\varepsilon} + \frac{1}{2} \boldsymbol{\varepsilon} : \mathbf{C}(d) : \boldsymbol{\varepsilon}$ leads to the stress $\boldsymbol{\sigma} = \partial w / \partial \boldsymbol{\varepsilon}$ non-zero for $\boldsymbol{\varepsilon} = \mathbf{0}$, and, using a dual (complementary) energy $u(\boldsymbol{\sigma}; d) = \boldsymbol{\sigma} : \boldsymbol{\varepsilon} - w(\boldsymbol{\varepsilon}, d)$, generating a non-zero, damage-induced strain for $\boldsymbol{\sigma} = \mathbf{0}$, see Fig. 2.1(a). The expression (2.3) leads to partial energy recovery with non residual, damage-induced strain, Fig. 2.1(b).

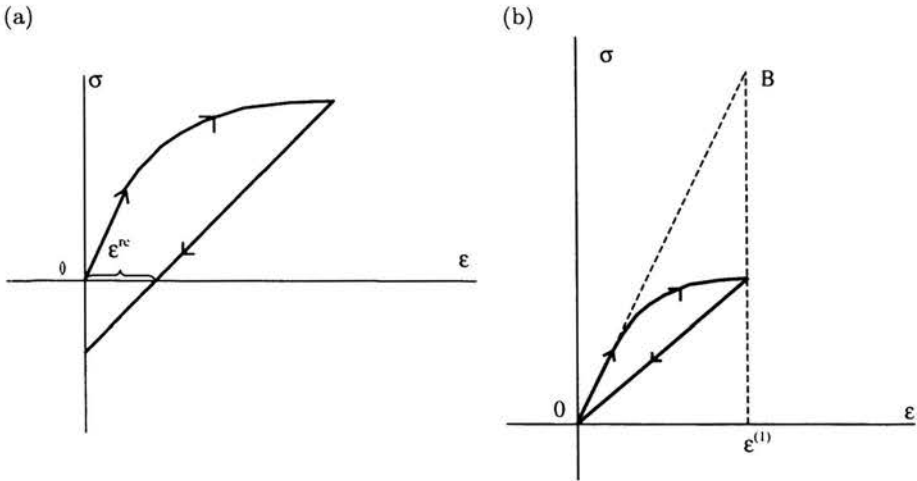


FIGURE 2.1. Elastic-damage stress-strain response; (a) the case of a non-homogeneous energy (thermodynamic potential) $w(\boldsymbol{\varepsilon}; d)$, effect of damage-induced residual strain $\varepsilon^{rc} \neq 0$; (b) the case of a homogeneous quadratic potential $w(\boldsymbol{\varepsilon}; d)$ according to (2.3).

The common, classical and phenomenological assumption is

$$\mathbf{C}(d) = (1 - d)\mathbf{C}, \quad d = [0, 1], \quad (2.4)$$

thus linearizing the elastic moduli degradation with respect to d , Lemaître, Chaboche [37], Marigo [34]. In such a way for a virgin material (absence of damage) the elastic rigidity is equal \mathbf{C} while for a hypothetically 'completely degraded' (fractured) solid $\mathbf{C}(d) = \mathbf{0}$.

The constitutive laws ('state' ones) related to (2.3) define respectively elastic stress response $\boldsymbol{\sigma}$ and the damage driving force (thermodynamic force)

F_d as follows:

$$\begin{cases} \sigma = \left. \frac{\partial w(\boldsymbol{\varepsilon}; d)}{\partial \boldsymbol{\varepsilon}} \right|_d = (1-d) \mathbf{C} : \boldsymbol{\varepsilon}, \\ F_d = - \left. \frac{\partial w(\boldsymbol{\varepsilon}; d)}{\partial d} \right|_{\boldsymbol{\varepsilon}} = \frac{1}{2} \boldsymbol{\varepsilon} : \mathbf{C} : \boldsymbol{\varepsilon}. \end{cases} \quad (2.5)$$

One can see that for a given damage state the elastic behaviour remains linear (see unloading curve, Fig. 2.1(b)) while the damage driving force representing the local energy release rate (with respect to d) analogous to global (field dependent) crack-driving force in Fracture Mechanics $\xi = -\frac{\partial \pi}{\partial s}$, where π is the total potential energy of the body with crack(s) while δs is the infinitesimal crack advance (growth of cracked area) which can be reduced in a two-dimensional context to a linear crack advance δa . As the energy is linear with respect to d , F_d is merely strain dependent quantity. For a given strain ($\boldsymbol{\varepsilon}^{(1)}$, say) F_d is represented by the area $0\boldsymbol{\varepsilon}^{(1)}\text{B}$ in Fig. 2.1(b).

As in classical plasticity, the laws (2.5) are not enough to describe the material behaviour. The dissipative evolution needs to be detailed, the only dissipative mechanism here being the damage one. The dissipation expression

$$\phi = \boldsymbol{\sigma} : \dot{\boldsymbol{\varepsilon}} - \rho \dot{\psi} \quad \text{with} \quad \psi = \psi(\boldsymbol{\varepsilon}; d) \quad (2.6)$$

is consequently reduced to

$$\phi = F_d \cdot \dot{d} \geq 0, \quad (2.7)$$

and ϕ should be non-negative to assure the thermodynamic admissibility of the model. The full normality is being postulated here; it is relative to the maximum dissipation hypothesis and is known to assure a priori the thermodynamic admissibility. As the normal dissipative mechanism (standard model) is supposed to govern time-independent (non-viscous) evolution of damage, there exists a convex non-transgressable reversibility domain $F \leq 0$ in the space of driving force, eventually dependent on d itself (as a parameter), such that

$$\begin{aligned} C_d &= \{F_d \mid F(F_d, d) \leq 0\}, \\ \dot{d} &= \lambda \frac{\partial F}{\partial F_d}, \quad \lambda \geq 0. \end{aligned} \quad (2.8)$$

One can see here an analogy with the inviscid plasticity, with a notable remark that the evolution of plastic strain is governed by a yield function

dependent on the stress tensor, the latter being the driving force for plastic strain-rate in the framework of plasticity theory. Here, the driving force is F_d (damage related energy release rate). However, from (2.5)₂ one can express F_d as a function of ε and, by inverting further (2.5)₁, as a function of σ . Consequently, the damage 'yield' function $F(F_d, d)$ can be represented respectively in the strain space and in the stress-space as well; Marigo [34, 38] postulated the following, simple form of F :

$$\begin{aligned} F(F_d, d) &= F_d - k(d), \\ k(d) &= \frac{1}{2} k_0(1 + 2md), \quad k_0 > 0, \quad m \geq 0. \end{aligned} \quad (2.9)$$

Thus, one obtains

$$\dot{d} = \begin{cases} 0 & \text{if } F < 0 \text{ or } F = 0, \dot{F} < 0 \text{ (elastic unloading),} \\ \dot{\lambda} & \text{if } F = 0, \dot{F} = 0. \end{cases} \quad (2.10)$$

The detailed expression of $\dot{\lambda}$ is obtained from the consistency equation $\dot{F} = 0$ stating that, while the damage criterion $F = 0$ is satisfied, the damage loading process is pursued (damage loading remains active with respect to any monotonous time scale). The kinematically controlled form of the evolution (2.10) can be obtained from the expression of F (via F_d) as a function of strain:

$$\begin{aligned} F[F_d(\varepsilon); d] &= \bar{F}(\varepsilon, d), \quad \dot{F} = 0 \iff \dot{\bar{F}} = 0, \\ \bar{F}(\varepsilon; d) &= \frac{1}{2} \varepsilon : \mathbf{C} : \varepsilon - k(d), \quad \dot{\bar{F}} = 0 \implies \mathbf{C} : \varepsilon : \dot{\varepsilon} - k_0 m \dot{\lambda} = 0, \\ \dot{\lambda} &= \frac{[\mathbf{C} : \varepsilon : \dot{\varepsilon}]^+}{k_0 m} \quad \text{with} \quad [a]^+ = \begin{cases} 0 & \text{if } a < 0, \\ a & \text{if } a \geq 0. \end{cases} \end{aligned} \quad (2.11)$$

Hence:

$$\dot{d} = \dot{\lambda} = \frac{[\mathbf{C} : \varepsilon : \dot{\varepsilon}]^+}{k_0 m} = \frac{[\mathbf{C} : \varepsilon : \dot{\varepsilon}]^+}{H}, \quad H = k_0 m \quad (2.12)$$

where the postulate $\dot{\lambda} \geq 0$ is satisfied by putting the brackets $[*]^+$ on the expression $\mathbf{C} : \varepsilon : \dot{\varepsilon}$ in the numerator. The symbol H for the denominator is chosen by some (formal) analogy with plasticity (hardening modulus) although herein a given finite and positive value of H induces non-linear σ - ε response with the initial pseudo-hardening stage followed by the softening one after a stress maximum (stress-peak). In the sequel it will be shown that

the softening branch may correspond to a non-unique response in relation to bifurcation phenomena occurring near the peak stress. One can see in Fig. 2.2 that $H = k_0 m > 0$ determines genuinely progressive damage evolution with m designating the progressivity-related material constant while k_0 being related to the damage threshold for the virgin i.e. non-damaged solid material. Several significant cases are illustrated in Fig. 2.2 including the two asymptotic ones corresponding to $m \Rightarrow 0$ (brutal damage) and $m \Rightarrow \infty$ (absence of damage evolution). The brutal damage ($m \Rightarrow 0, H \Rightarrow 0$) corresponds to the indeterminacy of \dot{d} ($\dot{d} \Rightarrow \infty$) at the very threshold point. It means that instantaneous total degradation of rigidity occurs together with pertaining instability depicted by dashed line in Fig. 2.2. The latter case can be viewed as having some *formal* analogy with the perfect plasticity ($\dot{\lambda}$ indeterminate $\Rightarrow \dot{\varepsilon}^P$ indeterminate) while *physically* both cases are opposite: infinite deformability for perfect plasticity and non-deformability beyond the strain attained at the damage limit for the brutal damage.

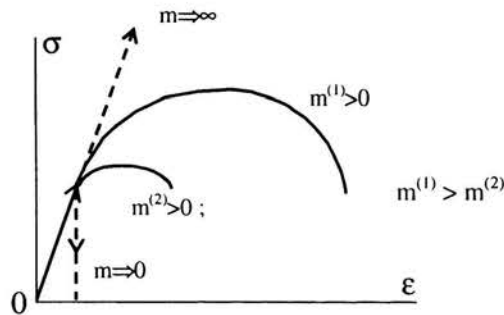


FIGURE 2.2. Progressive damage ($m > 0$) and brutal damage ($m \Rightarrow 0$) response as dependent on the progressivity parameter m .

The tangent stiffness, designated further by \mathbf{L} , corresponding to any non-linear, time-independent model is an essential input to structural analysis by Finite Element Method and a necessary prerequisite for studying local instabilities and, in particular, the localization bifurcation. The latter can be considered as a local bifurcation allowing two basic incremental solutions of the corresponding incremental equilibrium problem. One solution is exhibiting continuous deformation gradient increments (or rates) while the other (bifurcation branch) reveals a discontinuity. As such discontinuities in the deformation gradient increments are conceivable in some particular directions only – called characteristic directions – the localization incipience

corresponds to the loss of ellipticity of the incremental (rate) equations of a boundary value problem (Rice [39], Borré and Maier [40]).

The nowadays classical form of the criterion of localization inside the solid reading:

$$\det(\mathbf{n} \cdot \mathbf{L} \cdot \mathbf{n}) = 0 \quad (2.13)$$

involves the local direction of a characteristic surface S (its unit normal \mathbf{n}) and the tangent stiffness matrix \mathbf{L} corresponding to an assumed constitutive law, so that $\dot{\boldsymbol{\sigma}} = \mathbf{L} : \dot{\boldsymbol{\epsilon}}$, $\dot{\boldsymbol{\sigma}}$ and $\dot{\boldsymbol{\epsilon}}$ standing for the stress-rate and the strain-rate respectively. The associated localization-discontinuity mode is given by a vector \mathbf{g} collinear to a unit vector \mathbf{m} . The pair (\mathbf{n}, \mathbf{m}) indicates the orientation and nature of discontinuity, i.e. 'opening' or 'shearing' mode, frequently a combination of the both. The influence of the tangential stiffness \mathbf{L} in the characteristic (acoustic) tensor $\mathbf{Q} = \mathbf{n} \cdot \mathbf{L} \cdot \mathbf{n}$ makes it possible to study the singularity of \mathbf{Q} corresponding to the loss of ellipticity through the spectral analysis for a given class of constitutive relations. One can then establish analytical expressions for the spectral properties of \mathbf{Q} allowing explicit relations concerning singularity and some features of the bifurcation at stake. This way has been exploited by Ottosen and Runesson [41] who treat a class of non-associated plasticity laws regarding localization by spectral analysis approach. In fact the localization is taken up by these authors in a larger sense than in the classical approach recalled above: the discontinuity of displacement increment itself (or rate), i.e. strong discontinuity, is being incorporated in their bifurcation analysis. These authors argue that the classical bifurcation conditions linked to localization phenomena (under plastic/plastic and plastic/elastic response respectively on the characteristics surfaces and outside) are still valid under the restriction that the jump of displacement rate $[\dot{u}_i]$ remains constant along S . This step is one more argument allowing to link the study of localization to local failure, viz. macrocracking incipience.

The damage concept reflects explicitly deterioration phenomena in the framework of continuum modelling of nonlinear solid behaviour. Using this concept when studying localization, viz. transition from volume-diffused deterioration to surface-like localized one, takes on even more pertaining physical reference to failure incipience than localization study in the context of plasticity.

The tangent stiffness corresponding to the damage model introduced in the foregoing (formulae (2.3) to (2.12)) can be deduced by derivation with respect to time of (2.5)₁ and by replacing of (2.12) for \dot{d} . One obtains the

following form:

$$\dot{\sigma} = \mathbf{L}(\varepsilon; d) : \dot{\varepsilon} = (1 - d) \mathbf{C} : \dot{\varepsilon} - \frac{\Theta}{H} (\mathbf{C} : \varepsilon : \dot{\varepsilon}) (\mathbf{C} : \varepsilon) \quad (2.14)$$

with

$$\Theta = 0 \text{ if } \dot{\lambda} = 0 \text{ (non damage evolution),}$$

$$\Theta = 1 \text{ if } \dot{\lambda} > 0 \text{ (active damage: } \dot{d} > 0 \text{).}$$

Using the index (component) notation \mathbf{L} may be expressed in the form

$$L_{ijkl} = (1 - d) C_{ijkl} - \frac{\Theta}{H} (C_{ijmn} \varepsilon_{mn}) (C_{klrs} \varepsilon_{rs}) \quad (2.15)$$

Following Borré and Maier [40] we can approach the localization problem concerning the material obeying (2.14) with both loading-loading and loading-unloading bifurcations allowed. The first case (loading-loading) concerns dissipative evolution, i.e. active damage inside *and* outside the localization band (characterized by the surface S) while the second one regards the localization bifurcation event with unloading occurring outside the band. The criterion

$$\det \mathbf{Q} \leq 0, \quad \mathbf{Q} \equiv \mathbf{n} \cdot \mathbf{L} \cdot \mathbf{n} \quad (2.16)$$

represents a sufficient and necessary condition for bifurcation. In the same time the localization threshold itself is correctly determined from (2.13) for a linear comparison material and the loading-loading bifurcation, see Proposition 6, Borré and Maier [40].

Désoyer and Cormery [33] have proceeded with the spectral analysis for localization bifurcation of the model (2.14). The essential result is the bifurcation threshold d^{\min} given in terms of damage d as a function of the progressivity constant m ; it states

$$d^{\min}(m) = \frac{m - 1}{3m}. \quad (2.17)$$

It appears in particular that $d^{\min} \Rightarrow 0$ as $m \Rightarrow 1$, so that there exists positive values of m , namely $m \leq 1$, leading to local instabilities at the very threshold level (!) (in the sense that a bifurcation event is an instability precursor). The case $m \Rightarrow 0$ leading to strong precocious instability (brutal damage) as analysed before is only the special and extremal state concerning the 'immediate' bifurcation interval $0 \leq m \leq 1$ whereby the localization

bifurcation occurs at the very incipience of damage. One can now easily see why, at the beginning of this chapter, we have stated that $d = 1$ constitutes a *hypothetical* maximum for d . In fact, this maximum, corresponding to the ultimate degradation of elastic rigidity $\mathbf{C}(d) = \mathbf{0}$, see (2.4) is purely conceptual. It is preceded by bifurcation and instability events that may be equivalent to local fracture (macrocracking). Indeed, if one tries some reasonable values of m , say $m = 10$ and $m = 2$ one can see that the corresponding instability levels are $d^{\min} \cong 0.3$ and $d^{\min} \cong 0.16$ respectively (!), well below $d = 1$.

The result (2.17) concerning localization bifurcation is not surprising. While the latter bifurcation can be considered as a particular loss of uniqueness of the velocity field in the local rate problem, another important bifurcation event consists in a loss of positiveness of the second-order work (Hill [42], Raniecki and Bruhns [43]):

$$\xi \leq 0, \quad \xi = \frac{1}{2} \dot{\boldsymbol{\sigma}} : \dot{\boldsymbol{\varepsilon}} = \frac{1}{2} \dot{\boldsymbol{\varepsilon}} : \mathbf{L} : \dot{\boldsymbol{\varepsilon}}. \quad (2.18)$$

Désoyer and Cormery showed that the corresponding bifurcation limit d_s for the model (2.9) is

$$d_s = \frac{m-1}{3m} = d^{\min}(m). \quad (2.19)$$

Both bifurcation phenomena are thus coinciding for the material described by the actual isotropic damage model.

In the heading of this Section we used the expression “‘classroom’ damage model”. One of the reasons of such designation is the simplicity of the model: only four material constants (E, ν, k_0, m) appear in the above constitutive equations and in their condensed form (2.9). Using the notation of Kachanov [44] we can resume (2.3) and (2.4) as follows

$$w(\boldsymbol{\varepsilon}; d) = (1-d) w^0(\boldsymbol{\varepsilon}) \quad (2.20)$$

where $w^0(\boldsymbol{\varepsilon})$ is the elastic strain energy for linear isotropic elastic solid

$$w^0(\boldsymbol{\varepsilon}) = \frac{E}{2(1+\nu)} \left[\frac{\nu}{1-2\nu} \varepsilon_{kk}^2 + \varepsilon_{ij} \varepsilon_{ij} \right]. \quad (2.21)$$

Consequently, the energy (2.15) and the stress-strain relation (2.5)₁ for the damaged material are

$$w(\boldsymbol{\varepsilon}; d) = \frac{(1-d)E}{2(1+\nu)} \left[\frac{\nu}{1-2\nu} \varepsilon_{kk}^2 + \varepsilon_{ij} \varepsilon_{ij} \right], \quad (2.22)$$

$$\begin{aligned}\sigma_{kl} &= \frac{\partial w}{\partial \varepsilon_{kl}} = \frac{\nu(1-d)E}{(1+\nu)(1-2\nu)} \varepsilon_{mm} \delta_{kl} + \frac{(1-d)E}{1+\nu} \varepsilon_{kl} \\ &= \frac{\nu \tilde{E}}{(1+\nu)(1-2\nu)} \varepsilon_{mm} \delta_{kl} + \frac{\tilde{E}}{1+\nu} \varepsilon_{kl} \quad (2.23)\end{aligned}$$

with $\tilde{E} = (1-d)E$ designating the degraded Young's modulus. One can see above that only the Young's modulus is affected by damage while the Poisson's ratio is not. This leads to macroscopic interpretation of d :

$$d = 1 - \frac{\tilde{E}}{E} \quad (2.24)$$

which can be put in parallel with the micromechanical interpretations embodied respectively by the microcracks densities (2.1), (2.2). Considering arbitrary orientation distributions of penny-shaped (circular) noninteracting cracks, Kachanov [30, 44] synthesized earlier works in the field and gave detailed forms of energy and effective (degraded) moduli. For the case of isotropic (random) orientation distribution of cracks in the elastic isotropic matrix, the direct micromechanical analysis leads to the following energy and moduli estimations ($w^\mu, \tilde{E}^\mu, \tilde{\nu}^\mu$):

$$\begin{aligned}w^\mu(\varepsilon; d) &= w^0 + \Delta w, \\ \Delta w &= -\frac{8E(1-\nu)(1-\nu/5)}{9(1-\nu/2)(1+\nu)} d \left[\varepsilon_{ij}\varepsilon_{ij} + \frac{\nu(\nu^2 - 16\nu + 19)}{10(1-\nu/5)(1-2\nu)^2} \varepsilon_{kk}^2 \right], \quad (2.25)\end{aligned}$$

$$w^\mu \neq (1-d)w^0 \quad \text{in general,}$$

$$\frac{\tilde{E}^\mu}{E} = \left[1 + \frac{16(1-\nu^2)(1-3\nu/10)}{9(1-\nu/2)} d \right]^2 \quad (2.26)$$

$$\text{compared with } \frac{\tilde{E}}{E} = 1 - d \text{ (model),}$$

$$\frac{\tilde{\nu}^\mu}{E} = \frac{\tilde{E}^\mu}{E} \left[1 + \frac{8(1-\nu^2)}{45(1-\nu/2)} d \right] \cong \frac{\tilde{E}^\mu}{E} \quad (2.27)$$

$$\text{compared with } \frac{\tilde{\nu}}{\nu} = 1 \text{ (model).}$$

The above results (2.25)-(2.27) show that the model based on the energy expression $w = (1-d)w^0$ constitutes a crude approximation of micromechanical evaluation of effective elastic properties for the microcracked body with multiple circular cracks randomly oriented in space. This judgement can

be extended to a larger class of models of the type $\hat{g}(d)w^0$, where $\hat{g}(d)$ is any decreasing function of d . As concluded by Ju [45] and Kachanov [44], when starting from the micromechanical interpretation (2.1), i.e. the stipulation that $d = r^c$, the form (2.20) appears simplistic with respect to micromechanical evaluation involving the 'rigorous' form Δw given by (2.25). Moreover, the Poisson's ratio is reduced by the presence of microcracks approximately in the same proportion as the Young's modulus (for open microcracks). Moreover, the model's predictions of the effective moduli are not compatible with the micromechanical estimations for noninteracting defects whether the latter are cracks or cavities and d is considered as a measure of their respective densities and the internal variable in the thermodynamic potential $w = \rho\psi$.

However, the simplicity of the phenomenological form (2.20), a limited number of constants to be identified and its handy numerical implement, see Marigo [38], justify the model's usefulness as a tool for basic structural analysis involving damage and as a sort of a reference 'classroom' model in a sens parallel to the Prandtl-Reuss isotropic hardening J_2 -plasticity, viewed as the simplest reference plasticity model with respect to more sophisticated ones. As for the J_2 -plasticity, the damage threshold in the above model is symmetric with respect to tension vs. compression loadings in accordance with (2.9), F_d being a quadratic function of strain, see (2.5). Such a symmetry may be inaccurate for a number of microcracked (damaged) engineering materials, see Chapter 3. Still, the model presented constitutes a sort of 'reference prototype' in CDM, frequently employed as a starting point for more sophisticated developments, see e.g. [46, 47].

2.2. Ductile fracture damage. An example of coupled damage-plasticity modelling (Rousselier, 1981 [35])

Development of the line lattice (dislocation-like) defects constitutes a set of underlying microscale mechanisms of crystalline plasticity. It involves the rearrangement of the lattice bonds but not their loss. At the same time, due to microstructural heterogeneity of current metal polycrystals, these rearrangements are accompanied by emanation of numerous sites where the deterioration processes begin, promoted by the piling up of dislocation loops at obstacles such as grain boundaries, second phase inclusions, etc. The consecutive microdeterioration phenomena consisting in the growth of planar and volumetric defects (sharp cracks, voids) provoke the progressive loss

of structural bonds. They are relevant to damage analysis as coupled with the plasticity. The coupling of the two history-dependent mechanisms and, particularly, of their macroscopic consequences ('plastic degradation'), was evidently the focus of the plasticity community's attention in view of the assessment of the ductility limitations in deformed metals and alloys. The growth of voids formed around foreign inclusions and precipitates strongly connected to the ambient temperature plastic straining in metallic materials is classically termed "ductile fracture damage", see e.g. Dragon [48].

The continuum-like modelling of these phenomena was based on some micromechanical analyses as in the very well known approach by Gurson [49], see also Budiansky *et al.* [50], Leblond *et al.* [51]. The exponential effect of the stress triaxiality on the void growth is the most notable result of numerous works in the field. The first statements of the exponential amplification of void growth rates by stress triaxiality go back to McClintock [52] and Rice and Tracey [53], respectively for cylindrical and spherical isolated voids under remote stresses. Here, attention is focused on coherent continuum-like macroscopic modelling incorporating the remarkable aforementioned effect. The CDM model by Rousselier [35] is chosen in this respect as it displays a clear thermodynamic framework in its very formulation concerning various aspects of dissipative coupling.

The micromechanical motivation of the modelling at stake can be embodied by a 'unit cell' representing a typical cuboid (or other) element of the porous solid, i.e. an aggregate of voids around rigid inclusions and of a ductile homogeneous matrix. The latter is assumed as elastic-plastic with isotropic hardening α . The small strain framework will be considered for simplicity with the additivity of elastic and plastic contributions of total strain ϵ . The cavity initiation and growth considered as a predominant damage mechanism, the actual microporosity is designated by a dimensionless density $\bar{\rho}$ as follows

$$\bar{\rho} = \frac{1 - f_v}{1 - f_0}, \quad f_v \geq f_0 \quad (2.28)$$

where f_0 and f_v designate respectively the volume fraction of inclusions and the current volume fraction of voids assumed to include this of inclusions. During void growth the density $\bar{\rho}$ diminishes from its initial value $\bar{\rho}_{in} = 1$. The solid is considered as initially isotropic and its isotropy is supposed to be preserved under damage process. Damage kinetics consists in producing more porosity, it is thus natural to consider a damage internal variable as a

porosity-related one:

$$D = \bar{D}(\bar{\rho}). \quad (2.29)$$

The thermodynamic potential (free energy) is expressed as follows:

$$w = \rho \psi(\boldsymbol{\varepsilon}; \boldsymbol{\varepsilon}^P, \alpha, D) = \frac{1}{2} (\boldsymbol{\varepsilon} - \boldsymbol{\varepsilon}^P) : \mathbf{C} : (\boldsymbol{\varepsilon} - \boldsymbol{\varepsilon}^P) + p(\alpha) + m(D) \quad (2.30)$$

where $p(\alpha)$ and $m(D)$ represent respectively the strain-hardening and damage contributions to the stored energy, the latter one generally counterbalancing a hardening build-up, see e.g. Rousselier, 2000 [54]. It can be seen that the elastic degradation is neglected in (2.30): the model is entirely focused on damage vs. plasticity interaction. From (2.30) one deduces classically the elasticity response embodied here by a linear stress-strain (Hooke's) law and the respective conjugate forces related to α and D :

$$\left\{ \begin{array}{l} \boldsymbol{\sigma} = \frac{\partial w}{\partial \boldsymbol{\varepsilon}} = \mathbf{C} : (\boldsymbol{\varepsilon} - \boldsymbol{\varepsilon}^P) = \mathbf{C} : \boldsymbol{\varepsilon}^{\text{el}}, \\ A = -\frac{\partial w}{\partial \alpha} = -\frac{dp}{d\alpha}(\alpha), \\ F_D = -\frac{\partial w}{\partial D} = -\frac{dm}{dD}(D). \end{array} \right. \quad (2.31)$$

The expression of intrinsic dissipation contains the effects of plastic yielding and strain-hardening augmented by damage input:

$$\phi = \boldsymbol{\sigma} : \dot{\boldsymbol{\varepsilon}}^P + A \cdot \dot{\alpha} + F_D \cdot \dot{D}. \quad (2.32)$$

As the generalized normality framework (generalized standard model) is being postulated for irreversible evolutions of $\boldsymbol{\varepsilon}^P$, α and D , the non-negativity of the dissipation is assured by the existence of a convex pseudo-potential $\Omega(\boldsymbol{\sigma}, A, F_D)$ defined in the space of thermodynamic forces. Rousselier advances the following hypothesis:

$$\Omega(\boldsymbol{\sigma}, A, F_D) = \Omega [w_p(J_2^s, A) + w_D(\boldsymbol{\sigma}_{(m)}, F_D)] \quad (2.33)$$

expressing some dissipative coupling of plasticity and damage phenomena. For inviscid respective evolutions, the potential Ω reduces to the indicator pseudo-function supported by the reversibility domain $f(\boldsymbol{\sigma}, A, F_D) \leq 0$, $f = f_1(J_2^s, A) + f_2(\boldsymbol{\sigma}_{(m)}, F_D)$ with $J_2^s = (\frac{1}{2}s_{ij}s_{ij})^{1/2}$, $\boldsymbol{\sigma}_{(m)} = \frac{1}{3}\sigma_{kk}$, $s_{ij} = \sigma_{ij} - \frac{1}{3}\sigma_{kk}\delta_{ij}$, where \mathbf{s} designates the stress deviator tensor. The form of the

yield function f_1 corresponds to the Huber-Mises expression while this for f_2 is supposed linear in F_D :

$$C^{\text{plast-dam.}} = \{(\boldsymbol{\sigma}, A, F_D) \mid f(\boldsymbol{\sigma}, A, F_D) \leq 0\}, \quad (2.34)$$

$$f(\boldsymbol{\sigma}, A, F_D) = \left(\frac{1}{2} s_{ij} s_{ij}\right)^{1/2} - [k - A - F_D g(\sigma_{(m)})]$$

where k is the initial plasticity limit at simple shear; the actual limit is $k - A - F_D g(\sigma_{(m)})$. The corresponding evolution equations are:

$$\left\{ \begin{array}{l} \dot{\varepsilon}_{ij}^p = \lambda^f \frac{\partial f}{\partial \sigma_{ij}} = \lambda^f \left[\frac{s_{ij}}{2\sqrt{\frac{1}{2} s_{kl} s_{kl}}} + \frac{1}{3} F_D \frac{dg}{d\sigma_{(m)}} \delta_{ij} \right], \quad \lambda^f \geq 0 \\ \dot{\alpha} = \lambda^f \frac{\partial f}{\partial A} = \lambda^f = \sqrt{2} (\dot{\varepsilon}_{ij}^p \dot{\varepsilon}_{ij}^p)^{1/2}, \quad e_{ij} = \varepsilon_{ij} - \varepsilon_{(m)} \delta_{ij}, \\ \dot{D} = \lambda^f \frac{\partial f}{\partial F_D} = \lambda^f g(\sigma_{(m)}). \end{array} \right. \quad (2.35)$$

The effect of damage-induced porosity on the aggregate behaviour is clearly shown in (2.35)₁ via the volumetric contribution to the inelastic strain produced by the damage-yield function $f_2 = F_D g(\sigma_{(m)})$.

Contrarily to the energy form (2.30) exhibiting no apparent link between the respective contributions, the complementary relationships (2.35) indicate a strong coupling between the plasticity and damage events. Among other features one can see the common multiplier λ^f governing intensity of plasticity as well as that of damage growth. No supplementary input is necessary to quantify further damage growth. In fact, maintaining the foregoing hypotheses of predominant character of damage-plasticity interaction compared to the effect of damage on elasticity, it is stated that

$$\dot{\varepsilon}_{(m)} \cong \frac{1}{3} \dot{\varepsilon}_{ii}^p, \quad \varepsilon_{(m)} = \frac{1}{3} \varepsilon_{ii} \quad (2.36)$$

thus neglecting elastic volume change. The balance of mass equation expressed in a specific local version employing the dimensionless density $\bar{\rho}$ and accounting for (2.36) is

$$\dot{\bar{\rho}} + 3\bar{\rho} \dot{\varepsilon}_{(m)}^p = 0. \quad (2.37)$$

It yields

$$\dot{\varepsilon}_{(m)}^p = -\frac{\dot{\bar{\rho}}}{3\bar{\rho}}. \quad (2.38)$$

On the other hand, from (2.35)₁ one obtains

$$\dot{\varepsilon}_{(m)}^p = \lambda^f \frac{1}{3} F_D g'(\sigma_{(m)}) \quad (2.39)$$

where $g'(\sigma_{(m)}) = \frac{dg}{d\sigma_{(m)}}$.

This expression allows quantifying λ^f in a simple form

$$\lambda^f = \frac{3 \dot{\varepsilon}_{(m)}^p}{F_D g'(\sigma_{(m)})}. \quad (2.40)$$

Putting together (2.29) and (2.35)₃, the damage evolution can be expressed as follows:

$$\dot{D} = \frac{d\bar{D}}{d\bar{\rho}} \dot{\bar{g}} = \lambda^f g(\sigma_{(m)}) \quad (2.41)$$

and further, by use of (2.40)

$$\frac{d\bar{D}}{d\bar{\rho}} \dot{\bar{g}} = \frac{3 \dot{\varepsilon}_{(m)}^p g(\sigma_{(m)})}{F_D g'(\sigma_{(m)})}. \quad (2.42)$$

It follows from (2.38) that the above equation can be finally written in the form

$$\frac{g'(\sigma_{(m)})}{g(\sigma_{(m)})} = - \frac{1}{\bar{\rho} D'(\bar{\rho}) F_D(\bar{\rho})} \quad (2.43)$$

where $D'(\bar{\rho}) = \frac{d\bar{D}}{d\bar{\rho}}$. For given $\bar{\rho}$, the both members represent a (constant) quantity say, C^* , having the dimension of $[\sigma]^{-1}$. One can pose $C^* = \frac{C}{\sigma_0}$, $C = \text{const} > 0$ and σ_0 is the plasticity limit at uniaxial tension for the solid (non-damaged) material. We can thus write (2.43) in the form

$$\frac{g'(\sigma_{(m)})}{g(\sigma_{(m)})} = \frac{C}{\sigma_0}. \quad (2.44)$$

It easily follows from the above equation that

$$\begin{aligned} g(\sigma_{(m)}) &= \bar{\mu} \exp \frac{C \sigma_{(m)}}{\sigma_0}, \quad \bar{\mu} > 0, \\ \dot{D} &= \lambda^f \bar{\mu} \exp \left(\frac{C \sigma_{(m)}}{\sigma_0} \right), \quad \lambda^f \geq 0, \end{aligned} \quad (2.45)$$

which represents the exponential effect of the stress triaxiality $T = \frac{\sigma_{(m)}}{\sigma_0}$ on ductile fracture damage by void growth as mentioned at the beginning of

this Section and, as shown above, inherently arising from the hypotheses of the Rousselier's model, Rousselier [35].

The multiplier λ^f already quantified in (2.40) can be alternatively (and conventionally) determined from the consistency equation $\dot{f} = 0$ for plasticity-damage loading branch. One obtains the following strain-rate controlled expression:

$$\lambda^f = \frac{\frac{\partial f}{\partial \sigma} : \mathbf{C} : \dot{\epsilon}}{\frac{\partial f}{\partial \sigma} : \mathbf{C} : \frac{\partial f}{\partial \sigma} + \frac{\partial f}{\partial A} \frac{d^2 p}{d\alpha^2} \frac{\partial f}{\partial A} + \frac{\partial f}{\partial F_D} \frac{d^2 m}{dD^2} \frac{\partial f}{\partial F_D}} \quad (2.46)$$

where the last term in the denominator represents the specific damage input.

Particular versions of the aforementioned model are based on specific expressions concerning the functions $D(\bar{\rho})$ and $m(D)$, the latter conditioning the form of $F_D(D)$. The following application is illustrated below, Fig. 2.3:

$$\left\{ \begin{array}{l} D = \ln \left(1 + \frac{1 - \bar{\rho}}{\bar{\rho} f_0} \right), \quad \bar{\rho} \in [1, 0], \\ m(D) = -\frac{\sigma_0}{C} \ln(1 - f_0 + f_0 \exp D), \quad D \in [0, +\infty), \\ F_D(D) = \frac{\sigma_0}{C} \frac{f_0 \exp D}{1 - f_0 + f_0 \exp D}. \end{array} \right. \quad (2.47)$$

Equations (2.47) yield the following special form of the yield function f :

$$f(\sigma, A, F_D(D)) = \left[\frac{1}{2} s_{ij} s_{ij} \right]^{1/2} - \left[\frac{\sigma_0}{\sqrt{3}} - A - \frac{\sigma_0}{C} \frac{f_0 \exp D}{1 - f_0 + f_0 \exp D} \bar{\mu} \left(\exp \frac{C}{\sigma_0} \sigma_{(m)} \right) \right]. \quad (2.48)$$

It can be remarked that $F_D|_{D=0} = \frac{\sigma_0}{C} f_0$.

Two particular features of the form (2.48) can be viewed in Fig. 2.3: (i) there is a non-zero slope for a simple shear ($\sigma_{(m)} = 0$) thus allowing for volumetric dilatancy due to porosity growth for zero hydrostatic stress and (ii) a singular point (corner) exists for pure hydrostatic tension path ($J_2^s = 0$). These distinguish the Rousselier's model from that of Gurson [49]. The first property has some experimental support: tests for small triaxiality T including torsion stress-path (zero triaxiality) show clearly ductile fracture preceded by void growth for metallic specimens [55]. In this respect the

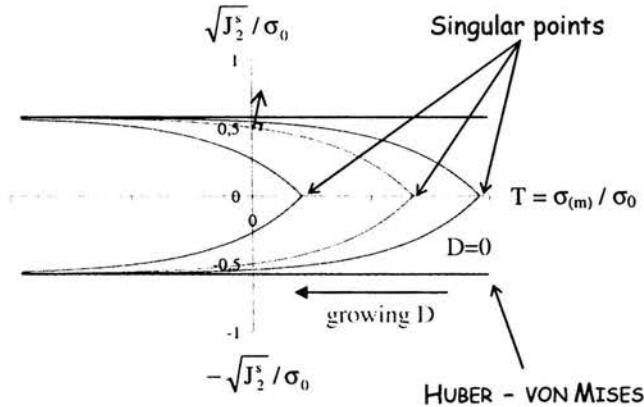


FIGURE 2.3. Aspect of consecutive yield loci for the Rousselier model in the stress-space $\sigma_{(m)}/\sigma_0 - J_2^s/\sigma_0$.

Rousselier's model is thus closer upon physical phenomena observed than the Gurson's one.

The Gurson model, based on explicit micromechanical considerations, is represented by the following yield function (here a special form resulting from modifications brought about by Tvergaard and Needleman [56] is given):

$$f(\boldsymbol{\sigma}, R, f_v) = \frac{\sigma_{\text{eq}}^2}{R^2} - 1 - q_1^2 (f^*)^2 + 2 q_1 f^* \cosh\left(\frac{3q_2 \sigma_{(m)}}{2R}\right) \quad (2.49)$$

where $\sigma_{\text{eq}} = \left(\frac{3}{2} s_{ij} s_{ij}\right)^{1/2}$, R is the actual tensile flow stress in the matrix (solid) material while q_1 , q_2 are adjustable phenomenological parameters. A particular, bilinear function $f^*(f_v)$ was introduced by Tvergaard and Needleman to account for the effects of advanced void growth and coalescence corresponding to the post-localization stage.

As in the model based on the potential (2.34) and its particular form (2.48), the model G-T-N (Gurson-Tvergaard-Needleman) embodied in (2.49) describes dilatational and pressure sensitive plastic flow due to the presence of micro-voids. Furthermore, although the matrix material continues to harden, the aggregate can soften. With continued deformation, the stress carrying capacity of the aggregate diminishes and this is linked to the creation of new free surface (damage by cavity growth).

Abundant work has been done to study material instabilities using the both models for microporous metallic aggregates in order to predict the onset of macroscopic ductile fracture. The occurrence of a localization (shear) band

instability viewed as an outcome of particular material response and considered as a favourite precursor of fracture as introduced in Sec. 2.1, has been widely investigated. For much synthetic comments regarding the localization bifurcation including progressively cavitating porous plastic solids and the Gurson model-based constitutive framework the reader can refer to the review by Needleman and Tvergaard [57]. Rousselier himself [54] has proceeded with a stability analysis of a linear perturbation employing his constitutive model presented above, Eqs. (2.28)-(2.48). As for the bifurcation approach leading to the criterion (2.13), the localization studied via a perturbation method can start from a relatively simple model problem for a solid subject to uniform straining. The hypothesis of instability of the fundamental solution is examined by postulating the planar perturbation of the displacement field $\mathbf{u}(\mathbf{x}, t)$ in the form:

$$\Delta \mathbf{u}(\mathbf{x}, t) = \delta \mathbf{U} \exp(i q \mathbf{n} \cdot \mathbf{x} + \omega t). \quad (2.50)$$

This perturbation being injected into the equilibrium equations leads to the expression $\mathbf{M}(\omega, n) \cdot \delta \mathbf{U} = 0$. Non-trivial solutions $\delta \mathbf{U} \neq \mathbf{0}$ exist if $\det \mathbf{M} = 0$, the latter representing a polynomial equation $\chi(\omega, \Theta, \varphi) = 0$ with respect to ω , the growth factor of the perturbation (2.50).

The characteristic direction of the perturbation is defined by the Euler angles (Θ, φ) . Localization occurs for the plane corresponding to the maximum root ω .

For an axisymmetric problem (axial and radial tensile loading) it is shown that with increasing f_v , the ratio $\dot{\varepsilon}_{(m)}^p / \dot{\varepsilon}_{\text{eq}}^p$ (where $\dot{\varepsilon}_{\text{eq}}^p = (\frac{2}{3} \dot{\varepsilon}_{ij}^p \dot{\varepsilon}_{ij}^p)^{1/2} = \frac{\sqrt{3}}{2} \dot{\alpha}$) increases as well as it can be deduced from Eq. (2.39) combined with (2.47). For $\dot{\varepsilon}_{(m)}^p / \dot{\varepsilon}_{\text{eq}}^p = 0.5$ the localization plane becomes perpendicular to the maximum principal stress direction while ω tends to infinity from that point on so that a bifurcation occurs. It can be remarked that for an elastic-viscoplastic version of the model, the limit value of the ratio $\dot{\varepsilon}_{(m)}^p / \dot{\varepsilon}_{\text{eq}}^p$ is smaller than 0.5 and ω remains finite. The critical value of $\dot{\varepsilon}_{(m)}^p / \dot{\varepsilon}_{\text{eq}}^p = 0.5$ corresponds to the uniaxial plastic extension: $\dot{\varepsilon}_{ij}^p = 0$ except for $\dot{\varepsilon}_{11}^p = 3\dot{\varepsilon}_{\text{eq}}^p/2$, Rousselier [54].

Independent numerical studies involving FE (finite element) approximations of the field equations for a cell containing a void indicate some pertinency of the critical strain-path condition $\dot{\varepsilon}_{(m)}^p / \dot{\varepsilon}_{\text{eq}}^p = 0.5$. For different global stress triaxialities a turning point regarding global strain path is observed in diagrams representing the ratio $\dot{\varepsilon}_{rr}^p / \dot{\varepsilon}_{zz}^p$ vs. $\dot{\varepsilon}_{\text{eq}}^p$, see Rousselier [54]. This turning point corresponds to $\dot{\varepsilon}_{rr}^p / \dot{\varepsilon}_{zz}^p = 0$, i.e. to $\dot{\varepsilon}_{(m)}^p / \dot{\varepsilon}_{\text{eq}}^p = 0.5$. The void growth

calculated from the cell-model approximations is exponential up to the turning point and becomes linear after. The results of cell-model simulations by Li *et al.* [58] are compared with the Rousselier and G-T-N models' predictions for a homogeneous problem near the critical state. It seems that the Rousselier's model is more adapted to follow the voided solid behaviour at the corresponding near- and post-localization stages of void growth.

An important issue concerns the ability of finite element approximations to treat localized shearing and alike bifurcation and post-bifurcation problems. The problem becomes ill-posed and mesh design, shape functions, etc., ill-adapted to deal with band-like deformation modes, notably for time-independant damage and/or plasticity models (the strain-rate dependency provides some 'regularizing' effect). In particular the numerical predictions show an inherent sensitivity corresponding to softening material behaviour leading to localization in regions as confined as possible within the mesh resolution. The problem can be overcome by incorporating a material length scale in the constitutive relations, e.g. by introducing a nonlocal formulation to a constitutive model via some ingredients, for example dissipative mechanisms exhibiting genuine nonlocal effects. Such nonlocal plasticity and damage models have been proposed by a number of authors (Aifantis [59], de Borst [60], Fleck *et al* [61], Pijaudier and Bazant [62], Leblond *et al* [63], Mroz and Seweryn [64]. In a nonlocal generalization of a relevant deformation and/or damage mechanism the corresponding local quantity, say κ , (plastic strain, damage variable, any other pertinent internal variable, its conjugate force, equivalent strain, etc.) is replaced by its spatially averaged form:

$$\bar{\kappa}(\mathbf{x}) = \frac{1}{V_r(\mathbf{x})} \int_{\Omega} \hat{\Psi}(\mathbf{x} - \mathbf{s}) \kappa(\mathbf{s}) d\mathbf{s}^3, \quad (2.51)$$

$$\text{with } V_r(\mathbf{x}) = \int_{\Omega} \hat{\Psi}(\mathbf{x} - \mathbf{s}) d\mathbf{s}^3, \quad d\mathbf{s}^3 \equiv d\Omega$$

where $\hat{\Psi}(\mathbf{x} - \mathbf{s})$ is the weight function, normalized over R^3 , for instance

$$\hat{\Psi}(\mathbf{x} - \mathbf{s}) = \exp \left[-\frac{4 \|\mathbf{x} - \mathbf{s}\|^2}{l_c^2} \right], \quad (2.52)$$

and \mathbf{s} is a relative position vector pointing to the infinitesimal volume $d\Omega$; Ω denotes the volume of the body studied. The normalization factor $V_r(\mathbf{x})$ can be considered as the representative volume at point \mathbf{x} . It is not necessarily

unity since the integral defining it above is taken over Ω instead of R^3 . As $\hat{\Psi}$ is normalized we have $\int_{R^3} \hat{\Psi}(\mathbf{s}) d\mathbf{s}^3 = 1$ [63].

The representation (2.51) can be used as a starting point for gradient models, called sometimes ‘differential nonlocal’ models, supposed more convenient to manage computationally in the context of incremental algorithms.

A way to transform the above nonlocal representation to a gradient one is to expand \mathbf{x} into Taylor series truncated (for instance) to the second order:

$$\kappa(\mathbf{x} + \mathbf{s}) = \kappa(\mathbf{x}) + \frac{\partial \kappa(\mathbf{x})}{\partial \mathbf{x}} \mathbf{s} + \frac{\partial^2 \kappa(\mathbf{x})}{\partial \mathbf{x}^2} \frac{\mathbf{s}^2}{2!} + \dots \quad (2.53)$$

Substitution of the latter in Eq. (2.51) and integration with respect to \mathbf{s} yields

$$\bar{\kappa}(\mathbf{x}) = \kappa(\mathbf{x}) + c \nabla^2 \kappa \quad (2.54)$$

where c is parameter of the dimension $[\text{L}]^2$; it depends on the type of weight function. Under some restrictions (see de Borst *et al.* [65]) it can be related to the internal length of the material: $\sqrt{c} \propto l_c$ reflecting thus the length scale for the deformation/damage process at stake.

Other ways to devise gradient damage models have been advanced, see e.g. Pijaudier and de Borst [47].

In the way outlined above by (2.51), (2.52) Leblond *et al.* [63] and Tvergaard and Needleman [66] have developed a nonlocal version of the Gurson model to study the influence of nonlocality on bifurcation by shear banding. These authors considered a nonlocal modification of damage evolution, the damage variable identified with the void volume fraction f_v . It is thus stipulated that the ductile damage mechanism in porous metals depends on a characteristic length as follows [66]:

$$\begin{aligned} \dot{f}_v(\mathbf{x}) &= \frac{1}{V_r(\mathbf{x})} \int_{\Omega} \hat{w}(\mathbf{x} - \mathbf{s}) \dot{f}_v(\mathbf{s}) d\mathbf{s}^3, \\ \text{with } \hat{w}(z) &= \left[\frac{1}{1 + (\frac{z}{l_c})^p} \right]^q, \quad l_c > 0, \end{aligned} \quad (2.55)$$

and $z = (z_i z_i)^{1/2}$. The local formulation corresponds to the limit $l_c \rightarrow 0$.

The authors cited above [63, 66] showed that the nonlocal damage approach removes the inherent mesh sensitivity in the predictions of failure by shear localization. It has been shown also that the values of the post-localization slopes for stress-strain curves predicted by the nonlocal continuum model depend significantly on the value chosen for l_c . A tentative to

provide a micromechanical basis for specifying the material characteristic length has been proposed in [66].

It is to be emphasized that the above analyses regarding the localization bifurcation governed by the condition (2.13), Rice [39], involving discontinuities, are facilitated by the fact that in spite of the nonlocal character of the constitutive equations, the jumps of the stress and strain rates through any surface are connected by a local relation, see [63] for details. From the early nineties on, a new class of damage models has emerged allowing for singular effects (strain-rate and/or velocity discontinuities) being incorporated in the very corpus of the constitutive model, see for instance Oliver [67].

Chapter 3

Anisotropic damage and normal unilateral effect: eigenvector approach for mesocracking damage

This chapter outlines the salient features of the anisotropic damage model by Dragon *et al.* [3], Halm and Dragon [4], which forms the framework for further developments presented in Chapters 4 and 5. An objective of the damage model summarized below is to describe – in a realistic manner applicable to structural calculus – the process of mesocrack-induced anisotropic degradation and relative inelastic behaviour of a rock-like ‘quasi-brittle’ solid. It stipulates evaluation of effective elastic moduli of a material with microcracks and an adequate description of the evolution of damage. The emphasis has been put on an “open” formulation of the model to allow further extensions and couplings. It is based on the hypotheses and developments ordered below in the items from (i) to (vi):

- (i) A single damage internal variable is constituted by a symmetric, second-order tensor \mathbf{D} indicating orientation of microcrack set(s) as well as the dissipative mechanism under consideration, namely generation and growth of decohesion microspheres:

$$\mathbf{D} = \sum_i d^i(s) \mathbf{n}^i \otimes \mathbf{n}^i. \quad (3.1)$$

The scalar density $d^i(s)$ is proportional to the extent s of decohesion surface and the unit normal vector \mathbf{n}^i describes orientation of the i -th

set of parallel crack-like defects. The form (3.1) is motivated by micromechanical considerations (see e.g. [30]) but in the context further on here the density $d(s)$ is reckoned as a macroscopic quantity. The expression (3.1) is in itself a guiding microstructural interpretation of damage-related internal variable \mathbf{D} . Since \mathbf{D} is a symmetric second-order tensor it has three positive eigenvalues D_k , ($k = 1, 2, 3$) and three orthogonal eigenvectors ν^k . This means that any system of microcracks (3.1), decomposed into $1, \dots, i, \dots, n$ of subsystems of parallel mesocracks can be reduced to three equivalent orthogonal sets of cracks characterized by densities D_k and normal vectors ν^k .

$$\mathbf{D} = \sum_{k=1}^3 D_k \nu^k \otimes \nu^k. \quad (3.2)$$

- (ii) The damage-dependent strain energy (free energy per unit volume) $w(\boldsymbol{\varepsilon}, \mathbf{D})$ generates a form of elastic orthotropy – in connection to the three eigensystems (3.2) – for $\mathbf{D} \neq \mathbf{0}$; w is assumed as linear function of \mathbf{D} and in this way corresponding to non-interacting cracks hypothesis. On the other hand, it contains linear and quadratic terms in $\boldsymbol{\varepsilon}$. A particular invariant form given below (formula (3.4)) comprises a single linear term reading $g \operatorname{tr}(\boldsymbol{\varepsilon} \cdot \mathbf{D})$; g is a constant, corresponding to damage-induced residual phenomena. The damage induced macroscopic residual stress for $\boldsymbol{\varepsilon} = \mathbf{0}$ is thus explicitly obtained equal to $g\mathbf{D}$. Inversely, for $\boldsymbol{\sigma} = \mathbf{0}$, non-zero residual strain is induced.
- (iii) Under predominantly compressive loading, favourably oriented cracks close leading to an elastic moduli recovery phenomenon in the direction normal to the closed cracks. It is called here normal unilateral effect – in the absence of frictional sliding (the latter, when accounted for later, will induce a shear recovery effect as well) – and requires more involved damage characterization. In fact, for a set of cracks constrained against opening a fourth-order tensorial density is necessary for a rigorous, micromechanically motivated description. A compromise solution has been advanced in [4] between micromechanical considerations imposing an additional fourth-order damage variable and macroscopic modelling efficiency. The formulation maintains the orthotropy of the effective, elastic properties, instead of eventual more general anisotropy induced by a new fourth-order damage tensor. The complementary fourth-order entity $\hat{\mathbf{D}}$, necessary to account for the normal unilateral effect, is di-

rectly assembled with the eigenvalues and eigenvectors of \mathbf{D} and cannot therefore be considered as a new damage internal variable:

$$\hat{\mathbf{D}} = \sum_{k=1}^3 D_k \boldsymbol{\nu}^k \otimes \boldsymbol{\nu}^k \otimes \boldsymbol{\nu}^k \otimes \boldsymbol{\nu}^k. \quad (3.3)$$

- (iv) A single scalar simultaneous invariant of $\hat{\mathbf{D}}$ and $\boldsymbol{\varepsilon}$, namely $\boldsymbol{\varepsilon} : \hat{\mathbf{D}} : \boldsymbol{\varepsilon}$, completes the expression of the free energy $w[\boldsymbol{\varepsilon}, \mathbf{D}, \hat{\mathbf{D}}(\mathbf{D})]$ (thermodynamic potential), with no additional material constant with respect to the basic form $w(\boldsymbol{\varepsilon}, \mathbf{D})$ postulated in (ii). Rigorous continuity analysis in the framework of multilinear elasticity (for a given damage state), recast in [4] and summarized under the item (v) below, leads to a simple microcrack closure condition for an equivalent set, namely: $\boldsymbol{\nu}^k \cdot \boldsymbol{\varepsilon} \cdot \boldsymbol{\nu}^k \leq 0$. The detailed expression of $w(\boldsymbol{\varepsilon}, \mathbf{D})$ including the supplementary term allowing for normal unilateral effect is:

$$w(\boldsymbol{\varepsilon}, \mathbf{D}) = \frac{1}{2} \lambda (\text{tr } \boldsymbol{\varepsilon})^2 + \mu \text{tr}(\boldsymbol{\varepsilon} \cdot \boldsymbol{\varepsilon}) + g \text{tr}(\boldsymbol{\varepsilon} \cdot \mathbf{D}) + \alpha \text{tr } \boldsymbol{\varepsilon} \text{tr}(\boldsymbol{\varepsilon} \cdot \mathbf{D}) + 2\beta \text{tr}(\boldsymbol{\varepsilon} \cdot \boldsymbol{\varepsilon} \cdot \mathbf{D}) - (\alpha + 2\beta) \boldsymbol{\varepsilon} : \left[\sum_{k=1}^3 H(-\boldsymbol{\nu}^k \cdot \boldsymbol{\varepsilon} \cdot \boldsymbol{\nu}^k) D_k \boldsymbol{\nu}^k \otimes \boldsymbol{\nu}^k \otimes \boldsymbol{\nu}^k \otimes \boldsymbol{\nu}^k \right] : \boldsymbol{\varepsilon}, \quad (3.4)$$

where H is the classical Heaviside function; α, β are material constants related to modified elastic moduli for a given damage state. λ and μ are the conventional Lamé constants for elastic (non damaged) solid matrix.

The corresponding damage-induced orthotropic elasticity representation $\boldsymbol{\sigma}(\boldsymbol{\varepsilon}, \mathbf{D})$ and the damage driving (thermodynamic) force \mathbf{F}^D are determined by corresponding partial derivation:

$$\begin{aligned} \boldsymbol{\sigma} &= \frac{\partial w}{\partial \boldsymbol{\varepsilon}} = \lambda (\text{tr } \boldsymbol{\varepsilon}) \mathbf{1} + 2\mu \boldsymbol{\varepsilon} + g \mathbf{D} \\ &+ \alpha [\text{tr}(\boldsymbol{\varepsilon} \cdot \mathbf{D}) \mathbf{1} + (\text{tr } \boldsymbol{\varepsilon}) \mathbf{D}] + 2\beta (\boldsymbol{\varepsilon} \cdot \mathbf{D} + \mathbf{D} \cdot \boldsymbol{\varepsilon}) \\ &- 2(\alpha + 2\beta) \sum_{k=1}^3 H(-\boldsymbol{\nu}^k \cdot \boldsymbol{\varepsilon} \cdot \boldsymbol{\nu}^k) D_k (\boldsymbol{\nu}^k \cdot \boldsymbol{\varepsilon} \cdot \boldsymbol{\nu}^k) \boldsymbol{\nu}^k \otimes \boldsymbol{\nu}^k, \end{aligned} \quad (3.5)$$

$$\begin{aligned} \mathbf{F}^D &= -\frac{\partial w}{\partial \mathbf{D}} = -g \boldsymbol{\varepsilon} - \alpha (\text{tr } \boldsymbol{\varepsilon}) \boldsymbol{\varepsilon} - 2\beta (\boldsymbol{\varepsilon} \cdot \boldsymbol{\varepsilon}) \\ &+ (\alpha + 2\beta) \sum_{k=1}^3 H(-\boldsymbol{\nu}^k \cdot \boldsymbol{\varepsilon} \cdot \boldsymbol{\nu}^k) (\boldsymbol{\nu}^k \cdot \boldsymbol{\varepsilon} \cdot \boldsymbol{\nu}^k)^2 \boldsymbol{\nu}^k \otimes \boldsymbol{\nu}^k. \end{aligned} \quad (3.6)$$

In spite of the presence of the Heaviside function $H(-\nu^k \cdot \varepsilon \cdot \nu^k)$, w , σ and \mathbf{F}^D remain continuous when passing from the open mesocracks configuration to the closed mesocracks configuration and vice versa. This is possible because the discontinuity of H takes place when the multiplier $\nu^k \cdot \varepsilon \cdot \nu^k$ entering Eqs. (3.6), (3.5), (3.6) becomes itself zero.

- (v) In the introduction of this text, the emphasis has been put on the difficulties in ensuring continuity of stress-strain response when damage deactivation takes place and corresponding unilateral conditions should be respected. Whereas some authors rectify a posteriori the discontinuity generated by the deactivation, see e.g. [68], the model given here satisfies continuity of the energy w and of the stress-strain response during crack opening/closure transition. Consider the free energy w written in two different forms, respectively $w^1(\varepsilon, \mathbf{D})$ for open microcracks and $w^2(\varepsilon, \mathbf{D}, \hat{\mathbf{D}})$ for closed ones:

$$w^1 = \frac{1}{2} \lambda (\text{tr } \varepsilon)^2 + \mu \text{tr}(\varepsilon \cdot \varepsilon) + g \text{tr}(\varepsilon \cdot \mathbf{D}) + \alpha_1 \text{tr } \varepsilon \text{tr}(\varepsilon \cdot \mathbf{D}) + 2\beta_1 \text{tr}(\varepsilon \cdot \varepsilon \cdot \mathbf{D}) + o(\varepsilon : \hat{\mathbf{D}} : \varepsilon), \quad (3.7a)$$

$$w^2 = \frac{1}{2} \lambda (\text{tr } \varepsilon)^2 + \mu \text{tr}(\varepsilon \cdot \varepsilon) + g \text{tr}(\varepsilon \cdot \mathbf{D}) + \underbrace{\alpha_2 \text{tr } \varepsilon \text{tr}(\varepsilon \cdot \mathbf{D}) + 2\beta_2 \text{tr}(\varepsilon \cdot \varepsilon \cdot \mathbf{D})}_{\Delta w'} + \underbrace{\gamma \varepsilon : \hat{\mathbf{D}} : \varepsilon}_{\Delta w''}. \quad (3.7b)$$

The model postulates a priori the continuity of stress between the states 1 and 2, i.e. $\sigma^1 = \sigma^2$ at opening/closure (and reverse) transition. Considering the current, damage influenced stiffness discontinuity (jump) $[\mathbf{C}] = (\partial^2 w^2 / \partial \varepsilon \partial \varepsilon) - (\partial^2 w^1 / \partial \varepsilon \partial \varepsilon)$, the condition stated can be written as an equation representing a surface \mathcal{S} in the strain space delimiting (for a given damage state) two linear elastic subdomains. This equation is of the form $h(\varepsilon) = [\mathbf{C}] : \varepsilon = 0$. The above condition of stress continuity is sufficient to impose the continuity of the energy w . Indeed, w is continuous if the stress jump is normal to the surface \mathcal{S} separating states 1 and 2, Wesolowski [69]. The condition on the stress discontinuity here is stronger: no jump was admitted.

Since \mathcal{S} separates the six-dimensional strain space \mathcal{E} into two six-dimensional subspaces, \mathcal{S} itself is five-dimensional (i.e., $\dim \text{Ker}[\mathbf{C}] = 5$) and $[\mathbf{C}]$ is of rank one: $\text{rank}[\mathbf{C}] = \dim \text{Im}[\mathbf{C}] = \dim \mathcal{E} - \dim \text{Ker}[\mathbf{C}] = 6 - 5 = 1$, cf. Curnier *et al.* [70]. It is then sufficient that all second order

determinants of $[\mathbf{C}]$ be equal to zero [69]. The relevant calculations give rise to the following sufficient conditions: $\alpha_1 = \alpha_2 = \alpha$, $\beta_1 = \beta_2 = \beta$, and thus $[\mathbf{C}] = 2\gamma \hat{\mathbf{D}}$. Each equivalent set of cracks of the normal ν^k , $k = 1, 2, 3$ can be considered independent. Let us examine for instance a single set ($k = 1$). The aforesaid equation determining the surface \mathcal{S} leads for the present model to the particular form: $h(\boldsymbol{\varepsilon}) = \nu \cdot \boldsymbol{\varepsilon} \cdot \nu = 0$, which represents the opening/closure criterion for the crack-set of normal ν . This criterion has been obtained by Halm and Dragon [4] and is based on the rigorous argument summed up hereby. The similar criterion was earlier postulated by Chaboche [71] on different grounds but in accordance with some micromechanical considerations, cf. Andrieux *et al.* [20].

The relation cited can be extended to each equivalent set: $h^k(\boldsymbol{\varepsilon}) = \nu^k \cdot \boldsymbol{\varepsilon} \cdot \nu^k = 0$, $k = 1, 2, 3$. An equivalent set (of normal ν^k) becomes inactive (resp. active) when the corresponding normal strain becomes negative (resp. positive). At this threshold, when passing from positive to negative $h^k(\boldsymbol{\varepsilon})$, the term $\boldsymbol{\varepsilon} : \hat{\mathbf{D}} : \boldsymbol{\varepsilon}$ with the constant γ appears in the expression of w^2 allowing for the recovery of stiffness in the direction normal to that of the closed crack-set. In a convenient local reference system related to the crack orientation (axis 1 normal to cracks, axes 2 and 3 in the crack plane), the corresponding stiffness recovery condition reads $\frac{\partial^2 \Delta w'}{\partial \varepsilon_{11} \partial \varepsilon_{11}} + \frac{\partial^2 \Delta w''}{\partial \varepsilon_{11} \partial \varepsilon_{11}} = 0$. This means that the damage-induced loss of normal stiffness obtained by derivation of the $\Delta w'$ -term in Eq. (3.7a) is recovered through the supplementary term $\Delta w''$. After calculation the condition above leads to the simple relation: $\gamma = -\alpha - 2\beta$. This result constitutes a major advantage: γ is not a new constant to be identified, it is calculated from the parameters α and β of the basic model. The form (3.4) of the energy w as well as the expressions (3.5), (3.6) account for the issues discussed in this paragraph.

- (vi) The evolution of \mathbf{D} , corresponding to the brittle, splitting-like crack kinetics, has been found to follow the normality rule with respect to a criterion in the space of components of the proper thermodynamic force (affinity) \mathbf{F}^D . The damage evolution is thus apparently following the principle of maximum (damage) dissipation, and is related here to tensile (positive) straining $\boldsymbol{\varepsilon}^+$ and to actual damage pattern. It should be stressed however that the particular damage criterion

$f(\mathbf{F}^D, \mathbf{D}) \leq 0$ is explicitly dependent only on the part $\mathbf{F}^{D1+} = -g\boldsymbol{\varepsilon}^+ = \mathbf{F}^D - \mathbf{F}^{D2} - \mathbf{F}^{D1-}$ of the driving force \mathbf{F}^D . \mathbf{F}^{D1} is the strain energy release rate term related to residual 'locked' effects: $\mathbf{F}^{D1} = -g\boldsymbol{\varepsilon}$, \mathbf{F}^{D2} represents the remaining recoverable energy release rate. The former term is decomposed into the splitting part $\mathbf{F}^{D1+} = -g\boldsymbol{\varepsilon}^+$, $\boldsymbol{\varepsilon}^+ = \mathbf{P}^+ : \boldsymbol{\varepsilon}$, with \mathbf{P}^+ a positive fourth-order projection operator selecting positive eigenvalues from strain, and the non-splitting part $\mathbf{F}^{D1-} = -g(\boldsymbol{\varepsilon} - \boldsymbol{\varepsilon}^+)$. The damage criterion and rate-independent damage evolution law are thus as follows:

$$\begin{aligned} f(\mathbf{F}^D - \mathbf{F}^{D2} - \mathbf{F}^{D1-}; \mathbf{D}) \\ = \sqrt{\frac{1}{2} \text{tr} [(\mathbf{F}^D - \mathbf{F}^{D2} - \mathbf{F}^{D1-}) \cdot (\mathbf{F}^D - \mathbf{F}^{D2} - \mathbf{F}^{D1-})]} \\ + B \text{tr} [(\mathbf{F}^D - \mathbf{F}^{D2} - \mathbf{F}^{D1-}) \cdot \mathbf{D}] - (C_0 + C_1 \text{tr} \mathbf{D}) \leq 0, \quad (3.8) \end{aligned}$$

$$\begin{aligned} \dot{\mathbf{D}} &= \Lambda_D \frac{\partial f}{\partial \mathbf{F}^D} \\ &= \begin{cases} 0, & \text{if } f < 0 \text{ or } f = 0, \dot{f} < 0; \\ \Lambda_D \left[\frac{\boldsymbol{\varepsilon}^+}{\sqrt{2 \text{tr}(\boldsymbol{\varepsilon}^+ \cdot \boldsymbol{\varepsilon}^+)}} + B \mathbf{D} \right], & \text{if } f = 0 \text{ and } \dot{f} = 0; \quad \Lambda_D \geq 0. \end{cases} \quad (3.9) \end{aligned}$$

Remarks

The hypotheses posed above lead to the normality rule (3.9) which does not correspond to the fully (generalized) standard schema in the sense codified by Halphen and Nguyen [72] requiring, among others, the yield function f (and the corresponding potential, namely the indicator function of $f = 0$ for an inviscid dissipative process) being defined in the non-truncated space of conjugate forces (here \mathbf{F}^D). The hypothesis herein is that the evolution of damage is governed by a criterion involving the particular ingredient \mathbf{F}^{D1+} of the conjugate force \mathbf{F}^D . This is equivalent to stating

$$f(\mathbf{F}^{D1+}, \mathbf{D}) = f(\boldsymbol{\varepsilon}^+, \mathbf{D}) = |g| \sqrt{\frac{1}{2} \boldsymbol{\varepsilon}^+ : \boldsymbol{\varepsilon}^+} - Bg \text{tr}(\boldsymbol{\varepsilon}^+ \cdot \mathbf{D}) - C_0 - C_1 \text{tr} \mathbf{D},$$

and postulating – as asserted above – the determinant role of positive straining in damage evolution. The complementary part of the actual damage

model (3.8), (3.9) – and of any dissipative model defined in the truncated space of a conjugate force preserving simultaneously the relative normality form – will be called in the sequel a pseudo-standard model. For this aspect and further analysis of the present model the reader can consult the dissertation of Badel [73].

The damage criterion (3.8) transferred to stress-space (see [3, 4]) represents a strongly pressure-sensitive surface with a marked dissymmetry of traction vs. compression limits.

The fourth-order tensor $\hat{\mathbf{D}}$ depends entirely on \mathbf{D} (see definition (3.3)); it does not require a separate evolution law.

In numerical calculations any loading path is considered as a collection of \mathbf{D} -proportional segments. The form of Eq. (3.6) is valid for such a segment, i.e. for a given configuration of principal directions of \mathbf{D} . Otherwise it should be completed to account for a novel configuration of the tensor $\hat{\mathbf{D}}$.

The model, non-linear as it is, contains eight material constants only: λ , μ , α , β , g , B , C_0 and C_1 , which can be relatively easily determined (see Sec. 5.3).

In order to illustrate the predictive capacities of the model, the curves in Fig. 3.1 show the stress-strain behaviour according to the basic damage model and experiment (Pecqueur *et al.* [74]) for Vosges sandstone submitted to axisymmetric triaxial compression with a confining pressure $P_c = 15$ MPa. The set of material constants, namely $\lambda = 3250$ MPa, $\mu = 4875$ MPa, $\alpha = 9925$ MPa, $\beta = -11180$ MPa, $g = -32$ MPa, $C_0 = 0.02$ MPa, $C_1 = 0.27$ MPa, $B = 0$, was determined according to the procedure described in Sec. 5.3. The dilatancy effect resulting from pronounced damage is well evidenced in Fig. 3.1(b)). The numerical simulations conform to experimental programme correspond to homogeneous stress-strain paths realized at a single Gauss point. For the location of bifurcation point with respect to stress-strain peak for a large spectrum of axisymmetric stress-strain paths, see Dragon *et al.* [3].

While the curves in Fig. 3.1 correspond to a routine experimental test for rock-like solids, the lateral overloading sequence following the foregoing compression test is much less common and needs somewhat sophisticated equipment. Three simulations of lateral overloading for previously damaged solid are shown in Fig. 3.2. The reference strain $\epsilon_1^{A,B,C}$ corresponds to the lateral strain value at the beginning of step c. The stiffness recovery occurring during overloading (step c) has been calculated following the extended

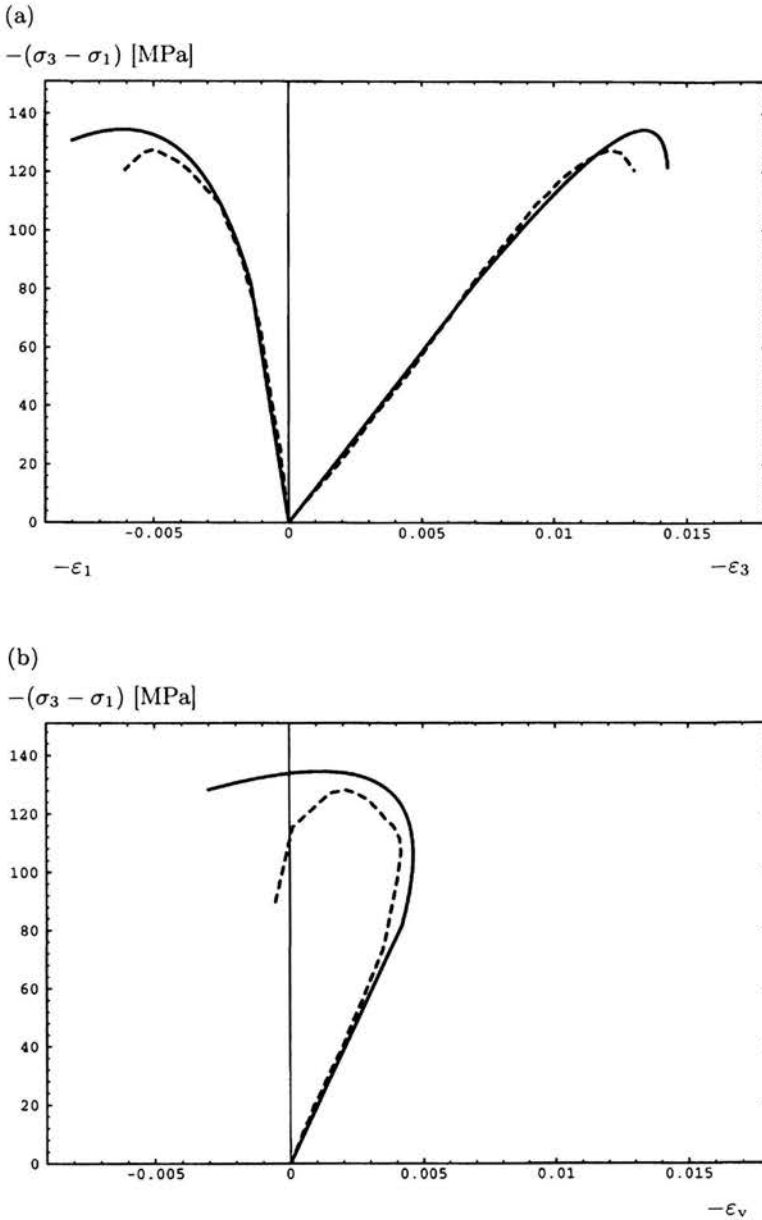


FIGURE 3.1. Comparison simulation (solid line) vs. experiment (dashed line) for a triaxial axisymmetric compression (confining pressure $P_c = 15$ MPa) on Vosges sandstone; (a) deviatoric stress $-(\sigma_3 - \sigma_1)$ vs. axial $-\epsilon_3$ and transversal $-\epsilon_1$ strain; (b) deviatoric stress $-(\sigma_3 - \sigma_1)$ vs. volumetric strain $-\epsilon_v$.

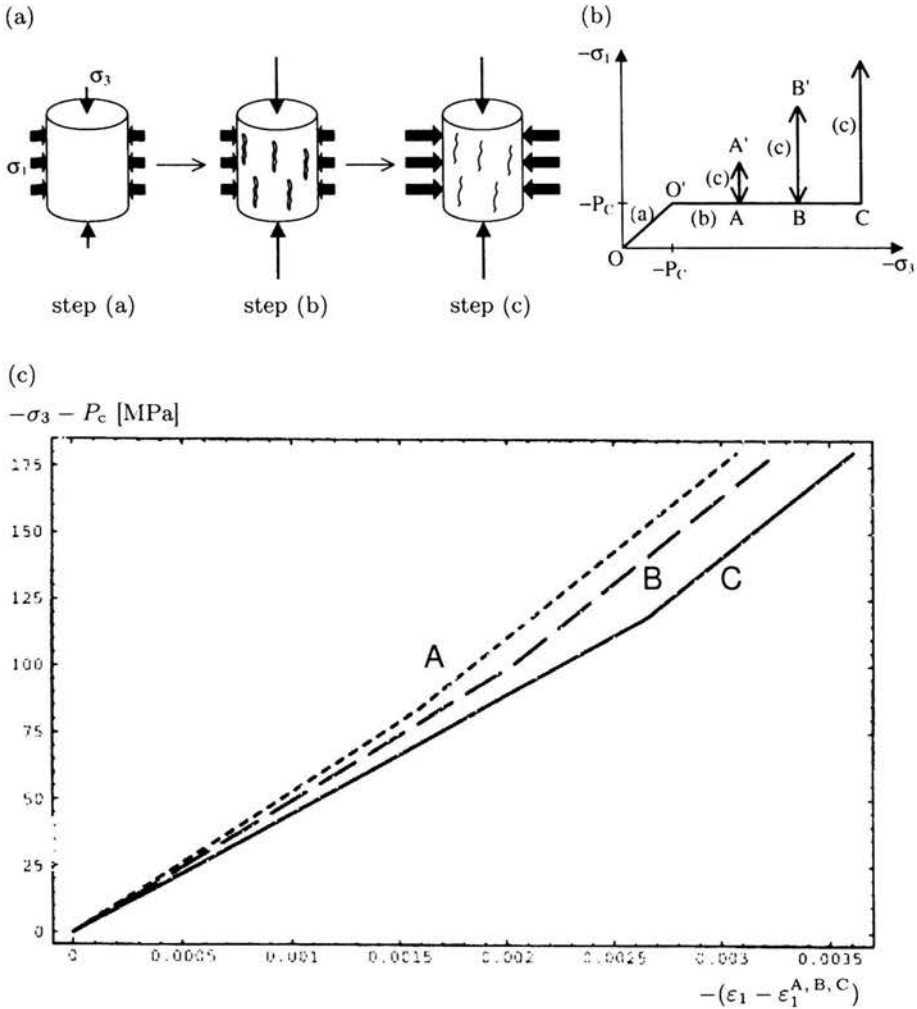


FIGURE 3.2. Triaxial axisymmetric compression with lateral overloading: loading paths and simulated lateral stress $-\sigma_3 - P_c$ vs. lateral strain $-(\epsilon_1 - \epsilon_1^{A,B,C})$ for Fontainebleau sandstone.

model presented above accounting for the unilateral, crack-closure related behaviour, see [4] for further details. Three successive simulations were performed for different values of the axial peak stress $|\sigma_3|_{\max}$, i.e. for different damage values corresponding to reduced moduli represented by initial segments in Fig. 3.2(c).

An operational, structural analysis approach employing the concept of damage should combine an efficient damage model implemented in robust

computer algorithm associated with proper tools for detection and control of bifurcation phenomena. The latter indicate eventual transition from distributed damage to surface-like localization considered as a precursor of macroscopic fracture. In any case bifurcation events point out an ill-posedness of the problem and necessity of remaking a computational scheme. Actually, the basic model presented, i.e. the one summarized above *except* the last, unilateral effect related term in $w(\boldsymbol{\varepsilon}; \mathbf{D})$, see Eq. (3.4) and counterparts in (3.5), (3.6), was extensively tested for its capacities to generate physically sound localized failure mechanisms, see e.g. [3]. Essential structure of the numerical scheme employed for the 3D localization detection and some notable results obtained with the basic damage model are summarized in the latter paper. The very fair predictions concerning the localization bifurcation obtained for homogeneous stress-strain paths as well as for boundary-value problems related to rock engineering applications have prompted further developments of the model itself including its coupling with a form of mesocrack-friction-induced plasticity as put forward in the next Chapter.

Chapter 4

Mesocrack friction induced plasticity

The unilateral normal effect included in the model summarized in Chapter 3 allows a moduli recovery in the direction normal to the closed mesocracks. It fails to capture a shear moduli recovery in the direction parallel to the crack plane, resulting from the blocking of mesocrack lips displacement due to roughness and corresponding friction phenomena. Experimental data involving loading-unloading cycles for specimens subjected for instance to torsion and hydrostatic compression show hysteretic effects generated by such a blocking and subsequent frictional sliding on closed mesocrack lips. The beginning of unloading is characterized by a quasi-vertical curve while further decreasing slope is linked to progressive sliding, see for instance Pecqueur [16]. Some attempts of micromechanical modelling of the phenomena deserve attention, [18-26]. However, they are not directly operational for an efficient structural analysis. Some of earlier attempts (Kachanov [18], Horii and Nemat-Nasser [19]) consider the influence of friction on effective moduli but do not provide satisfactory thermodynamic interpretation of sliding evolution. Most of existing approaches are limited to two-dimensional analyses, as e.g. [20], with the notable exception of the work by Gambarotta and Lagomarsino [24].

4.1. Energy expression and affinities related to damage-and-friction response

The global strain expression for a representative volume of elastic solid of stiffness \mathbf{C} containing microcracks (assumed plane and quasi-circular for simplicity) can be written as a sum of the solid matrix contribution $\boldsymbol{\varepsilon}^0$ and the crack contribution $\boldsymbol{\varepsilon}^c$:

$$\boldsymbol{\varepsilon} = \mathbf{C}^{-1} : \boldsymbol{\sigma} + \frac{1}{2V} \sum_i (\langle \mathbf{b} \rangle \otimes \mathbf{n} + \mathbf{n} \otimes \langle \mathbf{b} \rangle)^i s^i = \boldsymbol{\varepsilon}^e + \sum_i \boldsymbol{\varepsilon}^{ci} \quad (4.1)$$

with the crack displacement discontinuity \mathbf{b}^i being averaged ($\langle \mathbf{b}^i \rangle$) for the microcrack set i . For closed sliding cracks, as long as the orientation \mathbf{n}^i is preserved, $\langle \mathbf{b}^i \rangle$ is orthogonal to \mathbf{n}^i :

$$\langle \mathbf{b}^i \rangle = \xi^i \mathbf{g}^i, \quad \mathbf{g}^i \perp \mathbf{n}^i \text{ if } \mathbf{n}^i = \text{const.} \quad (4.2)$$

with ξ^i representing the amount of sliding in the direction \mathbf{g}^i . One can write furthermore:

$$\boldsymbol{\varepsilon}^{ci} = \frac{s^i}{2V} \xi^i (\mathbf{g}^i \otimes \mathbf{n}^i + \mathbf{n}^i \otimes \mathbf{g}^i) \quad (4.3)$$

Hence, for the microcrack system i , the sliding variable is chosen in the form:

$$\gamma^i = \frac{s^i \xi^i}{V} \text{sym}(\mathbf{n} \otimes \mathbf{g})^i \quad (4.4a)$$

the symmetrisation being operated for the expression in parentheses. The similarity with (3.1) is striking: as for \mathbf{D} , the form of γ is motivated by micromechanics; as for $d(s)$ the quantity $s^i \xi^i / V$ cannot be explicitly calculated in the framework of a macroscopic model. Moreover, as any system of microcracks represented by \mathbf{D} reduces to three equivalent sets according to (3.2), the sliding tensor γ can be written in the analogous manner:

$$\boldsymbol{\gamma} = \sum_{k=1}^3 \frac{s^k \xi^k}{V} \text{sym}(\boldsymbol{\nu} \otimes \mathbf{g})^k = \sum_{k=1}^3 \boldsymbol{\gamma}^k, \quad (4.4b)$$

where $\boldsymbol{\nu}^k$, $k = 1, 2, 3$, are \mathbf{D} -eigenvectors.

Let us consider, for a while, a single system of mesocracks characterized by the only principal non zero component D_3 and the normal (eigenvector) $\boldsymbol{\nu}^3$. The objective here is to argue for an enlarged form of the free-energy function $w(\boldsymbol{\varepsilon}, \mathbf{D}, \boldsymbol{\gamma})$ accounting for the frictional blocking and sliding effects for closed crack sets.

From (3.4), (3.5) one can infer that the anisotropic damage-induced shear moduli are entirely determined by μ (solid matrix shear modulus) and the term $2\beta \text{tr}(\boldsymbol{\varepsilon} \cdot \boldsymbol{\varepsilon} \cdot \mathbf{D})$. Hence, for the damage configuration at stake ($D_1 = D_2 = 0$, $D_3 \neq 0$) one obtains: $\sigma_{13} = 2\mu\varepsilon_{13} + 2\beta D_3 \varepsilon_{13}$, $\sigma_{23} = 2\mu\varepsilon_{23} + 2\beta D_3 \varepsilon_{23}$.

The degradation of moduli in the normal direction to the open crack set is described in the *conjugate* manner by the α -term as well as the β -one. The expression of the Young's modulus E_3 for the damage configuration as above is

$$E_3 = \lambda + 2\mu + 2\alpha D_3 + 4\beta D_3 - \frac{(\lambda + \alpha D_3)^2}{\lambda + \mu}.$$

Let us consider the transition from open cracks to closed ones, assuming friction resistant lips when in contact. The crack-open form of (3.4), with $H(-\nu^3 \cdot \boldsymbol{\varepsilon} \cdot \nu^3) = 0$ applies for the former case. When the cracks are closed and blocked by friction resistance at a given γ , the shear modulus μ is momentarily recovered and this should be properly reflected in the new modified expression $w(\boldsymbol{\varepsilon}, \mathbf{D}, \gamma)$. The β -term should be counterbalanced in this expression. The α -term, having no influence on shear moduli, enters as before. Additional invariants including γ can be only simultaneous (γ, \mathbf{D}) -invariants as there is no sliding on crack lips in the absence of damage. As from (4.3) one infers $\text{tr} \gamma = 0$ and $\text{tr}(\gamma \cdot \mathbf{D}) = 0$ (for conservative damage axes), only two simultaneous invariants of $\boldsymbol{\varepsilon}$, γ and \mathbf{D} convey useful information. They are: $\text{tr}(\boldsymbol{\varepsilon} \cdot \gamma \cdot \mathbf{D})$ and $\text{tr}(\gamma \cdot \gamma \cdot \mathbf{D})$. The argument for the quantity including β in the last term of (3.4) was to reconstitute the normal stiffness reduced by the term $2\beta \text{tr}(\boldsymbol{\varepsilon} \cdot \boldsymbol{\varepsilon} \cdot \mathbf{D})$ in the first line of (3.4), but since this latter term is going to be counterbalanced, the former quantity has to disappear from w . Doing so allows one to write tentatively the expression $w(\boldsymbol{\varepsilon}, \mathbf{D}, \gamma)$ for closed friction-resistant crack lips in the form (for a single crack system):

$$w(\boldsymbol{\varepsilon}, \mathbf{D}, \gamma) = \frac{1}{2} \lambda (\text{tr} \boldsymbol{\varepsilon})^2 + \mu \text{tr}(\boldsymbol{\varepsilon} \cdot \boldsymbol{\varepsilon}) + g \text{tr}(\boldsymbol{\varepsilon} \cdot \mathbf{D}) + \alpha \text{tr} \boldsymbol{\varepsilon} \text{tr}(\boldsymbol{\varepsilon} \cdot \mathbf{D}) \\ - \alpha (\boldsymbol{\varepsilon} : \hat{\mathbf{D}} : \boldsymbol{\varepsilon}) + \eta_1 \text{tr}(\boldsymbol{\varepsilon} \cdot \gamma \cdot \mathbf{D}) + 2\eta_2 \text{tr}(\gamma \cdot \gamma \cdot \mathbf{D}) \quad (4.5)$$

where η_1 and η_2 are material constants to be identified.

From the micromechanical viewpoint there are infinity of crack-closure paths possible (straight, slantwise, mixed, . . .). The macroscopic model continuity requires continuity for expressions of $w(\boldsymbol{\varepsilon}, \mathbf{D}, \gamma)$ and $\boldsymbol{\sigma}$ for crack opening-to-closure (and reverse) transition. The analysis analogous to that

summarized in Chapter 3 under the item (v) is to be applied again here in the enlarged damage-and-friction context. This leads to the following condition at the closure-point:

$$\begin{cases} \boldsymbol{\varepsilon} \cdot \mathbf{D} = \boldsymbol{\gamma} \cdot \mathbf{D} \\ \mathbf{D} \cdot \boldsymbol{\varepsilon} = \mathbf{D} \cdot \boldsymbol{\gamma} \end{cases} \iff \gamma_{ij} = \text{sym}(\varepsilon_{ik} \nu_k \nu_j) \text{ at closure-point.} \quad (4.6)$$

The latter formula constitutes an initialization for the sliding variable $\boldsymbol{\gamma}$ and can be explained as follows: at closure point, the sliding quantity $\boldsymbol{\gamma}$ is equal to the strain $\boldsymbol{\varepsilon}$ in the crack plane, the matrix transmits its deformation to the crack.

According to the continuity conditions for multilinear elasticity (Wesołowski [69], Curnier *et al.* [70]) already employed in [4] in the context of unilateral normal effect, see Eqs. (3.4)-(3.6) in Chapter 3, the jump of effective elastic stiffness $[\mathbf{C}]$ between open crack and closed crack respective configurations should be a singular operator. The corresponding energy expressions are designated respectively w^1 and w^2 , as in (v) in Chapter 3. It is sufficient that all second-order determinants of $[\mathbf{C}]$ be equal to zero.

In the present context – Eq. (4.5) at the very closure point, taking into account (4.6) – $[\mathbf{C}]$ is given as follows:

$$[\mathbf{C}] = \left. \frac{\partial^2 w^2}{\partial \boldsymbol{\varepsilon} \partial \boldsymbol{\varepsilon}} \right|_{\boldsymbol{\gamma}, D} - \left. \frac{\partial^2 w^1}{\partial \boldsymbol{\varepsilon} \partial \boldsymbol{\varepsilon}} \right|_D,$$

$$[\mathbf{C}_{ijkl}] = \left(\frac{1}{2} \eta_1 + \eta_2 - \beta \right) \left(\delta_{ik} D_{jl} + \delta_{jl} D_{ik} + \delta_{il} D_{jk} + \delta_{jk} D_{il} \right) - 2\alpha \hat{D}_{ijkl}.$$

The above-mentioned singularity requirement and the additional stronger condition allowing no stress jump in the strain space across the surface $\boldsymbol{\nu} \cdot \boldsymbol{\varepsilon} \cdot \boldsymbol{\nu} = 0$, applied by Halm and Dragon [5] (in the way similar to [4]) lead respectively to:

$$\begin{cases} \frac{1}{2} \eta_1 + \eta_2 - \beta = 0, \\ \eta_1 = 4\beta. \end{cases} \quad (4.7)$$

The free-energy $w(\boldsymbol{\varepsilon}, \mathbf{D}, \boldsymbol{\gamma})$ can now be written as follows (for either open or closed cracks):

$$\begin{aligned} w(\boldsymbol{\varepsilon}; \mathbf{D}, \boldsymbol{\gamma}) = & \frac{1}{2} \lambda (\text{tr } \boldsymbol{\varepsilon})^2 + \mu \text{tr}(\boldsymbol{\varepsilon} \cdot \boldsymbol{\varepsilon}) + g \text{tr}(\boldsymbol{\varepsilon} \cdot \mathbf{D}) + \alpha \text{tr } \boldsymbol{\varepsilon} \text{tr}(\boldsymbol{\varepsilon} \cdot \mathbf{D}) \\ & + 2\beta \text{tr}(\boldsymbol{\varepsilon} \cdot \boldsymbol{\varepsilon} \cdot \mathbf{D}) + H(-\boldsymbol{\nu} \cdot \boldsymbol{\varepsilon} \cdot \boldsymbol{\nu}) \left[-\alpha \boldsymbol{\varepsilon} : \hat{\mathbf{D}} : \boldsymbol{\varepsilon} - 2\beta \text{tr}(\boldsymbol{\varepsilon} \cdot \boldsymbol{\varepsilon} \cdot \mathbf{D}) \right. \\ & \left. + 4\beta \text{tr}(\boldsymbol{\varepsilon} \cdot \boldsymbol{\gamma} \cdot \mathbf{D}) - 2\beta \text{tr}(\boldsymbol{\gamma} \cdot \boldsymbol{\gamma} \cdot \mathbf{D}) \right]. \quad (4.8) \end{aligned}$$

The expression (4.8) can be generalized to three non-interactive equivalent crack sets represented by eigenvectors ν^k associated with the principal components D_k , $k = 1, 2, 3$. One can select the k -th set using the following projection operator \mathbf{L}^k :

$$\begin{aligned}\mathbf{L}^k &= \nu^k \otimes \nu^k \otimes \nu^k \otimes \nu^k, \\ \mathbf{D}^k &= D_k \nu^k \otimes \nu^k = \mathbf{L}^k : \mathbf{D}.\end{aligned}\quad (4.9)$$

This allows to write counterpart equations of (3.4)-(3.6) independently for each equivalent set, all possible configurations being included (open or closed, sliding or non sliding sets):

$$\begin{aligned}w(\boldsymbol{\varepsilon}, \mathbf{D}, \boldsymbol{\gamma}) &= \frac{1}{2} \lambda (\text{tr } \boldsymbol{\varepsilon})^2 + \mu \text{tr}(\boldsymbol{\varepsilon} \cdot \boldsymbol{\varepsilon}) + g \text{tr}(\boldsymbol{\varepsilon} \cdot \mathbf{D}) + \alpha \text{tr } \boldsymbol{\varepsilon} \text{tr}(\boldsymbol{\varepsilon} \cdot \mathbf{D}) + 2\beta \text{tr}(\boldsymbol{\varepsilon} \cdot \boldsymbol{\varepsilon} \cdot \mathbf{D}) \\ &+ \sum_{k=1}^3 H(-\nu^k \cdot \boldsymbol{\varepsilon} \cdot \nu^k) \left[-\alpha \boldsymbol{\varepsilon} : (D_k \mathbf{L}^k) : \boldsymbol{\varepsilon} - 2\beta \text{tr}(\boldsymbol{\varepsilon} \cdot \boldsymbol{\varepsilon} \cdot \mathbf{D}^k) \right. \\ &\quad \left. + 4\beta \text{tr}(\boldsymbol{\varepsilon} \cdot \boldsymbol{\gamma}^k \cdot \mathbf{D}^k) - 2\beta \text{tr}(\boldsymbol{\gamma}^k \cdot \boldsymbol{\gamma}^k \cdot \mathbf{D}^k) \right],\end{aligned}\quad (4.10)$$

$$\begin{aligned}\boldsymbol{\sigma} = \frac{\partial w}{\partial \boldsymbol{\varepsilon}} &= \lambda (\text{tr } \boldsymbol{\varepsilon}) \mathbf{1} + 2\mu \boldsymbol{\varepsilon} + g \mathbf{D} + \alpha [\text{tr}(\boldsymbol{\varepsilon} \cdot \mathbf{D}) \mathbf{1} + (\text{tr } \boldsymbol{\varepsilon}) \mathbf{D}] + 2\beta (\boldsymbol{\varepsilon} \cdot \mathbf{D} + \mathbf{D} \cdot \boldsymbol{\varepsilon}) \\ &+ \sum_{k=1}^3 H(-\nu^k \cdot \boldsymbol{\varepsilon} \cdot \nu^k) \left[-2\alpha D_k (\nu^k \cdot \boldsymbol{\varepsilon} \cdot \nu^k) \nu^k \otimes \nu^k - 2\beta (\boldsymbol{\varepsilon} \cdot \mathbf{D}^k + \mathbf{D}^k \cdot \boldsymbol{\varepsilon}) \right. \\ &\quad \left. + 2\beta (\boldsymbol{\gamma}^k \cdot \mathbf{D}^k + \mathbf{D}^k \cdot \boldsymbol{\gamma}^k) \right],\end{aligned}\quad (4.11)$$

$$\begin{aligned}\mathbf{F}^D = -\frac{\partial w}{\partial \mathbf{D}} &= -g \boldsymbol{\varepsilon} - \alpha (\text{tr } \boldsymbol{\varepsilon}) \boldsymbol{\varepsilon} - 2\beta (\boldsymbol{\varepsilon} \cdot \boldsymbol{\varepsilon}) \\ &+ \sum_{k=1}^3 H(-\nu^k \cdot \boldsymbol{\varepsilon} \cdot \nu^k) \left[\alpha (\nu^k \cdot \boldsymbol{\varepsilon} \cdot \nu^k)^2 \nu^k \otimes \nu^k + 2\beta \mathbf{L}^k : (\boldsymbol{\varepsilon} \cdot \boldsymbol{\varepsilon}) \right. \\ &\quad \left. - 4\beta \mathbf{L}^k : (\boldsymbol{\varepsilon} \cdot \boldsymbol{\gamma}^k) + 2\beta \mathbf{L}^k : (\boldsymbol{\gamma}^k \cdot \boldsymbol{\gamma}^k) \right].\end{aligned}\quad (4.12)$$

As each equivalent set of the normal ν^k is to be considered independently, the corresponding affinity (thermodynamic force) is:

$$\begin{aligned}\mathbf{F}^{\boldsymbol{\gamma}^k} = -\frac{\partial w}{\partial \boldsymbol{\gamma}^k} &= H(-\nu^k \cdot \boldsymbol{\varepsilon} \cdot \nu^k) \left[-2\beta (\boldsymbol{\varepsilon} \cdot \mathbf{D}^k + \mathbf{D}^k \cdot \boldsymbol{\varepsilon}) \right. \\ &\quad \left. + 2\beta (\boldsymbol{\gamma}^k \cdot \mathbf{D}^k + \mathbf{D}^k \cdot \boldsymbol{\gamma}^k) \right].\end{aligned}\quad (4.13)$$

The remark concerning Eq. (3.6) stating its validity for a \mathbf{D} -proportional segment, i.e. for a given configuration of principal directions of \mathbf{D} , is still valid for Eq. (4.12).

4.2. Sliding criterion and evolution

The model herein considers frictional non-sliding/sliding phenomena on mesocrack lips on a macroscopic scale, by an approach similar to that to damage, notwithstanding the micromechanical background and interpretations of \mathbf{D} and γ . So, the Coulomb criterion form, function of the corresponding shear and normal tractions on a crack lip, employed in micromechanical models (Horii and Nemat-Nasser [19], Andrieux *et al.* [20], Gambarotta and Lagomarsino [24]), is methodologically less suitable in the present context. The pertinent thermodynamic affinity governing frictional sliding on an equivalent system k , ($k = 1, 2, 3$) is the entity $\mathbf{F}\gamma^k$ defined above as the strain energy release-rate with respect to γ^k .

The frictional non sliding/sliding complementary law is based on the hypotheses as follows:

- (i) The sliding criterion depends explicitly on the norm of the tangential part $\mathbf{F}\gamma^{Tk}$ of the "force" $\mathbf{F}\gamma^k$ and on the normal strain $\nu^k \cdot \boldsymbol{\varepsilon} \cdot \nu^k$ consecutively to the strain-related representation of the energy w and the crack-closure criterion at stake ($\nu^k \cdot \boldsymbol{\varepsilon} \cdot \nu^k \leq 0$).
- (i) Contrarily to inconsistencies relative to the normality rule in the classical Coulomb framework affected by appearance of a normal separating velocity (cf. for example [75]) a pseudo-standard scheme in the space of forces conjugate to γ^k keeps physical pertinence. The apparent normality rule appears to relate the frictional sliding rate to the tangential force $\mathbf{F}\gamma^{Tk}$ indicating its leaning to the crack plane (for a \mathbf{D}^k -proportional loading segment).

Consequently, the corresponding convex reversibility domain $h^k \leq 0$ can be written as:

$$\begin{aligned}
 h^k & \left(\mathbf{F}\gamma^k - \mathbf{F}\gamma^{Nk}, \nu^k \cdot \boldsymbol{\varepsilon} \cdot \nu^k \right) \\
 & = \sqrt{\frac{1}{2} \operatorname{tr} \left[(\mathbf{F}\gamma^k - \mathbf{F}\gamma^{Nk}) \cdot (\mathbf{F}\gamma^k - \mathbf{F}\gamma^{Nk}) \right]} + \hat{\rho} \nu^k \cdot \boldsymbol{\varepsilon} \cdot \nu^k \leq 0, \\
 & \quad \text{if } \nu^k \cdot \boldsymbol{\varepsilon} \cdot \nu^k \leq 0, \quad (4.14)
 \end{aligned}$$

where $\hat{\rho}$ is a material constant, a strain-related friction coefficient in the space $(\mathbf{F}^{\gamma^k}, \boldsymbol{\varepsilon})$ and

$$\begin{aligned}\mathbf{F}^{\gamma^k} &= \mathbf{F}^{\gamma T k} + \mathbf{F}^{\gamma N k}, \\ \mathbf{F}^{\gamma T k} &= \mathbf{F}^{\gamma^k} - (\boldsymbol{\nu}^k \cdot \mathbf{F}^{\gamma^k} \cdot \boldsymbol{\nu}^k) \boldsymbol{\nu}^k \otimes \boldsymbol{\nu}^k, \\ \mathbf{F}^{\gamma N k} &= (\boldsymbol{\nu}^k \cdot \mathbf{F}^{\gamma^k} \cdot \boldsymbol{\nu}^k) \boldsymbol{\nu}^k \otimes \boldsymbol{\nu}^k.\end{aligned}\quad (4.15)$$

The normality rule for $\dot{\gamma}^k$ is then

$$\begin{aligned}\dot{\gamma}^k &= \Lambda_\gamma^k \frac{\partial h^k(\mathbf{F}^{\gamma^k} - \mathbf{F}^{\gamma N k}, \boldsymbol{\nu}^k \cdot \boldsymbol{\varepsilon} \cdot \boldsymbol{\nu}^k)}{\partial \mathbf{F}^{\gamma^k}} \\ &= \begin{cases} \mathbf{0}, & \text{if } h^k < 0 \text{ or } h^k = 0, \dot{h}^k < 0, \\ \Lambda_\gamma^k \frac{\mathbf{F}^{\gamma T k}}{\sqrt{2 \operatorname{tr}(\mathbf{F}^{\gamma T k} \cdot \mathbf{F}^{\gamma T k})}}, & \text{if } h^k = 0 \text{ and } \dot{h}^k = 0, \Lambda_\gamma^k \geq 0. \end{cases}\end{aligned}\quad (4.16)$$

Detailed comments on salient aspects of the criterion $h^k = 0$ in the strain space are given by Halm and Dragon [5]. Figure 4.1 shows the corresponding form together with a hardening-like phenomenon (for $\gamma^k \neq \mathbf{0}$) in reduced

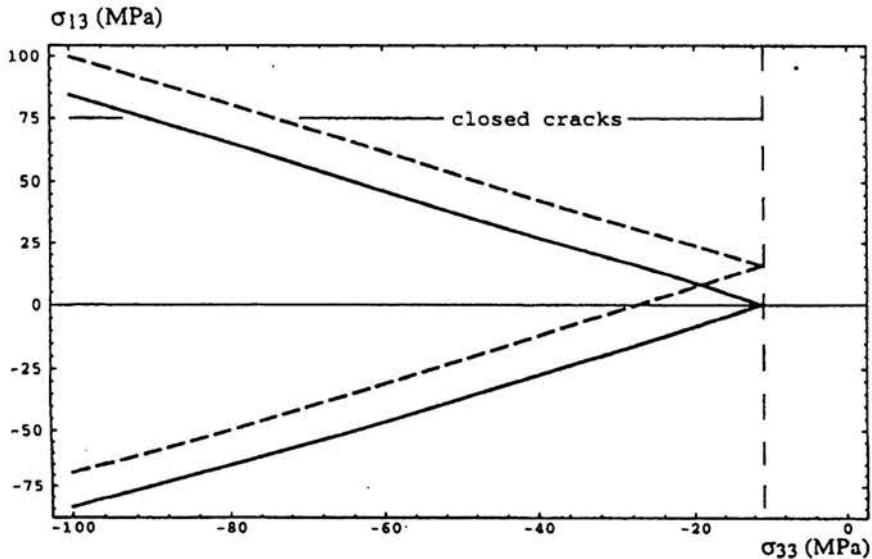


FIGURE 4.1. Frictional sliding criterion and the relative sliding-induced hardening mechanism in the reduced stress-space $(\sigma_{33}, \sigma_{13})$ for $\gamma^k = \mathbf{0}$ (solid line) and $\gamma^k \neq \mathbf{0}$ (dashed line).

stress space $(\sigma_{33}, \sigma_{13})$. The similitude between the actual yield surface and the Coulomb one can be clearly noticed. In connection with the crack opening/closure condition (a single crack system $D_3 \neq 0$ is considered for illustration) the cone $h^k = 0$ is shifted to the left: it corresponds to negative value of σ_{33} at the closure point.

By examining the complete set (4.10)-(4.16) of the equations of the model, one can see that the frictional sliding does not sweep away the relative simplicity of the enlarged model (see the end of Chapter 3). Only one additional constant $\hat{\rho}$ adds to eight material constants $(\lambda, \mu, \alpha, \beta, C_0, C_1, g, B)$. It can be stressed that $\hat{\rho}$ governs the slope of the cone in Fig. 4.1.

It can also be proved that the slope is inversely proportional to the amount of damage, thus implying that a higher crack density is favouring sliding.

Chapter 5

Damage and frictional sliding interaction. Fully coupled model, its numerical implementation and applications (rock-like solids)

The model completed in Chapter 4 incorporating friction-induced blocking and sliding on equivalent mesocrack-sets is valid for a given ('frozen') damage state or for conservative damage evolution (\mathbf{D}^k -proportional loading paths). It has proved conclusive in representing multistage loading-and-unloading dissipative cycles due to blocking-and-sliding sequences, see Halm and Dragon [5] for illustrations. In particular a dissipative unloading blocking-and-sliding sequence could be obtained while for the same stress-strain cycle the frictionless model of Chapter 3 gave purely elastic unloading, see Fig. 5.1 for a shear-loading cycle for pre-damaged material.

5.1. Generalized coupled model

The splitting-like damage kinetics considered in Chapter 3 is regarded as approximately valid for closed sliding mesocracks even when some branching occurs, see for example Horii and Nemat-Nasser [76], Barquins *et al.* [77] for some experimental insight. This type of splitting kinetics will be still considered as the predominant mechanism furthest for \mathbf{D}^k -non-proportional loading. This means the complementary damage law (3.8)-(3.9) being reconducted for more complex stress-strain paths involving varying \mathbf{D}^k orientations. However, as the frictional blocking-and-sliding is inevitably affecting

the stress-strain response, so for instance the stress threshold corresponding to damage criterion $f = 0$ is subsequently affected. For example, in the stress subspace analogous to that of Fig. 4.1, the frontier $f = 0$ corresponding to closed cracks under frictional blocking/sliding is farther beyond the limit for frictionless cracks, see e.g. Fig. 9 in [5].

This is mostly the sliding complementary rule (4.15)-(4.16) which needs to be perfected to describe fairly the \mathbf{D}^k -non-proportional loading paths. If the principal axes of \mathbf{D}^k rotate the orthogonality $\boldsymbol{\gamma}^k : \mathbf{D}^k = 0$ is no longer true and discontinuities may arise, especially for crack closure-opening transition. So, an enhanced form of $h^k \leq 0$ needs to account for the \mathbf{D}^k -axes rotation. The form (4.14), depending on $\mathbf{F}\boldsymbol{\gamma}^k$, produced – via normality rule (4.14) – sliding $\dot{\boldsymbol{\gamma}}^k$ in the mesocrack plane. A judicious modification of this basic assumption should be compatible with sliding and damage departure from the actual mesocrack equivalent plane. This is achieved by means of the following partition of $\mathbf{F}\boldsymbol{\gamma}^k$, given below for a single crack set of normal $\boldsymbol{\nu}^k$:

$$\begin{aligned} \mathbf{F}\boldsymbol{\gamma}^k &= \mathbf{F}\boldsymbol{\gamma}^k + \mathbf{F}\boldsymbol{\gamma}^k \\ &= \underbrace{\mathbf{F}\boldsymbol{\gamma}^k + 4\beta(\boldsymbol{\gamma}^k : \mathbf{D}^k)\boldsymbol{\nu}^k \otimes \boldsymbol{\nu}^k}_{\mathbf{F}^k} - 4\beta(\boldsymbol{\varepsilon} : \mathbf{D}^k)\boldsymbol{\nu}^k \otimes \boldsymbol{\nu}^k \quad (5.1) \\ &= \mathbf{F}^k - 4\beta(\boldsymbol{\varepsilon} : \mathbf{D}^k)\boldsymbol{\nu}^k \otimes \boldsymbol{\nu}^k. \end{aligned}$$

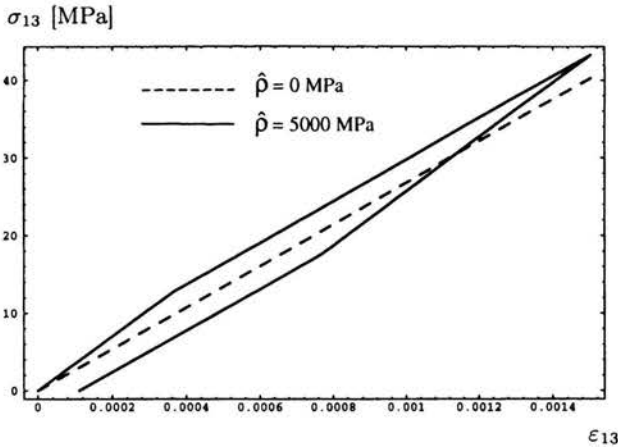


FIGURE 5.1. Influence of frictional resistance and sliding on stress-strain response for a shear loading under constant damage (single crack system perpendicular to torsion axis).

\mathbf{F}^k is the appropriate part of \mathbf{F}^{γ^k} to enter the more general expression of $h^k \leq 0$ suitable for the model including \mathbf{D}^k -axes rotation. First, one obtains that for \mathbf{D}^k -proportional loading \mathbf{F}^k reduces to \mathbf{F}^{γ^k} (as $\gamma^k : \mathbf{D}^k = 0$) and the new representation $h^k(\mathbf{F}^k, \boldsymbol{\nu}^k \cdot \boldsymbol{\varepsilon} \cdot \boldsymbol{\nu}^k)$ reduces to (4.14). Secondly, the above-mentioned, crucial stress continuity problem is effectively dealt with. In fact, comparing (4.6), (4.13), (4.15), (5.1), one can see that the closure-opening transition point for sliding crack-set can be alternatively defined as:

$$\mathbf{F}^k = \mathbf{F}^{\gamma^k} = \mathbf{0} \iff \boldsymbol{\varepsilon} \cdot \mathbf{D}^k + \mathbf{D}^k \cdot \boldsymbol{\varepsilon} = \boldsymbol{\gamma}^k \cdot \mathbf{D}^k + \mathbf{D}^k \cdot \boldsymbol{\gamma}^k. \quad (5.2)$$

Despite the fact that the above equation represents weaker condition than (4.6), it allows to verify the singularity requirement for $[\mathbf{C}]$ (cf. Sec. 4.1) leading to the stress continuity.

It can be remarked that though $\boldsymbol{\gamma}^k : \mathbf{D}^k \neq 0$ as equivalent crack-axes rotate no additional invariants are necessary in the strain energy expression (4.10). They are not required by the continuity considerations (see above) and bring neither significant information. For example, introducing $\text{tr} \boldsymbol{\varepsilon} \text{tr}(\boldsymbol{\gamma}^k \cdot \mathbf{D}^k)$, $\text{tr} \boldsymbol{\gamma}^k \text{tr}(\boldsymbol{\gamma}^k \cdot \mathbf{D}^k)$ and $\boldsymbol{\gamma}^k : D_k \mathbf{L}^k : \boldsymbol{\gamma}^k$ contributes to no more record on shear moduli degradation than existing invariants $\text{tr}(\boldsymbol{\varepsilon} \cdot \boldsymbol{\gamma}^k \cdot \mathbf{D}^k)$ and $\text{tr}(\boldsymbol{\gamma}^k \cdot \boldsymbol{\gamma}^k \cdot \mathbf{D}^k)$.

The above considerations lead to the following improved expression for the sliding complementary rule:

$$h^k(\mathbf{F}^k, \boldsymbol{\nu}^k \cdot \boldsymbol{\varepsilon} \cdot \boldsymbol{\nu}^k) = \sqrt{\frac{1}{2} \text{tr}(\mathbf{F}^k \cdot \mathbf{F}^k)} + \hat{\rho} \boldsymbol{\nu}^k \cdot \boldsymbol{\varepsilon} \cdot \boldsymbol{\nu}^k \leq 0, \quad (5.3)$$

$$\dot{\boldsymbol{\gamma}}^k = \Lambda_\gamma^k \frac{\partial h(\mathbf{F}^k, \boldsymbol{\nu}^k \cdot \boldsymbol{\varepsilon} \cdot \boldsymbol{\nu}^k)}{\partial \mathbf{F}^{\gamma^k}} = \begin{cases} \mathbf{0}, & \text{if } h^k < 0 \text{ or } h^k = 0, \dot{h}^k < 0, \\ \Lambda_\gamma^k \frac{\mathbf{F}^k}{\sqrt{2 \text{tr}(\mathbf{F}^k \cdot \mathbf{F}^k)}}, & \text{if } h^k = 0 \text{ and } \dot{h}^k = 0, \Lambda_\gamma^k \geq 0. \end{cases} \quad (5.4)$$

The direction of $\dot{\boldsymbol{\gamma}}^k$ is thus allowed to leave the equivalent crack-set plane consecutively to the rotation of the latter. In such a manner \mathbf{D}^k -non-proportional loading can be followed by the model which takes into account the interaction of the two dissipative mechanisms: damage and frictional sliding. The corresponding combined dissipation is:

$$\mathbf{D} = \mathbf{F}^D : \dot{\mathbf{D}} + \sum_{k=1}^3 \mathbf{F}^{\gamma^k} : \dot{\boldsymbol{\gamma}}^k \geq 0. \quad (5.5)$$

Despite of the corresponding normality rules, i.e. the formulae (3.9) and (5.4) respectively for damage growth and frictional sliding, and the convexity characterizing the domains $f \leq 0$ and $h \leq 0$ one should check the non-negativity of D in the process of numerical integration. This is because of the partition of the respective thermodynamic forces, i.e. the sole parts $\mathbf{F}^D - \mathbf{F}^{D2} - \mathbf{F}^{D1-}$ and $\mathbf{F}^{\gamma^k} - [-4\beta(\boldsymbol{\varepsilon} : \mathbf{D}^k)\boldsymbol{\nu}^k \otimes \boldsymbol{\nu}^k]$ entering respectively into the corresponding damage and sliding-yield functions (pseudo-standard modelling). The convex domains at stake should contain their origin respectively in the \mathbf{F}^D -space and in the \mathbf{F}^{γ^k} -space to ensure thermodynamically admissible evolutions (one can note in this point some analogy with the kinematic hardening rule in classical plasticity). In this respect the algorithmic approximation of the coupled

TABLE 5.1. Rate-independent anisotropic damage-friction coupled model.

Free energy: (per unit volume)	$w(\boldsymbol{\varepsilon}, \mathbf{D}, \boldsymbol{\gamma}) = \frac{1}{2} \lambda (\text{tr } \boldsymbol{\varepsilon})^2 + \mu \text{tr}(\boldsymbol{\varepsilon} \cdot \boldsymbol{\varepsilon}) + g \text{tr}(\boldsymbol{\varepsilon} \cdot \mathbf{D}) + \alpha \text{tr } \boldsymbol{\varepsilon} \text{tr}(\boldsymbol{\varepsilon} \cdot \mathbf{D})$ $+ 2\beta \text{tr}(\boldsymbol{\varepsilon} \cdot \boldsymbol{\varepsilon} \cdot \mathbf{D}) + \sum_{k=1}^3 H(-\boldsymbol{\nu}^k \cdot \boldsymbol{\varepsilon} \cdot \boldsymbol{\nu}^k) [-\alpha \boldsymbol{\varepsilon} : (D_k \mathbf{L}^k) : \boldsymbol{\varepsilon}$ $- 2\beta \text{tr}(\boldsymbol{\varepsilon} \cdot \boldsymbol{\varepsilon} \cdot \mathbf{D}^k) + 4\beta \text{tr}(\boldsymbol{\varepsilon} \cdot \boldsymbol{\gamma}^k \cdot \mathbf{D}^k) - 2\beta \text{tr}(\boldsymbol{\gamma}^k \cdot \boldsymbol{\gamma}^k \cdot \mathbf{D}^k)]$
Stress-strain and Internal variable relations:	$\boldsymbol{\sigma} = \frac{\partial w}{\partial \boldsymbol{\varepsilon}}, \text{ see (4.11), } \mathbf{F}_D = -\frac{\partial w}{\partial \mathbf{D}}, \text{ see (4.12),}$ $\mathbf{F}^{\gamma^k} = -\frac{\partial w}{\partial \boldsymbol{\gamma}^k}, \text{ see (4.13) for details}$
Damage complementary rule:	$\mathbf{F}(\mathbf{F}^D - \mathbf{F}^{D2} - \mathbf{F}^{D1-}, \mathbf{D}) \leq 0, \text{ see (3.8) for details,}$ $\dot{\mathbf{D}} = \Lambda_D \frac{\partial f}{\partial \mathbf{F}^D} = \Lambda_D \left[\frac{\boldsymbol{\varepsilon}^+}{\sqrt{2 \text{tr}(\boldsymbol{\varepsilon}^+ \cdot \boldsymbol{\varepsilon}^+)}} + B \mathbf{D} \right], \quad \Lambda_D \geq 0$
D-consistency:	$\dot{f} \Lambda_D = 0$
Frictional sliding related plasticity:	$h^k(\mathbf{F}^k, \boldsymbol{\nu}^k \cdot \boldsymbol{\varepsilon} \cdot \boldsymbol{\nu}^k) = \sqrt{\frac{1}{2} \text{tr}(\mathbf{F}^k \cdot \mathbf{F}^k)} + \hat{\rho} \boldsymbol{\nu}^k \cdot \boldsymbol{\varepsilon} \cdot \boldsymbol{\nu}^k \leq 0,$ <p style="text-align: center;">see (4.15), (5.1) for detailed form of \mathbf{F}^k,</p> $\dot{\boldsymbol{\gamma}}^k = \Lambda_\gamma^k \frac{\partial h^k}{\partial \mathbf{F}^{\gamma^k}} = \Lambda_\gamma^k \frac{\mathbf{F}^k}{\sqrt{2 \text{tr}(\mathbf{F}^k \cdot \mathbf{F}^k)}}, \quad \Lambda_\gamma^k \geq 0$
$\boldsymbol{\gamma}^k$ -consistency:	$\dot{h}^k \Lambda_\gamma^k = 0$

model should control the dissipation issue for each step and integration point. The incremental procedure leading to numerical integration of the equations of the model is summarized further in this chapter.

For completeness, the coupled rate-independent anisotropic damage-frictional sliding constitutive equations are summarized in Table 5.1.

5.2. Numerical integration of damage and sliding constitutive relations

This section provides an outline of several computational aspects involved in the finite-element implementation of the coupled model presented above. The incremental weak form of the equilibrium equation is formulated for a body $\Omega \subset R^3$ with boundary $\partial\Omega$ in the time interval $t \in I = [0, T]$. Let \mathbf{f}_d be the given body forces per unit volume, \mathbf{u}_d the displacements imposed on the part $\partial_1\Omega$ of $\partial\Omega$ and \mathbf{F}_d the traction vectors prescribed on the complementary part $\partial_2\Omega$. With the time partition: $I = \cup_{r=1}^N [t_r, t_{r+1}]$, the weak problem is formulated as follows: for each time increment $[t_r, t_{r+1}]$, find the displacement field \mathbf{u} such as, at time t_{r+1} ,

$$\int_{\Omega} \boldsymbol{\sigma}(\nabla_s \mathbf{u}) : \nabla_s \delta \mathbf{u} \, d\Omega - \int_{\Omega} \mathbf{f}_d(t_{r+1}) \cdot \delta \mathbf{u} \, d\Omega - \int_{\partial_2\Omega} \mathbf{F}_d(t_{r+1}) \cdot \delta \mathbf{u} \, dS = 0,$$

with $\mathbf{u} \in U_{ad}$, $U_{ad} = \{\mathbf{u} \mid \mathbf{u} = \mathbf{u}_d(t_{r+1}) \text{ on } \partial_1\Omega\}$, and $\forall \delta \mathbf{u} \in U_0$, $U_0 = \{\mathbf{u} \mid \mathbf{u} = \mathbf{0} \text{ on } \partial_1\Omega\}$.

The highly non-linear character of the constitutive laws, brought together in Chapters 3-4, requires that a time integration algorithm for the evolution of the damage variable \mathbf{D} and that of the sliding variable γ be accurate and stable. Such an algorithm forms, together with a spatial finite-element discretization, the finite-element implementation of the problem outlined above.

The incremental procedure leading to numerical integration of the equations of the model consists in the standard strain discretization for the loading path under consideration. At time t_r the strain $\boldsymbol{\varepsilon}_r$, the internal variables \mathbf{D}_r and γ_r^k as well as the stress $\boldsymbol{\sigma}_r$ are known. The stress $\boldsymbol{\sigma}_{r+1}$ and the internal variables \mathbf{D}_{r+1} and γ_{r+1}^k at time t_{r+1} are looked for. Since each dissipative mechanism (damage and sliding) may occur independently and since each of them offers some particularities, the two corresponding integration algorithms are commented separately. The coupling is discussed afterwards.

(i) **Local integration for the damage model.** The damage evolution Eq. (3.9) is integrated point-wise (at each quadrature point of a finite-element in the spatial discretization) in the strain-driven setting. The set of state variables \mathbf{q}_r is assumed to be known at the end of the step r : $\mathbf{q}_r = (\boldsymbol{\varepsilon}_r, \mathbf{D}_r, \gamma_r^k)$. Since only damage evolution is concerned in this paragraph, γ^k is considered constant, i.e. $\gamma_{r+1}^k = \gamma_r^k$. The integration problem amounts to updating the mechanical state, i.e. to determine \mathbf{q}_{r+1} and $\boldsymbol{\sigma}_{r+1}$, from \mathbf{q}_r and prescribed strain increment $\Delta\boldsymbol{\varepsilon}$ (such as $\boldsymbol{\varepsilon}_{r+1} = \boldsymbol{\varepsilon}_r + \Delta\boldsymbol{\varepsilon}$):

$$\begin{aligned}\mathbf{q}_{r+1} &= (\boldsymbol{\varepsilon}_{r+1}, \mathbf{D}_{r+1}, \gamma_{r+1}^k), \\ \boldsymbol{\sigma}_{r+1} &= \mathbf{G}_\sigma(\boldsymbol{\varepsilon}_{r+1}, \mathbf{D}_{r+1}, \gamma_{r+1}^k),\end{aligned}\quad (5.6)$$

$$\text{with } \boldsymbol{\varepsilon}_{r+1} = \boldsymbol{\varepsilon}_r + \Delta\boldsymbol{\varepsilon}, \quad \mathbf{D}_{r+1} = \mathbf{D}_r + \Delta\mathbf{D},$$

where the symbol \mathbf{G}_σ summarizes relation (4.11).

The following scheme furnishes a well-grounded, stable algorithm for the damage model:

(a) *Calculation of the components of $\boldsymbol{\varepsilon}_{r+1}^+$*

Given $\boldsymbol{\varepsilon}_{r+1}$, \mathbf{Q}_{r+1}^+ and then \mathbf{P}_{r+1}^+ are directly determined from the expression $P_{ijkl}^+ = Q_{ik}^+ Q_{jl}^+$, where $\mathbf{Q}^+ = \sum_{n=1}^3 H(\varepsilon_n) \mathbf{r}^n \otimes \mathbf{r}^n$; ε_n , \mathbf{r}^n being the eigenvalues and eigenvectors of $\boldsymbol{\varepsilon}$, H the Heaviside function. \mathbf{P}_{r+1}^+ extracts the positive components of $\boldsymbol{\varepsilon}_{r+1}$:

$$\boldsymbol{\varepsilon}_{r+1}^+ = \mathbf{P}_{r+1}^+ : \boldsymbol{\varepsilon}_{r+1}.$$

(b) *Elastic predictor*

The increment is first assumed to be purely elastic:

$$\Delta\mathbf{D} = \mathbf{0}, \quad \mathbf{D}_{r+1} = \mathbf{D}_r.$$

The value of $f(\boldsymbol{\varepsilon}_{r+1}, \mathbf{D}_r)$ is then checked:

$$\begin{aligned}f(\boldsymbol{\varepsilon}_{r+1}, \mathbf{D}_r) &= \sqrt{\frac{g^2}{2} \text{tr}(\boldsymbol{\varepsilon}_{r+1}^+ \cdot \boldsymbol{\varepsilon}_{r+1}^+) - Bg \text{tr}(\boldsymbol{\varepsilon}_{r+1}^+ \cdot \mathbf{D}_r)} \\ &\quad - (C_0 + C_1 \text{tr} \mathbf{D}_r).\end{aligned}\quad (5.7)$$

If $f(\boldsymbol{\varepsilon}_{r+1}, \mathbf{D}_r) \leq 0$, the elastic prediction is confirmed and \mathbf{q}_{r+1} is updated with $\mathbf{D}_{r+1} = \mathbf{D}_r$. Otherwise, \mathbf{D}_{r+1} has to be corrected and $\Delta\mathbf{D}$ is calculated as follows.

(c) *Damage correction*

The damage increment is given by the evolution Eq. (3.9) in its discretized form:

$$\Delta \mathbf{D} = \Delta \Lambda_D \left[\frac{\boldsymbol{\varepsilon}_{r+\theta}^+}{\sqrt{2 \operatorname{tr}(\boldsymbol{\varepsilon}_{r+\theta}^+ \cdot \boldsymbol{\varepsilon}_{r+\theta}^+)}} + B \mathbf{D}_{r+\theta} \right], \quad (5.8)$$

where one writes:

$$\boldsymbol{\varepsilon}_{r+\theta}^+ = (1 - \theta) \boldsymbol{\varepsilon}_r^+ + \theta \boldsymbol{\varepsilon}_{r+1}^+,$$

$$\mathbf{D}_{r+\theta} = (1 - \theta) \mathbf{D}_r + \theta \mathbf{D}_{r+1}.$$

The choice of $\theta = 1$ corresponds to a purely implicit integration scheme; in this framework, Cormery [78] showed that the damage condition $f(\boldsymbol{\varepsilon}_{r+\theta}, \mathbf{D}_{r+\theta}) = 0$ with $\theta = 1$ reduces to a simple linear equation in $\Delta \Lambda_D$. The solution of this equation is:

$$\Delta \Lambda_D = \frac{A_{r+1}}{B A_{r+1} + C_1 C_{r+1} + B g F_{r+1}}, \quad (5.9)$$

with

$$A_{r+1} = \sqrt{\frac{g^2}{2} \operatorname{tr}(\boldsymbol{\varepsilon}_{r+1}^+ \cdot \boldsymbol{\varepsilon}_{r+1}^+) - B g \operatorname{tr}(\boldsymbol{\varepsilon}_{r+1}^+ \cdot \mathbf{D}_r) - (C_0 + C_1 \operatorname{tr} \mathbf{D}_r)},$$

$$C_{r+1} = \frac{\operatorname{tr} \boldsymbol{\varepsilon}_{r+1}^+}{\sqrt{2 \operatorname{tr}(\boldsymbol{\varepsilon}_{r+1}^+ \cdot \boldsymbol{\varepsilon}_{r+1}^+)}} + B \operatorname{tr} \mathbf{D}_r,$$

$$F_{r+1} = \sqrt{\frac{1}{2} \operatorname{tr}(\boldsymbol{\varepsilon}_{r+1}^+ \cdot \boldsymbol{\varepsilon}_{r+1}^+) + B \operatorname{tr}(\boldsymbol{\varepsilon}_{r+1}^+ \cdot \mathbf{D}_r)},$$

$\Delta \mathbf{D}$ is then known as well as the mechanical state \mathbf{q}_{r+1} .

Remark: A purely implicit integration scheme has been chosen. Indeed, Ortiz and Popov [79] showed for a general formulation of elastoplasticity that this scheme ensures unconditional stability properties of relevant integration algorithms, whatever the strain increment $\Delta \boldsymbol{\varepsilon}$ is, even for strongly non linear behaviour. Moreover, this scheme is well adapted to the above damage model: the value of $\Delta \Lambda_D$ is the solution of a linear equation enforcing incremental damage consistency condition and does not require iterative procedure, unlike for most of elastoplastic models.

- (ii) **Local integration for the sliding model.** Damage is tentatively assumed to be constant ($\mathbf{D}_{r+1} = \mathbf{D}_r$). The key aspect in the formulation of the discrete time stepping procedure for the frictional sliding related plasticity concerns the integration of the evolution equation for the sliding variable γ^k , Eq. (4.16) or (5.4), the latter for general, damage axes rotation accompanied loading. The elastic predictor/plastic corrector scheme is employed here in a way parallel to damage integration.

(a) *Elastic predictor*

One assumes $\Delta\gamma^k = \mathbf{0}$ (i.e. $\gamma_{r+1}^k = \gamma_r^k$). The damage eigenvalues D_{r+1}^k and eigenvectors ν_{r+1}^k are known, the part \mathbf{F}_{r+1}^k of the thermodynamic force related to γ^k entering the expression of h^k is given by (see (5.1)):

$$\mathbf{F}_{r+1}^k = \mathbf{F}_{r+1}^{\gamma^k} + 4\beta D_{r+1}^k (\nu_{r+1}^k \cdot \boldsymbol{\varepsilon}_{r+1} \cdot \nu_{r+1}^k) \nu_{r+1}^k \otimes \nu_{r+1}^k. \quad (5.10)$$

The value of h^k is checked:

$$h^k(\mathbf{F}_{r+1}^k, \nu_{r+1}^k \cdot \boldsymbol{\varepsilon}_{r+1} \cdot \nu_{r+1}^k) = \sqrt{\frac{1}{2} \text{tr}(\mathbf{F}_{r+1}^k \cdot \mathbf{F}_{r+1}^k) + \hat{\rho} \nu_{r+1}^k \cdot \boldsymbol{\varepsilon}_{r+1} \cdot \nu_{r+1}^k}. \quad (5.11)$$

If $h^k \leq 0$, the set of variables $\mathbf{q}_{r+1} = (\boldsymbol{\varepsilon}_{r+1}, \mathbf{D}_{r+1}, \gamma_{r+1}^k)$ as well as $\boldsymbol{\sigma}_{r+1}$ is then determined as confined to reversible domain. If $h^k > 0$, the mechanical state has to be corrected, i.e. frictional sliding evolution accounted for through the plastic correction below.

(b) *Plastic correction*

The aim is to solve the following system:

$$\boldsymbol{\sigma}_{r+1} = \mathbf{G}_\sigma(\boldsymbol{\varepsilon}_{r+1}, \mathbf{D}_{r+1}, \gamma_{r+1}^k), \quad (5.12a)$$

$$\mathbf{F}_{r+1}^{\gamma^k} = \mathbf{G}_F \gamma^k(\boldsymbol{\varepsilon}_{r+1}, \gamma_{r+1}^k), \quad (5.12b)$$

$$\Delta\gamma^k = \Delta\Lambda_\gamma^k \mathbf{G}_\gamma(\mathbf{F}_{r+\theta}^k), \quad (5.12c)$$

$$h_{r+1}^k = 0, \quad (5.12d)$$

where (5.12a), (5.12b) and (5.12c) respectively stand for Eqs. (4.11), (4.13) and (4.16) or (5.4) for general loading.

Unlike the case of damage integration, the implicit scheme applied to sliding does not lead to the resolution of a linear equation for $\Delta\Lambda_\gamma^k$:

Eqs. (5.12a)-(5.12d) are a set of non-linear algebraic equations to be solved for the unknowns σ_{r+1} , γ_{r+1}^k , $\mathbf{F}_{r+1}^{\gamma^k}$ and $\Delta\Lambda_\gamma^k$. The solution is approximated by a Newton-Raphson algorithm.

(iii) **Coupling.** Both above dissipative mechanisms (damage and frictional sliding) may occur along particular loading paths. The problem is then to determine the increments $\Delta\mathbf{D}$ and $\Delta\gamma^k$ simultaneously. The integration is here facilitated by the low degree of interference between f on one hand and h^k on the other: whereas h^k is a function of \mathbf{D} and γ^k , f depends only on \mathbf{D} and Eq. (5.8) can be solved without explicit reference to sliding. The general algorithm is as follows:

1. The value $\nu^k \cdot \boldsymbol{\varepsilon} \cdot \nu^k$ of the normal strain for each equivalent micro-crack system is checked.
2. If $\nu^k \cdot \boldsymbol{\varepsilon} \cdot \nu^k > 0$, the corresponding system is open; sliding does not occur and $\Delta\mathbf{D}$ is calculated as described in paragraph (i) above.
3. If $\nu^k \cdot \boldsymbol{\varepsilon} \cdot \nu^k \leq 0$, the corresponding system is closed and may slide. Both criteria $f \leq 0$, $h^k \leq 0$ are checked; $\Delta\mathbf{D}$ and $\Delta\gamma^k$ are calculated by solving successively Eqs. (5.8) and (5.12c). The relation (5.12a) generalized to coupled process yields σ_{r+1} .

5.3. Identification of the material parameters

The model presented in the foregoing has been conceived for engineering applications. The emphasis has been put on the accessibility of a small number of material constants: only nine parameters are required for fully coupled model (λ , μ , α , β , g , C_0 , C_1 , B , $\hat{\rho}$). Seven of them can be relatively easily determined by conventional axisymmetric “triaxial” compression tests (Fig. 5.2). The friction coefficient $\hat{\rho}$ is identified by torsional tests involving frictional sliding. To determine B , a less common off-axis loading for pre-damaged specimen has to be exploited. The identification procedure has been described in details by Pham [80] and Cormery [78]. Some guiding indications are summarized below.

Consider a triaxial compression test on a cylindrical sample assumed as approximately initially undamaged and isotropic. One can determine the conventional elastic constants λ and μ from E_0 and ν_0 (initial Young’s modulus and Poisson ratio) relevant to the stress-strain relationships $(\sigma_3 - \sigma_1)$ vs. ε_3 and $(\sigma_3 - \sigma_1)$ vs. ε_1 respectively, in the elastic range without damage

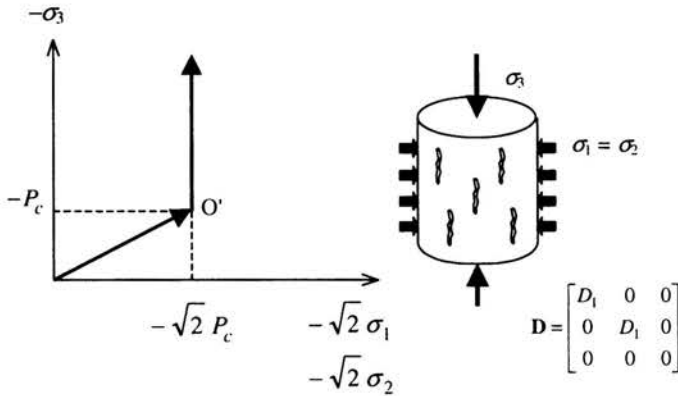


FIGURE 5.2. Conventional triaxial compression loading path.

growth ($f < 0$). To determine the values of α , β and g , the non-linear, i.e. damage affected portion and the subsequent unloading are exploited. The point at which unloading is performed should correspond to pronounced oriented damage but has to be reasonably far from the localization bifurcation-onset point to avoid interference. The unloading portion corresponding to \mathbf{D} -modified degraded moduli is being linearized according to the frictionless damage-elastic model (Chapter 3). By inverting (3.5) and specifying to axisymmetric stress-strain-damage path one can establish finally three independent equations (Eqs. (5.13)-(5.15) below) with respect to the unknowns αD_1 , βD_1 and $g D_1$.

Let be B and B' the starting point for the unloading (see Fig. 5.3). The values of αD_1 and βD_1 are related to E_3 and ν_{31} (i.e. the unloading slopes) by:

$$E_3 = \lambda + 2\mu - \frac{L_2^2}{L_1}, \quad (5.13)$$

$$\nu_{31} = \frac{L_2}{2L_1}, \quad (5.14)$$

with

$$L_1 = \lambda + \mu + 2(\alpha + \beta) D_1, \quad L_2 = \lambda + \alpha D_1.$$

The expression related to damage-induced residual effects can be expressed as follows:

$$g D_1 = \frac{E_3 \varepsilon_3 - \sigma_3 + 2\nu_{31} \sigma_1}{2\nu_{31}}. \quad (5.15)$$

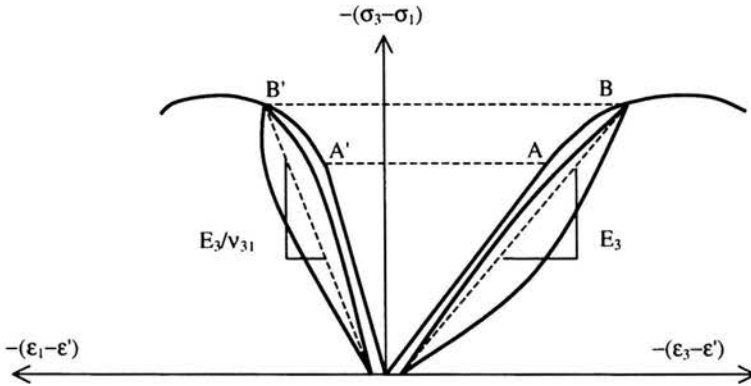


FIGURE 5.3. Determination of degraded moduli.

The next stage consists in determining C_0 and C_1 . At the initial damage threshold on the experimental curves (points A and A'), we have from (3.8):

$$|g| \varepsilon_1^A - C_0 = 0. \quad (5.16)$$

At the above-mentioned unloading point B, damage has reached a given value D_1 ; checking the criterion leads to:

$$|g| \varepsilon_1^B - (C_0 + 2 C_1 D_1) = 0. \quad (5.17)$$

According to the actual 'phenomenological' procedure based solely on stress-strain curves, one needs now to 'disentangle' the expressions αD_1 , βD_1 , $g D_1$, $C_1 D_1$, i.e. find D_1 corresponding to the loading-unloading point B in order to obtain the constants involved. This is the purpose of the final stage of the identification at stake and is done by an iterative procedure comprising the following steps:

- (i) set any admissible value D_1 as (tentative) damage at the point concerned and calculate α , β , g , C_1 and C_0 from Eqs. (5.13)-(5.17);
- (ii) calculate $-(\sigma_3 - \sigma_1)$ vs. ε_1 and ε_3 respectively;
- (iii) check locally and/or globally the gap between the trial values (ii) and the experimental ones with a norm set in advance;
- (iv) if no convergence, loop backwards to (i) with a new D_1 . The choice of a loading-unloading point can eventually be reviewed.

The set $(\lambda, \mu, \alpha, \beta, g, C_0, C_1)$ may thus be formally determined by means of a single loading-unloading test in axisymmetric triaxial apparatus. In fact,

it is preferable to cover a reasonable range of confining pressure values, i.e. exploit several curves and settle ultimate values of the constants concerned through averaging process. The hypothesis of an initially ‘virgin’ undamaged and isotropic solid can be eventually circumvented and an initial microcrack-damage state may be accounted for. Some initial, non damage-induced anisotropy may be eventually introduced as for example for ceramic-matrix composites. However, it requires additional terms in the energy representation, see further, Chapter 6.

To determine $\hat{\rho}$ for friction-induced plasticity, one resorts to torsional tests: on experimental curves giving the torque C vs. the angular deformation w for pre-damaged material (see Fig. 5.6 at the end of this section), the first change of slope is due to the onset of frictional sliding. For this point, the sliding yield condition is reached and solving $h^k = 0$ provides the value of $\hat{\rho}$.

A partial identification, discarding the constant B set to zero has been performed for a Vosges sandstone tested by Pecqueur [16] (Table 5.2) and a Fontainebleau sandstone (Table 5.3).

TABLE 5.2. Constitutive parameters (Vosges sandstone).

λ [MPa]	μ [MPa]	α [MPa]	β [MPa]	g [MPa]	C_0 [MPa]	C_1 [MPa]	B -	$\hat{\rho}$ [MPa]
3250	4875	9925	-11180	-32	0.02	0.27	0	1565

TABLE 5.3. Constitutive parameters (Fontainebleau sandstone).

λ [MPa]	μ [MPa]	α [MPa]	β [MPa]	g [MPa]	C_0 [MPa]	C_1 [MPa]	B -	$\hat{\rho}$ [MPa]
26250	17500	1900	-20400	-110	0.001	0.55	0	2500

5.4. Applications: rock-like solids

To illustrate the pertinency of the coupled model and efficiency of the integration algorithms summarized above two selected numerical examples are given below. They are concerned with brittle rock behaviour and examine the effect of loading involving necessarily the closed mesocrack related phenomena thus bringing forward the efficiency of the fully coupled model.

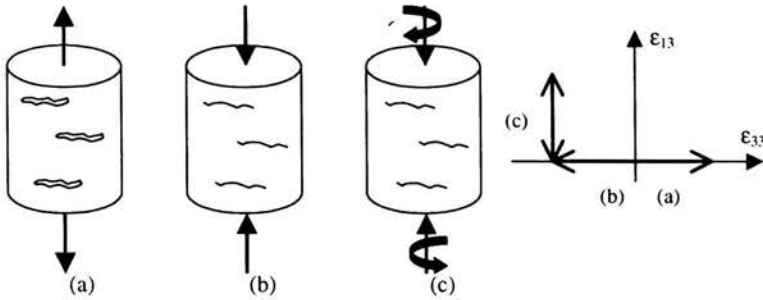


FIGURE 5.4. Steps of the homogeneous torsion-and-compression simulation (the corresponding cyclic stress-strain curve is shown in Fig. 5.5).

The first example is the analysis of a homogeneous stress-strain path relative to the third step of the complex loading programme as follows (see Fig. 5.4):

Step a: Uniaxial tension, $\sigma_3 > 0$, induces damage $D_3 > 0$ (a set of parallel mesocracks of normal 3).

Step b: Unloading then reloading under compression beyond the crack closure threshold are considered. The corresponding numerical simulation is strain-controlled; $\epsilon_{33} < \epsilon_{11} = \epsilon_{22}$.

Step c: Upon a given (frozen) configuration ($\epsilon_{33}, \epsilon_{11} = \epsilon_{22}$) corresponding to mesocracks closure is superposed additional shear strain-controlled loading: $\epsilon_{13} = \epsilon_{23}$ and subsequent unloading. Three loading-unloading cycles are simulated. In Fig. 5.5 the corresponding σ_{13} vs. ϵ_{13} loading and unloading curves are plotted. Damage growth, accompanied with principal **D**-axes rotation is calculated for each loading cycle. Friction blocking or sliding effects are accounted for.

The initial oversteiffened portion O-A in Fig. 5.5 is due to friction-induced blocking effect corresponding to recovery of the solid elastic shear modulus μ . Beyond A frictional sliding is evolving, the slope of the portion A-B is lower than the slope O-A. From B to C damage growth accompanied with frictional sliding occurs. The loading path at stake is a **D**-non-proportional one; there is some rotation of equivalent crack-axes and a complex damage state is brought about. The unloading portions are here non-linear curves: multiform unloading process with successive sliding sequences occurs (blocking on one equivalent set, two remaining sets open, followed by closure of a second one

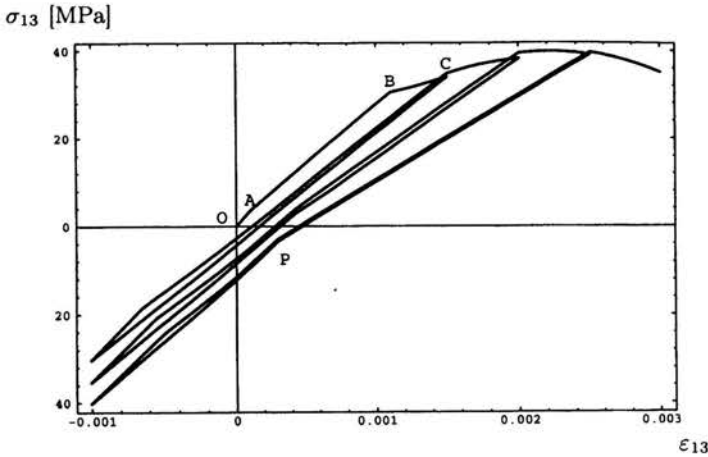


FIGURE 5.5. Shear stress σ_{13} -shear strain ϵ_{13} loading and unloading cycles corresponding to damage and frictional sliding variation. Non-proportional damage growth is simulated preceded by an initial tension-induced damage ($D_3 > 0$) and subsequent compression-induced crack closure. Complex hysteresis is exhibited.

and frictional sliding on one then two sets, etc). Here, the simulated curve σ_{13} vs. ϵ_{13} is presented to illustrate the capacity of the model to deal with multiple stage loading/unloading loops involving, eventually coupled damage-and-sliding effects and stiffening due to crack closure (for example, at point P, for the last unloading). The material under consideration is Fontainebleau sandstone (Table 5.3).

The second example refers to experimental tests by Pecqueur *et al.* [74], Pecqueur [16], consisting in a torsional loading applied to hollow cylinder specimens under hydrostatic compression. The cylinder is cut in brittle rock (Vosges sandstone, Table 5.2). Pecqueur [16] showed that the stress field is homogeneous in the central third of the cylinder. Based on this statement, the following homogeneous simulation has been carried out: an hydrostatic compression ($P_c = 10$ MPa) is first applied to a pre-damaged material with a set of mesocracks perpendicular to the cylinder axis in compression-induced closure range, next a torque C is superimposed.

Again, an initial stiffened portion is observed corresponding to friction-related blocking phenomenon. It is followed by a stage where frictional sliding evolution is noticed. This explains the reduced slope observed in Fig. 5.6, the solid line (1) leaning closely to the experimental dashed one (2). Finally, for the last stage, the simultaneous complex damage growth and sliding take

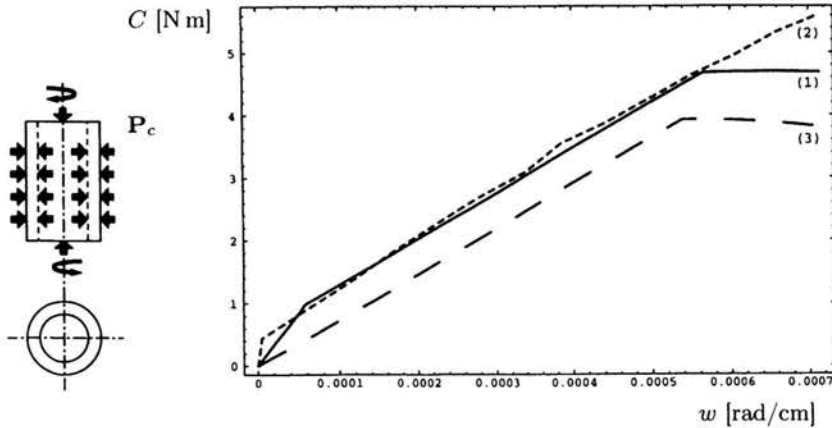


FIGURE 5.6. Torque C vs. angular deformation w for hollow cylinder example. The solid line (1) gives homogeneous response (for $P_c = 10$ MPa) of the model when both damage and frictional blocking/sliding (for closed mesocracks) are active. It appears fairly close to experimental response (dashed line (2)). The frictionless model response is given by the dashed line (3).

place and the slope becomes even smaller. The same simulation (with the same initial damage level and configuration) has been carried out for a prior version of the model (dashed line (3)) involving only the anisotropic damage propagation (cracks are allowed to slide, but without friction; the ‘basic model’ according to the terminology of Chapter 3 here, see also Dragon *et al.* [3]). The curves clearly indicate that the hypothesis of perfectly lubricated cracks underestimates the torque value whereas friction stiffens the material and predicts behaviour closer to experiment.

The last point to be commented concerns applications of the model on the level of structural analysis. This has been done for different modular segments of growing complexity. A boundary-value problem involving the fully coupled damage-and-friction model for a slab with a symmetrical double edge notch, has been recently studied by Halm *et al.* [81]. The constitutive parameters are those of Table 5.3. This has been a part of a larger programme (see also [73]) under the auspices of *Electricité de France*. It shows the capacity of the model to follow complex degradation (multiple mesocrack growth in the structure and the recovery of effective properties under a cycle of loading. The damage localization instabilities prevented frictional sliding from spreading notably.

Earlier applications employed the basic (frictionless) anisotropic damage model including the localization bifurcation analysis performed with

the 3D localization detector settled by the present authors' coworkers (Cormery, [78]). Salient algorithmic features and applications of this detector are given in [3]. The latter references bring forward structural analyses for a set of blocks with a hole, see also Dragon [83]. Numerical simulations were carried on in parallel to careful experimental investigations regarding failure incipience in the hole area. These investigations were done at the Institut Français du Pétrole (Onaisi, [82]). The numerical localization detector was employed for each computation step as a post-processor.

The computations involving *isotropic* damage modelling indicated quite erroneously the localization onset around the hole (at symmetric poles placed perpendicularly to the ones where the macrocracking was effectively starting out). By contrast, the computations applying the present 'basic' *anisotropic* damage model indicated the localized failure onset at the poles in accordance with the experimental observations by Onaisi. The slope of the localization plane was fairly reproduced by the simulations.

The calculations performed, employing the 'basic' as well as more complete modelling including frictional effects, indicate a rather strong tendency to concentrate and/or to localize damage. It seems that there is a somewhat inherent model feature to favour brittleness to the detriment of other, ductility preserving, features (as e.g. frictional resistance). The enriched, e.g. non-local damage growth description as well as time-dependent damage-kinetics variants of the present model would hopefully suppress this tendency to overestimate (accelerate) brittleness. Some work in this direction, namely a visco-damage counterpart of (3.8), (3.9), has been proposed for polymer modified concrete, Pascal [84] in view of applications for specific concrete structures.

As it is indicated at the headline of Chapter 3, the modelling of damage and notably this of damage activation/deactivation related to the normal unilateral effect is based herein on the spectral decomposition (3.1) for the second-order tensor \mathbf{D} and the extrapolation of the latter leading to the restrictive fourth-order entity $\hat{\mathbf{D}}$ in (3.3). The corresponding hypotheses involve maintaining of the form of damage-induced orthotropy of the effective elastic properties (to the detriment of more general anisotropy) and the relevant equivalence postulate stipulating that any system of mesocrack can be reduced to three commensurate orthogonal sets. The latter are embodied by eigen-densities D_k of \mathbf{D} and its eigenvectors \mathbf{v}^k . The maintaining of orthotropy was arguably justified on some micromechanical basis by Kachanov [36, 44]. The equivalence postulate is an important component of

the theory presented in Chapters 3-5 as it concerns not only the damage segment of the coupled model but is, through (4.4b), (4.9)-(4.13), reconducted for the mesocrack friction plasticity model (Chapters 4 and 5).

The damage description including unilateral effect based on the spectral decomposition of a second-order damage tensor was earlier postulated by Chaboche [71], cited in the foregoing (Chapter 3).

Recently, Cormery and Welemene [85] and Badel [73] have put forward critical analyses regarding the spectral decomposition-based damage models. As one could expect, difficulties appear for the damage configurations involving multiple principal bases characterizing purely isotropic spatial damage distribution $\mathbf{D} = d_0 \mathbf{1}$ and the like subspace, partial symmetries of \mathbf{D} like transverse planar isotropic distribution, say, $\mathbf{D} = d_0(\mathbf{e}_1 \otimes \mathbf{e}_1 + \mathbf{e}_2 \otimes \mathbf{e}_2)$, \mathbf{e}_1 and \mathbf{e}_2 representing orthogonal unit vectors. For such configurations involving infinity of principal bases (non-uniqueness), the choice of a particular set of eigenvectors leads to a form of the energy function $w(\boldsymbol{\varepsilon}; \mathbf{D})$ different from a form obtained for an other licit system. One observes thus in general non-uniqueness of the energy $w(\boldsymbol{\varepsilon}; \mathbf{D})$ and of the resulting response (e.g. stiffness $\mathbf{C}(\mathbf{D})$) for specific (sub)spatially uniform damage distributions. It has been shown in detail for the present model (Chapter 3) as well for the model by Chaboche [71]. Furthermore, such a non-uniqueness may produce the loss of continuity of the energy function $w(\boldsymbol{\varepsilon}; \mathbf{D})$ with respect to \mathbf{D} and thus brings into question the very definition of \mathbf{F}_D (thermodynamic force) and corresponding evolution laws. It should be thus stressed that aforesaid isotropic and the like damage configurations involving the multiplicity of principal bases should be tentatively excluded from the operational domain of any spectral decomposition-based damage model. More fundamentally, some topological safeguards should be searched for to assure the energy uniqueness (i.e. the existence of the thermodynamic potential) in the close neighbourhood of such configurations.

Following the critical study [85], a very stimulating work on anisotropic damage with unilateral effects due to microcrack closure has been proposed in 2002 by Welemene [86] without resorting to spectral decomposition of damage. The microcracking is embodied in the microcrack density distribution $\tilde{\rho}(\mathbf{n}, \mathbf{d}_0, \mathbf{d}_2, \mathbf{d}_4, \dots, \mathbf{D}_p)$ written in terms of the even-order damage tensors \mathbf{D}_p , following Onat and Leckie [87], Lubarda and Krajcinovic [88] and other authors. A very good approximation of directional moduli recovery due to crack closure is obtained for a truncated representation limited

to the order $p = 4$ when the defects are either all open or all closed. For a material containing simultaneously some microcracks systems open and other closed, evaluations involving $p > 4$ are significant, see [86] for details. The Welemane's model describes directional variations of Poisson's ratio under the transition opening-closure, contrarily to the ours, less sophisticated model given in Chapter 3.

The evolution laws for the tensors \mathbf{d}_p in [86] obey the truly standard modelling assumptions. A somewhat deceiving feature of the model results probably from this fully standard form: for uniaxial and axisymmetric-triaxial compression paths the directional distribution of damage obtained from the model corresponds to slight anisotropy only ([86], pp.103-105) in contradiction to most of experimental evidence for rock-like solids. It should be remarked that frictional sliding effects at microcracks are not accounted for in the Welemane's model.

Chapter 6

Interaction of primary anisotropy with the damage-induced one (CMC's)

6.1. Introduction

The model discussed in Chapters 3-5 concerns materials whose initial behaviour (i.e. that of non-damaged solid) is isotropic. This assumption is found too restrictive for a number of materials (e.g. sedimentary rocks, fiber-reinforced composites, etc.). In this part, the introduction of initial orthotropy effects is considered by using a parsimonious optimised method consisting in combining three transverse isotropy operators (fabric tensors). One obtains a small number of constants to be determined compared to other approaches. It is worth noting that multiple matrix-cracking is the primary dissipative mechanism considered here. An important issue in this framework is the interaction of oriented damage (and respective secondary anisotropy) with an initial anisotropy. Some micromechanical studies (Mauge and Kachanov [89]) address this problem and propose some tools to quantify the respective coupling. Those tools can be hardly exploited in general 3D context. An alternative is thus advanced involving conjunction of damage and fabric tensors to deal with coupling effects of primary anisotropy vs. those of evolving damage microcracking induced one. This latter phenomenon is described by a formalism keeping the wish to propose an efficient alternative with respect to some micromechanical results. The capability of the model is validated by simulating tension tests on CMC plates. Whereas the model presented in Chapters 3-5 puts forward the role played by damage induced

residual effects for rock-like solids as, e.g. residual strain exhibited by tension vs. compression cycles, this permanent stress/strain is not manifest for a large family of brittle matrix composites (e.g. CMC's), at least for matrix-cracking stage of degradation. Thus, this chapter also attempts to relax some residual damage-induced effects in order to cope with initially anisotropic materials without irreversible strain.

6.2. Initial anisotropy

6.2.1. Transverse isotropy

The mechanical properties of a transversely isotropic material are identical in planes orthogonal to a given 'axial' direction. Relevant works in the literature deal with initial anisotropy by formulating the thermodynamic potential related to initial elasticity, w^0 (the superscript "0" means initial stiffness), within the framework of the tensor function representation theory, Boehler [90]: the form of w^0 must remain invariant with respect to the coordinate transformation expressing the material symmetries and is built by use of polynomial invariants (see Talreja [91] for the general formulation and a 2D application, or Ladevèze [92] for a 3D example). The present section is based on a method employing the same mathematical tools. Its particularity lies in the fact that it *explicitly* uses a second-order orientation tensor \mathbf{A} , whose principal axes coincide with the material symmetry axes, unlike the above cited works that implicitly formulate the thermodynamic potential in the orthotropy axes. The way chosen here to model the primary anisotropy of the material is to use "fabric tensors", which quantify directional data (see e.g. Kanatani [93], for an exhaustive study on these tensors). Let w^0 be the free energy of the undamaged material. Linear elasticity is assumed for this class of materials so that w^0 is a quadratic function of the strain tensor $\boldsymbol{\varepsilon}$. Classically, w^0 takes the following form in the case of initial isotropy:

$$w^0(\boldsymbol{\varepsilon}) = \frac{\lambda}{2}(\text{tr } \boldsymbol{\varepsilon})^2 + \mu \text{tr}(\boldsymbol{\varepsilon} \cdot \boldsymbol{\varepsilon}), \quad (6.1)$$

where λ and μ are the Lamé constants. For initially isotropic materials, the expression of w^0 (see Eq. (6.1)) only contains the strain tensor. The case of the transverse isotropy (and, more generally, anisotropy) requires a directional

(fabric) tensor \mathbf{A} . The problem is then equivalent to finding w^0 such that:

$$\begin{cases} w^0(\mathbf{Q} \cdot \boldsymbol{\varepsilon} \cdot \mathbf{Q}^T, \mathbf{Q} \cdot \mathbf{A} \cdot \mathbf{Q}^T) = w^0(\boldsymbol{\varepsilon}, \mathbf{A}), & \forall \mathbf{Q} \in \mathcal{O}, \\ w^0(\mathbf{Q} \cdot \boldsymbol{\varepsilon} \cdot \mathbf{Q}^T, \mathbf{A}) = w^0(\boldsymbol{\varepsilon}, \mathbf{A}), & \forall \mathbf{Q} \in \mathcal{T}, \end{cases} \quad (6.2)$$

where \mathcal{O} is the full proper orthogonal group, i.e. $\mathcal{O} = \{\mathbf{Q} \mid \mathbf{Q} \cdot \mathbf{Q}^T = \mathbf{Q}^T \cdot \mathbf{Q} = \mathbf{I}\}$ and $\mathcal{T} \subset \mathcal{O}$ the symmetry group corresponding to transverse isotropy. Relations (6.2) mean that w^0 is an isotropic invariant of $\boldsymbol{\varepsilon}$ and \mathbf{A} . The tensor function representation theory, Boehler [90], guides one to obtain the expression of w^0 .

As it can be found in the literature, Spencer [94], Matzenmiller and Sackman [95], let us define \mathbf{A} by:

$$\mathbf{A} = \mathbf{a} \otimes \mathbf{a}, \quad \|\mathbf{a}\| = 1, \quad (6.3)$$

where \mathbf{a} is the transverse isotropy direction. The tensor \mathbf{A} thus contains the information on anisotropy, e.g. the direction of the reinforcement in unidirectional fiber-reinforced composites.

According to Cowin [96], the expression of w^0 must include quadratic terms in \mathbf{A} : transverse isotropic symmetry could not be represented by the solution of (6.2) if only linear terms in \mathbf{A} entered w^0 . After some calculation, the following expression of w^0 has been found to be sufficient to properly model the initial transverse isotropy:

$$\begin{aligned} w^0(\boldsymbol{\varepsilon}, \mathbf{A}) = & \frac{a_1}{2} (\text{tr } \boldsymbol{\varepsilon})^2 + a_2 \text{tr}(\boldsymbol{\varepsilon} \cdot \mathbf{A}) \text{tr } \boldsymbol{\varepsilon} \\ & + \frac{b_1}{2} [\text{tr}(\boldsymbol{\varepsilon} \cdot \mathbf{A})]^2 + 2c_1 \text{tr}(\boldsymbol{\varepsilon} \cdot \boldsymbol{\varepsilon}) + 2c_2 \text{tr}(\boldsymbol{\varepsilon} \cdot \boldsymbol{\varepsilon} \cdot \mathbf{A}). \end{aligned} \quad (6.4)$$

It is worth noting that a rigorous use of the representation theory of tensor functions would lead to include in Eq. (6.4) terms of higher degree in \mathbf{A} . However, the purpose here is to reach a compromise between the mathematical formulation and the number of parameters to be identified. The five parameters a_1, a_2, b_1, c_1, c_2 are easily identified from the coefficients of the stiffness tensor \mathbf{C}^0 (considered as experimentally known).

6.2.2. Extension to orthotropy

The previous paragraph showed the transversely isotropic elasticity expressed with a single fabric tensor in the energy function w^0 . This now allows

one to model the initial response of a given class of composites, for example those that are reinforced by unidirectional fibers. Most composites (e.g. woven composites) exhibit orthotropic behaviour. This paragraph aims at extending the case of transverse isotropy to orthotropy.

The modelling of the orthotropic behaviour is based here on the fact that orthotropy may be considered as equivalent to a combination of three transverse symmetries with respect to three orthogonal directions. Instead of a single fabric tensor, three directional operators \mathbf{A}_i ($i = 1, 2, 3$) enter the expression of w^0 . The following additive decomposition for orthotropy can be proposed by assuming that the \mathbf{A}_i are unit and mutually orthogonal tensors:

$$w^0(\boldsymbol{\varepsilon}; \mathbf{A}_1, \mathbf{A}_2, \mathbf{A}_3) = \sum_{i=1}^3 [\bar{a}_i \operatorname{tr} \boldsymbol{\varepsilon} \operatorname{tr}(\mathbf{A}_i \cdot \boldsymbol{\varepsilon}) + \bar{b}_i [\operatorname{tr}(\mathbf{A}_i \cdot \boldsymbol{\varepsilon})]^2 + \bar{c}_i \operatorname{tr}(\mathbf{A}_i \cdot \boldsymbol{\varepsilon} \cdot \boldsymbol{\varepsilon})]. \quad (6.5)$$

The values of the nine constants \bar{a}_i , \bar{b}_i , \bar{c}_i ($i = 1, 2, 3$) are determined in the same way as for the case of the transverse isotropy, i.e. by identifying the stiffness tensor components expressed in the orthotropy directions 1, 2, 3:

$$C^0 = \frac{\partial^2 w}{\partial \boldsymbol{\varepsilon} \partial \boldsymbol{\varepsilon}} \Rightarrow \left\{ \begin{array}{l} C_{11}^0 = 2\bar{a}_1 + 2\bar{b}_1 + 2\bar{c}_1, \\ C_{22}^0 = 2\bar{a}_2 + 2\bar{b}_2 + 2\bar{c}_2, \\ C_{33}^0 = 2\bar{a}_3 + 2\bar{b}_3 + 2\bar{c}_3, \\ C_{12}^0 = \bar{a}_1 + \bar{a}_2, \\ C_{13}^0 = \bar{a}_1 + \bar{a}_3, \\ C_{23}^0 = \bar{a}_2 + \bar{a}_3, \\ 2C_{44}^0 = \bar{c}_2 + \bar{c}_3, \\ 2C_{55}^0 = \bar{c}_1 + \bar{c}_3, \\ 2C_{66}^0 = \bar{c}_1 + \bar{c}_2. \end{array} \right. \quad C_{ij} = 0 \quad \text{otherwise.} \quad (6.6)$$

Remark 6.1. The solution proposed here (orthotropy modelled by three fabric tensors) is highly advantageous and differs from others found in the literature. For example, Cowin [96], Biegler and Mehrabadi [97] model orthotropy by a single tensor \mathbf{A} and, according to the representation theory of tensor functions, the most general form of the stiffness tensor involving one fabric tensor \mathbf{A} is:

$$C_{ijkl}^0 = a_1 \delta_{ij} \delta_{kl} + a_2 (A_{ij} \delta_{kl} + A_{kl} \delta_{ij}) + a_3 (\delta_{ij} A_{km} A_{ml} + A_{im} A_{mj} \delta_{kl}) + b_1 A_{ij} A_{kl} + b_2 (A_{ij} A_{km} A_{ml} + A_{in} A_{nj} A_{kl}) + \dots \quad (6.7)$$

$$\begin{aligned}
& \dots + b_3 A_{im} A_{mj} A_{kn} A_{nl} + c_1 (\delta_{ik} \delta_{jl} + \delta_{il} \delta_{jk}) \\
& + c_2 (A_{ik} \delta_{jl} + A_{jk} \delta_{il} + A_{il} \delta_{jk} + A_{jl} \delta_{ik}) \\
& + c_3 (A_{im} A_{mk} \delta_{jl} + A_{jm} A_{ml} \delta_{ik} + A_{im} A_{ml} \delta_{jk} + A_{jm} A_{mk} \delta_{il}).
\end{aligned} \tag{6.7}$$

[cont.]

Cowin [96], proved that the least material symmetry that can be represented by (6.7) is orthotropy and that the material orthotropy axes coincide with the principal axes of \mathbf{A} . In these axes, \mathbf{A} can be written as:

$$\mathbf{A} = \begin{bmatrix} \alpha_1 & 0 & 0 \\ 0 & \alpha_2 & 0 \\ 0 & 0 & \alpha_3 \end{bmatrix}. \tag{6.8}$$

There are then 12 parameters to be identified: $\alpha_1, \alpha_2, \alpha_3, a_1, a_2, a_3, b_1, b_2, b_3, c_1, c_2, c_3$. Two cases have to be considered:

1. If \mathbf{A} is unknown, Eq. (6.7) leads to a non linear system of 9 equations with 12 unknowns. The difficulty encountered to solve this system is a good reason to prefer the formulation (6.5).
2. If \mathbf{A} is known a priori, then Eq. (6.7) reduces to a regular system. However, the preliminary identification of \mathbf{A} may not be simple: not only the principal directions of \mathbf{A} have to be determined but also the eigenvalues $\alpha_1, \alpha_2, \alpha_3$, i.e. the respective influence of each orthotropy direction. This non trivial identification stage is not necessary in the method proposed in this paper.

Remark 6.2. Equation (6.5) allows one to model different levels of initial anisotropy:

- orthotropy, requiring the identification of the nine parameters $\bar{a}_i, \bar{b}_i, \bar{c}_i$ ($i = 1, 2, 3$).
- tetragonal symmetry (orthotropic symmetry and equivalence between two orthogonal axes, for example 1 and 2), when $\bar{a}_1 = \bar{a}_2, \bar{b}_1 = \bar{b}_2, \bar{c}_1 = \bar{c}_2$,
- cubic symmetry (orthotropic symmetry and equivalence between the three symmetry axes), when $\bar{a}_1 = \bar{a}_2 = \bar{a}_3, \bar{b}_1 = \bar{b}_2 = \bar{b}_3, \bar{c}_1 = \bar{c}_2 = \bar{c}_3$,
- transverse isotropy (for example, with respect to axis 1), when $\bar{a}_2 = \bar{a}_3, \bar{b}_2 = \bar{b}_3 = 0, \bar{c}_2 = \bar{c}_3$,
- isotropy when $\bar{a}_1 = \bar{a}_2 = \bar{a}_3, \bar{b}_1 = \bar{b}_2 = \bar{b}_3 = 0, \bar{c}_1 = \bar{c}_2 = \bar{c}_3$. The free energy density w^0 then reduces to the classical expression with two parameters, λ and μ (Eq. (6.1)).

However, because of the limited number of invariants entering Eq. (6.5), orthotropy is the weakest material symmetry (the strongest anisotropy) that can be modelled by the simplified method proposed here, see also Halm *et al.* [98].

6.3. Anisotropic damage effects

The previous section was concerned with the initial anisotropic elasticity (primary anisotropy). This initial anisotropy may strongly affect the matrix-cracking mechanism. Consequently, the aim of this section is to propose a model introduced in [98], accounting for primary anisotropy, mesocrack growth and interaction between both kinds of anisotropy (initial and induced by the presence of defects). The model is assumed to concern material degradation mechanisms not exhibiting notable irreversible stress/strain effects after loading/unloading cycles, unlike the case of the materials at stake in Chapters 3-5. This is especially valid for brittle matrix composites when the matrix alone is damaged. As a contrary mechanism, one can mention for example permanent strain caused by fiber debonding and sliding at the fiber/matrix interface in fiber-reinforced composites. These mechanisms follow the matrix cracking and intervene at an advanced stage of loading; it is not the subject of this section.

6.3.1. Damage variable and thermodynamic potential

The version of the model detailed in Chapters 3-5 assumes the initial isotropy of the material and postulates that any damage configuration is described by the single variable \mathbf{D} . For the sake of simplicity, an active damage is here considered and the fourth-order term corresponding to crack closure effects and detailed in Chapter 3 will not enter the constitutive equations.

While the above conventional damage parameter \mathbf{D} *alone* is sufficient to deal with active damage for initially isotropic materials, Mauge and Kachanov [89] prove that it should be accompanied with further insight into cracking when considering anisotropic materials. The enhanced proper crack density parameter that adjusts “relative weight” of a given crack system ‘ k ’ according to its *orientation* with respect to the matrix is, for each crack, a four-order tensor proportional to $\mathbf{n}^{(k)} \otimes \mathbf{B}^{(k)} \otimes \mathbf{n}^{(k)}$ (see [89]) where $\mathbf{n}^{(k)}$ is the normal to the k -th crack and $\mathbf{B}^{(k)}$ the crack opening displacement

second-order tensor related to a system 'k', namely the tensor which links the average displacement discontinuity vector to the traction vector. The tensor \mathbf{B} reflects the fact that, e.g. cracks normal to the stiffer direction of the matrix produce a stronger impact on the effective stiffness than the ones normal to the softer direction. It depends on the crack orientation with respect to the anisotropy axes of the matrix. Its expression is difficult to find in the closed form in the most general case. An alternative approach advanced here circumvents this difficulty by keeping a macroscopic while physically motivated formulation: no reference is made to the exact micromechanical form of $\mathbf{n} \otimes \mathbf{B} \otimes \mathbf{n}$ (which is anyway hardly known) while a macroscopic fourth-order tensor involving both \mathbf{D} (characterizing orientation and extend of the crack array) and \mathbf{A} (i.e. the orthotropy direction, see previous section) enters explicitly the equations of the model. The form of this term is chosen by extension of the basic version of the model dealing with initially isotropic materials (Chapter 3). Indeed, the stiffness tensor \mathbf{C} related to this version is:

$$\mathbf{C} = \mathbf{C}^0 + \alpha (\mathbf{I} \otimes \mathbf{D} + \mathbf{D} \otimes \mathbf{I}) + 2\beta (\mathbf{I} \overline{\otimes} \mathbf{D} + \mathbf{D} \overline{\otimes} \mathbf{I}), \quad (6.9)$$

where \mathbf{C}^0 is the initial elastic stiffness tensor, α and β two material parameters and the tensor products \otimes and $\overline{\otimes}$ defined by:

$$(\mathbf{a} \otimes \mathbf{b})_{ijkl} = a_{ij}b_{kl}, \quad (6.10a)$$

$$(\mathbf{a} \overline{\otimes} \mathbf{b})_{ijkl} = \frac{1}{2} (a_{ik}b_{jl} + a_{il}b_{jk}). \quad (6.10b)$$

The anisotropic enhanced version accounting for the relative weight of equivalent crack (through \mathbf{D}) systems with respect to primary anisotropy axes is obtained by replacing the identity ("isotropic") tensor \mathbf{I} by the orientation ("anisotropic") tensors \mathbf{A}_i :

$$\begin{aligned} \mathbf{C} = \mathbf{C}^0 + \sum_{i=1}^3 \alpha_i (\mathbf{A}_i \otimes \mathbf{D} + \mathbf{D} \otimes \mathbf{A}_i) \\ + 2\beta_i (\mathbf{A}_i \overline{\otimes} \mathbf{D} + \mathbf{D} \overline{\otimes} \mathbf{A}_i) = \mathbf{C}^0 + \Delta \mathbf{C}. \end{aligned} \quad (6.11)$$

Now, the initial \mathbf{A}_i -embodied anisotropy co-exists with the damage-induced one: the fourth-order tensors involving \mathbf{A}_i and \mathbf{D} combine initial orthotropy and (evolving) damage effects. The expression of $\Delta \mathbf{C}$, like that of \mathbf{B} , contains information on damage and primary anisotropy. The group of elastic symmetry of the properties is an intersection of the group of symmetry of \mathbf{C}^0

(orthotropy of the matrix without cracks) and the one characterizing $\Delta\mathbf{C}$. If the principal axes of \mathbf{D} coincide with the orthotropy axes of \mathbf{C}^0 , the material remains orthotropic. If they do not effective properties have no elements of symmetry. Six parameters ($\alpha_i, \beta_i, i = 1, 2, 3$) have to be identified compared to two in the basic version. Expression (6.11) of \mathbf{C} leads to the following thermodynamic potential (free energy per unit volume):

$$w(\boldsymbol{\varepsilon}, \mathbf{D}; \mathbf{A}_i) = \sum_{i=1}^3 [\bar{a}_i \operatorname{tr} \boldsymbol{\varepsilon} \operatorname{tr}(\mathbf{A}_i \cdot \boldsymbol{\varepsilon}) + \bar{b}_i [\operatorname{tr}(\mathbf{A}_i \cdot \boldsymbol{\varepsilon})]^2 + \bar{c}_i \operatorname{tr}(\mathbf{A}_i \cdot \boldsymbol{\varepsilon} \cdot \boldsymbol{\varepsilon})] \\ + \sum_{i=1}^3 [\alpha_i \operatorname{tr}(\boldsymbol{\varepsilon} \cdot \mathbf{A}_i) \operatorname{tr}(\boldsymbol{\varepsilon} \cdot \mathbf{D}) + 2\beta_i \operatorname{tr}(\boldsymbol{\varepsilon} \cdot \mathbf{A}_i \cdot \boldsymbol{\varepsilon} \cdot \mathbf{D})]. \quad (6.12)$$

The second term represents the variation of free energy due to damage and the effects of interaction of primary anisotropy with the damage induced one leading eventually to further loss of material symmetry. Unlike the expression of the energy for the basic version of the reference model, see Chapter 3, the term $g \operatorname{tr}(\boldsymbol{\varepsilon} \cdot \mathbf{D})$ giving rise to residual macroscopic stress for $\boldsymbol{\varepsilon} = \mathbf{0}$ (and dually $\boldsymbol{\varepsilon} \neq \mathbf{0}$, for $\boldsymbol{\sigma} = \mathbf{0}$) is not considered in Eq. (6.12).

The corresponding elastic stress $\boldsymbol{\sigma}$ and thermodynamic force related to damage \mathbf{F}^D are determined by partial derivation of w :

$$\boldsymbol{\sigma} = \frac{\partial w}{\partial \boldsymbol{\varepsilon}} = \sum_{i=1}^3 \left\{ \bar{a}_i [\operatorname{tr}(\mathbf{A}_i \cdot \boldsymbol{\varepsilon}) \mathbf{I} + (\operatorname{tr} \boldsymbol{\varepsilon}) \mathbf{A}_i] \right. \\ \left. + 2\bar{b}_i \operatorname{tr}(\mathbf{A}_i \cdot \boldsymbol{\varepsilon}) \mathbf{A}_i + \bar{c}_i (\mathbf{A}_i \cdot \boldsymbol{\varepsilon} + \boldsymbol{\varepsilon} \cdot \mathbf{A}_i) \right\} \\ + \sum_{i=1}^3 \left\{ \alpha_i [\operatorname{tr}(\boldsymbol{\varepsilon} \cdot \mathbf{D}) \mathbf{A}_i + \operatorname{tr}(\boldsymbol{\varepsilon} \cdot \mathbf{A}_i) \mathbf{D}] \right. \\ \left. + 2\beta_i (\mathbf{A}_i \cdot \boldsymbol{\varepsilon} \cdot \mathbf{D} + \mathbf{D} \cdot \boldsymbol{\varepsilon} \cdot \mathbf{A}_i) \right\}, \quad (6.13)$$

$$\mathbf{F}^D = -\frac{\partial w}{\partial \mathbf{D}} = \sum_{i=1}^3 [-\alpha_i \operatorname{tr}(\boldsymbol{\varepsilon} \cdot \mathbf{A}_i) \boldsymbol{\varepsilon} - 2\beta_i \boldsymbol{\varepsilon} \cdot \mathbf{A}_i \cdot \boldsymbol{\varepsilon}]. \quad (6.14)$$

6.3.2. Damage evolution law

The threshold $f = 0$ delimiting the elastic domain is expressed in the proper space of components of \mathbf{F}^D , the thermodynamic force related to \mathbf{D}

(damage driving force). The evolution of \mathbf{D} is assumed to follow the normality rule, corresponding to the principle of maximum dissipation and exhibiting splitting-like damage mechanism commonly observed in brittle solids. The previously discussed (see Chapter 3) hypothesis regarding the pseudo-standard modelling is here again put forward: the thermodynamic force splits into two parts and the damage criterion $f(\mathbf{F}^D; \mathbf{D}) = 0$ as well as the corresponding potential are assumed to depend on the part \mathbf{F}^{D+} of \mathbf{F}^D involving the positive strain $\boldsymbol{\varepsilon}^+$:

$$\begin{aligned}\mathbf{F}^{D+} &= \sum_{i=1}^3 [-\alpha_i \operatorname{tr}(\boldsymbol{\varepsilon} \cdot \mathbf{A}_i) \boldsymbol{\varepsilon}^+ - 2\beta_i \boldsymbol{\varepsilon}^+ \cdot \mathbf{A}_i \cdot \boldsymbol{\varepsilon}^+], \\ \mathbf{F}^{D-} &= \mathbf{F}^D - \mathbf{F}^{D+}, \quad \boldsymbol{\varepsilon} = \boldsymbol{\varepsilon}^+ + \boldsymbol{\varepsilon}^-. \end{aligned} \quad (6.15)$$

The threshold $f = 0$ is thus chosen as follows:

$$\begin{aligned}f(\mathbf{F}^D - \mathbf{F}^{D-}, \mathbf{D}) &= \sqrt{\frac{1}{2} \operatorname{tr}[(\mathbf{F}^D - \mathbf{F}^{D-}) \cdot (\mathbf{F}^D - \mathbf{F}^{D-})]} \\ &\quad + B \operatorname{tr}[(\mathbf{F}^D - \mathbf{F}^{D-}) \cdot \mathbf{D}] - (C_0 + C_1 \operatorname{tr} \mathbf{D}) = 0, \end{aligned} \quad (6.16)$$

where C_0 , C_1 and B keep the same signification as in Chapter 3. The rate-independent damage evolution law obeying pseudo-standard rule is written as follows:

$$\dot{\mathbf{D}} = \begin{cases} \mathbf{0}, & \text{if } f < 0 \text{ or } f = 0, \dot{f} < 0, \\ \Lambda_D \frac{\partial f}{\partial \mathbf{F}^D} = \Lambda_D \left[\frac{\mathbf{F}^{D+}}{\sqrt{2 \operatorname{tr}(\mathbf{F}^{D+} \cdot \mathbf{F}^{D+})}} + B\mathbf{D} \right], & \Lambda_D \geq 0, \\ & \text{if } f = 0 \text{ and } \dot{f} = 0. \end{cases} \quad (6.17)$$

The importance of the positive strain appears in the first term involving \mathbf{F}^{D+} . The second term ($B\mathbf{D}$), called drag-term, represents the influence of the current value of damage on its instantaneous evolution.

6.3.3. Example

The predictive capacity of the foregoing approach is tested by simulating tension tests on a bi-directional ($0^\circ, 90^\circ$) ceramic-ceramic composite produced by the SEP. This material consists of 2D plates of a chemical vapor infiltration processed SiC matrix reinforced with plies of Nicalon fibers. The

components of the stiffness tensor are identified by an ultrasonic evaluation technique, Audoin and Baste [99], which makes it possible to measure the nine stiffness coefficients describing orthotropy. From these stiffness components, the following set of parameters $(\bar{a}_i, \bar{b}_i, \bar{c}_i)$, $i = 1, 2, 3$ is identified (see Table 6.1).

TABLE 6.1.

$\bar{a}_1 = 23.0$ GPa	$\bar{a}_2 = 71.0$ GPa	$\bar{a}_3 = 74.0$ GPa
$\bar{b}_1 = 83.5$ GPa	$\bar{b}_2 = 13.5$ GPa	$\bar{b}_3 = 11.0$ GPa
$\bar{c}_1 = 24.0$ GPa	$\bar{c}_2 = 90.0$ GPa	$\bar{c}_3 = 96.0$ GPa

Tension tests (Aubard [100]) have been carried out on these woven plates with different orientations θ of the tension axis (tension along axis 3, in the plane (2,3), see Fig. 6.1) with respect to fiber axis. The parameters $C_0, C_1, B, \alpha_2, \alpha_3, \beta_2, \beta_3$ are identified on 0° - and 45° -tests. Note that no experimental information on the direction 1 is available. Thus, in this particular case, the parameters α_1 and β_1 are arbitrarily chosen equal to zero. Table 6.2 collects the values of the different parameters. A third tension test ($\theta = 20^\circ$) is used as a preliminary validation test.

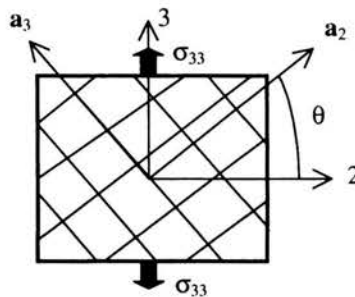
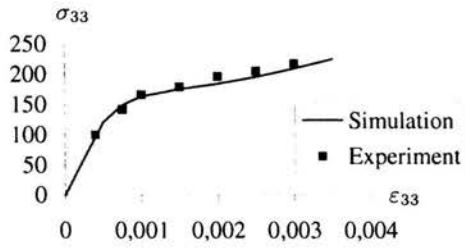
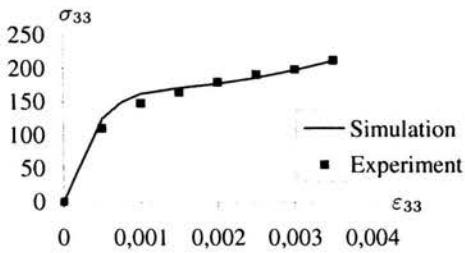
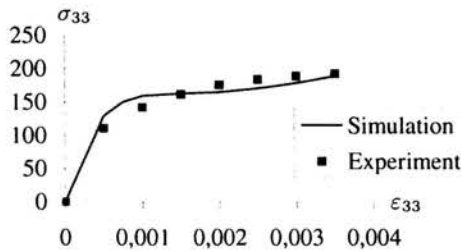
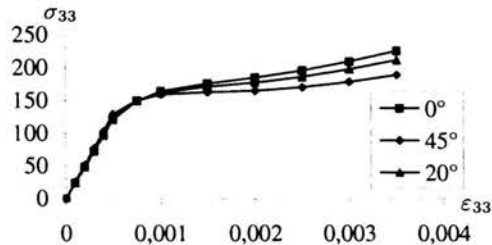


FIGURE 6.1. Schematization of the plate under tension.

TABLE 6.2. Material constants.

C_0 [MPa]	C_1 [MPa]	B -	α_2 [MPa]	β_2 [MPa]	α_3 [MPa]	β_3 [MPa]
0.017	0.058	-0.7	0	-62000	0	-48000

Figures 6.2-6.4 exhibit a fair correlation between the experimental data and the corresponding simulation. Note in particular the respective position (Fig. 6.5) of each curve in agreement with the experiment: even if the

FIGURE 6.2. Comparison simulation/experiment $\theta = 0^\circ$.FIGURE 6.3. Comparison simulation/experiment $\theta = 45^\circ$.FIGURE 6.4. Comparison simulation/experiment $\theta = 20^\circ$.FIGURE 6.5. Respective position of the simulated response for $\theta = 0^\circ, 20^\circ, 45^\circ$.

elastic response of the composite for $\theta = 45^\circ$ is initially stiffer than the response in the direction parallel to fibers ($\theta = 0^\circ$), the subsequent stress level is lower for $\theta = 45^\circ$ than for $\theta = 0^\circ$ or 20° . This illustrates the interaction effect between (oriented) cracking and the primary orthotropy on resultant material degradation in accordance with the postulates formulated in Sec. 6.3.1.

6.4. Conclusion

The work presented in this chapter completes the modular strategy followed since Chapter 3 by adding a supplementary level to the structure of the damage model, namely the competition between initial anisotropy and induced one. This has been done by pursuing a methodology which can be considered as phenomenological yet still strongly micromechanically motivated. The existing framework includes damage growth by oriented microcracking, effects of opening/closure (and inverse) transition for microcrack sets and complementary dissipation effects due to frictional resistance and sliding on closed crack sets. The extension proposed in the present chapter concerns quasi-brittle solids exhibiting a marked initial anisotropy independently of secondary damage induced one. The initial orthotropy has been introduced here in a particular thrifty manner allowing for tractable identification due to a reduced number of material constants compared to other existing schemes. The model allows furthermore to take into account major coupling effects between the primary anisotropy and the secondary, damage induced and evolving anisotropy. This has been done by introducing invariant terms involving simultaneously damage tensor and material fabric tensor in the representation of the free energy (thermodynamic potential). This representation is an alternative to the micromechanical expression posulated in Mauge and Kachanov [89] comprising the crack compliance tensor \mathbf{B} and indicators of crack orientation. An illustration of the interactional effects at stake (primary vs. damage induced anisotropy) has been given for a brittle matrix fiber reinforced composite.

Chapter 7

Mesocrack interaction via morphology-based micromechanical approach

It is useful at this stage to recapitulate briefly progression of the present notes from the introductory damage modelling background (Chapter 2), to more advanced microcracking related anisotropic pseudo-standard modelling consisting in modular approach incorporating gradually essential accompanying phenomena. The four-fold anisotropic model detailed above (Chapters 3-6) includes:

1. the basic frictionless version for mesocracking damage inducing a form of orthotropy, dilatancy and some residual effect for initially isotropic solid,
2. the enhanced version including normal unilateral effect,
3. the coupled model involving the latter one connected with friction sliding related plasticity,
4. the combined model incorporating a primary fabric tensors-embodied anisotropy with a secondary damage-induced one.

A number of micromechanical studies has been cited through the foregoing developments supporting some essential hypotheses and ingredients of the model and putting emphasis on its micromechanical motivations. Several simplifications persist, one of most notable being connected to linear dependence of the energy $w(\boldsymbol{\varepsilon}, \mathbf{D}, \dots)$ on the damage tensor \mathbf{D} pertaining – as it is stated in Chapter 3 – to the hypothesis of non-interaction of mesocracks. Obviously, this hypothesis is a strongly limiting one. In the context of the

macroscopic local model of Chapters 3-6 the rather precocious localization bifurcation (see comments at the end of Chapter 5) represents in fact a sort of inherent transformation of dilute distributed damage evolution into concentrated, clustering mesocracking. In this sense the localization bifurcation can be considered as a sort of phenomenological palliative for the advanced damage process involving crack interaction marked mesocracking stage. Further work should be focused on robust modelling including this kind of transformation of the damage kinetics and overcoming related instabilities [73]. Consensual nonlocal damage modelling, implemented in reliable engineering computational schemes, is probably one of ways to accomplish this task in the near future.

The problem of microcrack interaction (within an elastic matrix) was extensively studied by Kachanov on micromechanical ground, see for instance the recapitulative study [44]. One can consult also Fond and Berthaud [25] putting stress on friction effects.

Many paradoxical crack configurations and effects are listed in Kachanov's paper. The efficient "pseudo-tractions technique" proposed by this author, gives reasonable approximations for prescribed distributions of defects.

The problem of the crack interaction impact on the effective moduli and, furthermore, the problem of essential structure of a macroscopic theory accounting for this effect in an advanced formulation as stemming, e.g. from the developments presented above (Chapters 3-6) is a non-trivial one. The comments by Kachanov [44], p. 386, point out essential non-uniqueness factors regarding the relationship between crack arrangements and averaging schemes tending to predict global energy and effective moduli. As stressed by Krajcinovic [2], the nonlocal character and loss of statistical uniformity may affect damage process by interaction marked microcracking, in connection with degree of pressure confinement and clustering phenomena.

It is not intended here to comment furthermore micromechanical studies quoted above. The aim of this chapter is to introduce a non-classical micromechanical analysis dealing with microcracking and capturing crack interaction phenomena. Its non-classical character stems much from kinematical and morphological assumptions regarding the microstructure and constituting the very basis of the methodology itself. Indeed, many authors search nowadays morphologically enhanced representations which in term should bridge the gap between 'disordered' and 'periodic' representations in micromechanics. A systematic approach involving 'morphologically representative patterns'

has been recently advanced by Bornert *et al.* [101]. Herein, the present authors team's work [28, 102] based on the homogenization scheme proposed by Christoffersen in 1983 [103] is outlined and commented in relation to the macroscopic model of Chapters 3-6. This contribution, focusing on elastic particulate composites, attempts to extend further the Christoffersen's technique by accounting for microcracking damage at the interfaces grain/matrix. Another extension involving viscoelastic matrix and related two-stage 'direct' homogenization is presented by Nadot-Martin *et al.* in [104].

7.1. Microstructure schematization and local problem approach

Figure 7.1 shows a close-up schematic for grains separated by matrix layers according to the scheme proposed by Christoffersen [103] for a broad class of "bonded granulates". The grains are considered as polyhedral; any two of them are interconnected by a material layer of a given uniform thickness. The grain-layer interfaces are characterized by their orientation and their area (respectively \mathbf{n}^α and A^α for the α -th layer). Some granulometry is accounted for through the vectors linking grain centroids (\mathbf{d}^α for the α -th layer). Moreover, no restriction being imposed concerning grain sizes, the representation allows granulometric variations.

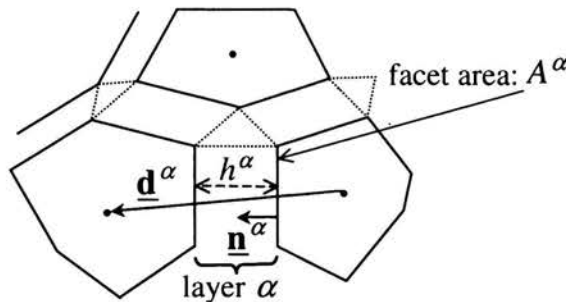


FIGURE 7.1. Two neighbouring grains with an interconnecting material layer according to Christoffersen [103].

The local problem approach is based on the definition of a simplifying kinematical context. The latter is defined by four assumptions consisting in piecewise linearization of the microscopic displacement field with respect to the geometrical schematization of the microstructure presented above:

1. The kinematics of grain centroids is characterized by the macroscopic displacement gradient $\nabla \underline{\mathbf{U}} = \bar{\mathbf{f}}$.
2. The grains are supposed homogeneously deformed and the corresponding displacement gradient $\nabla \underline{\mathbf{u}}^0 = \mathbf{f}^0$ assumed to be common to all members of the statistically representative volume element (SRVE).
3. Each interconnecting layer is subject to homogeneous deformation, proper to the layer α under consideration. The corresponding displacement gradient is noted $\nabla \underline{\mathbf{u}}^\alpha = \mathbf{f}^\alpha$ for the α -th layer.
4. Local disturbances at grain edges and corners are neglected on basis of thinness of the layers.

With the previous assumptions, the continuity of displacements on the grain-layer interfaces leads to the expression of the kinematics of the layer α as follows:

$$f_{ij}^\alpha = f_{ij}^0 + (\bar{f}_{ik} - f_{ik}^0) d_k^\alpha n_j^\alpha / h^\alpha, \quad (7.1)$$

where h^α is the thickness of layer α . In view of (7.1), strain as well as rotation are controlled by $\bar{\mathbf{f}}$, \mathbf{f}^0 but also by the geometrical features of the layer α under consideration. One may emphasize that such a dependence on local geometrical parameters allows to account for microstructure effect on deformation mechanisms of the matrix. Note that due to the fourth assumption neglecting interlayer zones, each layer is in fact uniquely loaded on its boundaries with the grains. In this way, there is no direct interaction between layers; the transmission through grains-and-layers assembly is described via grains as illustrated in Fig. 7.2 and expressed through the presence of \mathbf{f}^0 in (7.1).

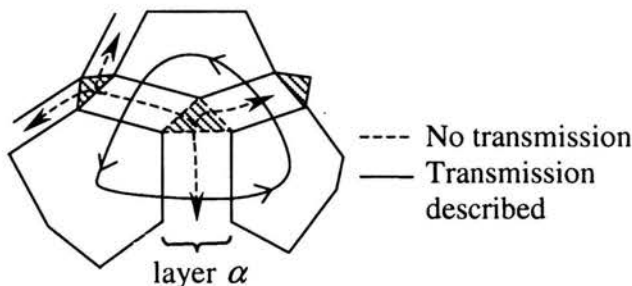


FIGURE 7.2. Grain-layer interaction modelling according to Christoffersen [03].

In order to ensure compatibility between local motion according to the above description and global motion characterized by $\bar{\mathbf{f}}$, the following average

relation is imposed:

$$\bar{f}_{ij} = \langle u_{i,j} \rangle_V = (1 - c)f_{ij}^0 + \frac{1}{|V|} \sum_{\alpha} f_{ij}^{\alpha} A^{\alpha} h^{\alpha}, \quad c = \frac{1}{|V|} \sum_{\alpha} A^{\alpha} h^{\alpha}, \quad (7.2)$$

where $|V|$ represents the volume of grains and layers excluding interlayer zones and c the ratio of layers volume to volume $|V|$. The summations in (7.2) are over all layers contained in the Statistically Representative Volume Element (SRVE). Inserting (7.1) shows that compatibility is satisfied only if

$$\frac{1}{|V|} \sum_{\alpha} d_i^{\alpha} n_j^{\alpha} A^{\alpha} = \delta_{ij}, \quad (7.3)$$

where δ_{ij} is the Kronecker's symbol, (see [103] for geometrical interpretation of (7.3)).

Consider now the SRVE to be loaded on its boundaries by uniform tractions represented by a given macroscopic stress Σ . Then, the well-known Hill-Mandel principle of macro-homogeneity specialised to the above geometrical and kinematical description takes here the following particular form:

$$\Sigma_{ij} \bar{f}_{ij} = (1 - c)\sigma_{ij}^0 f_{ij}^0 + \frac{1}{|V|} \sum_{\alpha} \sigma_{ij}^{\alpha} f_{ij}^{\alpha} A^{\alpha} h^{\alpha}, \quad (7.4)$$

for any arbitrary $\bar{\mathbf{f}}$ and \mathbf{f}^0 and any stress field statically admissible with Σ . σ^0 and σ^{α} represent average stresses in the grains and in the α -th layer respectively. By inserting (7.1) and taking successively two particular values for \mathbf{f}^0 , it can be shown from (7.4) that:

$$\left\{ \begin{array}{l} \Sigma_{ij} = \langle \sigma_{i,j} \rangle_V = (1 - c)\sigma_{ij}^0 + \frac{1}{|V|} \sum_{\alpha} \sigma_{ij}^{\alpha} A^{\alpha} h^{\alpha}, \\ \Sigma_{ij} = \frac{1}{|V|} \sum_{\alpha} t_i^{\alpha} d_j^{\alpha} = \frac{1}{|V|} \sum_{\alpha} t_j^{\alpha} d_i^{\alpha}, \quad t_j^{\alpha} = \sigma_{kj}^{\alpha} n_k^{\alpha} A^{\alpha}, \end{array} \right. \quad (7.5)$$

where \underline{t}^{α} represents the total force transmitted through the α -th layer. Note that, although the first relation is largely exploited in the context of 'classical' homogenization methods, the second one remains specific to the Christofersen approach: stresses are seen from a granular viewpoint as forces transmitted from grain to grain by layers acting as contacts zones, namely according to solid line in Fig. 7.2.

The following consists in searching \mathbf{f}^0 in such a way that the real stress field, namely this associated to the strain field by local constitutive laws,

satisfies the system (7.5) where (7.1) is substituted for \mathbf{f}^α . Christoffersen proceeds along the determination of \mathbf{f}^0 for isotropic and linear-elastic constituents by considering uniform moduli for grains noted \mathbf{L}^0 and different uniform moduli for layers noted $\mathbf{L}^{(e)\ell}$. Note that, in this way, $\boldsymbol{\sigma}^0$ and $\boldsymbol{\sigma}^\alpha$ represent uniform fields in the grains and in the α -th layer respectively and \mathbf{t}_α becomes the mean force transmitted through the grain-layer interface. \mathbf{f}^0 is then obtained as follows:

$$\begin{aligned} \mathbf{f}^0 &= \bar{\mathbf{f}} - \mathbf{B}^{-1} : \mathbf{A} : \bar{\mathbf{f}}, \\ \mathbf{A} &= \langle \mathbf{L}^{(e)} \rangle_V - \mathbf{L}^{(e)\ell}, \quad \langle \mathbf{L}^{(e)} \rangle_V = (1-c)\mathbf{L}^0 + c\mathbf{L}^{(e)\ell}, \end{aligned} \quad (7.6)$$

$$\begin{aligned} B_{ijkl} &= A_{ijkl} - L_{ijkl}^{(e)\ell} + L_{mjnl}^{(e)\ell} \bar{R}_{imkn}, \\ \bar{R}_{ijkl} &= \frac{1}{|V|} \sum_{\alpha} d_i^\alpha n_j^\alpha d_k^\alpha n_l^\alpha A^\alpha / h^\alpha. \end{aligned} \quad (7.7)$$

Inserting (7.6) in (7.1) leads to the expression of \mathbf{f}^α as a function of $\bar{\mathbf{f}}$. From the localization relations concerning the displacement gradient, one may finally deduce the local strain field in the grains and in the layers with respect to the microscopic coordinates $\underline{\mathbf{y}}$ in the SRVE.

$$\boldsymbol{\varepsilon}(\underline{\mathbf{y}}) = \mathbf{C}(\underline{\mathbf{y}}) : \mathbf{E}, \quad (7.8)$$

$$C_{ijkl}(\underline{\mathbf{y}}) = \begin{cases} C_{ijkl}^0 = (\mathbf{Id} - \mathbf{Id} : \mathbf{B}^{-1} : \mathbf{A})_{ijkl} & \text{for } \underline{\mathbf{y}} \in \text{grains,} \\ C_{ijkl}^\alpha = Id_{ijkl} - Id_{ijuv} (\mathbf{B}^{-1} : \mathbf{A})_{vmkl} \Pi_{mu}^\alpha & \text{for } \underline{\mathbf{y}} \in \text{layer } \alpha. \end{cases}$$

with $Id_{ijkl} = \frac{1}{2}(\delta_{ik}\delta_{jl} + \delta_{il}\delta_{jk})$ and $\Pi_{ij}^\alpha = \delta_{ij} - d_i^\alpha n_j^\alpha / h^\alpha$. At last, the overall stress is derived from (7.5)₁:

$$\boldsymbol{\Sigma}(\mathbf{E}) = \mathbf{L} : \mathbf{E}, \quad \mathbf{L} = \mathbf{L} \langle \mathbf{L}^{(e)} \rangle_V - \mathbf{A} : \mathbf{B}^{-1} : \mathbf{A}. \quad (7.9)$$

It is to be stressed that $\mathbf{C}(\underline{\mathbf{y}})$ stands above, in (7.8), for the strain concentration tensor.

7.2. Extension in presence of damage

The purpose consists in incorporating the material discontinuities and relative displacement jumps in a compatible way with the above Christoffersen's kinematical assumptions. In addition to imply the displacement jump linearity, these assumptions, and more precisely the second one regarding \mathbf{f}^0 as

common to all grains, impose only two possible configurations for a layer α : either its two boundaries are cohesive, either they are both debonded. The second configuration is described with two mean displacement discontinuity vectors $\langle \underline{b}^\alpha \rangle_{I_i^\alpha}$ ($i = 1, 2$) of opposite signs. By taking into account relative conditions of displacement jump, the extended formula for the displacement gradient \mathbf{f}^α , the counterpart of (7.1) for a debonded layer α (see Fig. 7.3), is given by:

$$\begin{aligned} f_{ij}^\alpha &= f_{ij}^0 + (\bar{f}_{ik} - f_{ik}^0) d_k^\alpha n_j^\alpha / h^\alpha + f_{ij}^{\alpha D}, \\ \langle b_i^\alpha \rangle_{I_1^\alpha} &= -\langle b_i^\alpha \rangle_{I_2^\alpha} = -\frac{1}{2} f_{ij}^{\alpha D} c_j^\alpha. \end{aligned} \quad (7.10)$$

The supplementary term $\mathbf{f}^{\alpha D}$ represents the contribution of microcracks to the α -th layer's motion; \mathbf{c}^α is the vector connecting the centres of two opposite facets.

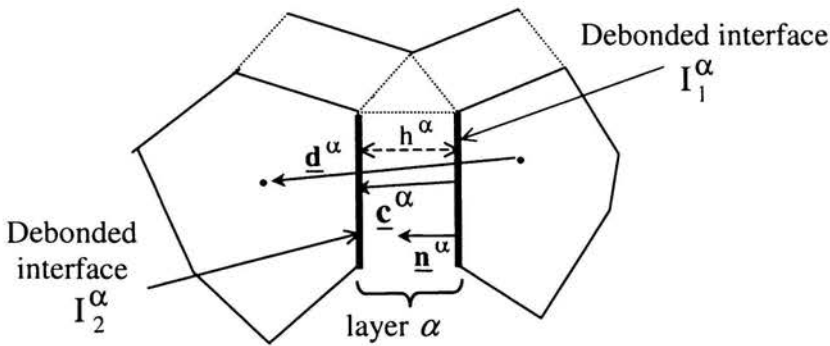


FIGURE 7.3. A layer with cracks at its boundaries.

Equations (7.2) and (7.4) are no longer valid. The following extended formulae include the discontinuities $\langle b_i \rangle$:

$$\bar{f}_{ij} = \langle f_{ij} \rangle_V + \frac{2}{|V|} \sum_k \langle b_i^k \rangle_{I_1^k} n_j^k A^k, \quad (7.11)$$

$$\begin{aligned} \Sigma_{ij} \bar{f}_{ji} &= (1 - c) \sigma_{ij}^0 f_{ji}^0 + \frac{1}{|V|} \sum_\alpha \sigma_{ij}^\alpha f_{ji}^\alpha A^\alpha h^\alpha \\ &+ \frac{1}{|V|} \sum_k \left\{ \int_{I_1^k} \sigma_{ij} n_j^k b_i^k da - \int_{I_2^k} \sigma_{ij} n_j^k b_i^k da \right\}. \end{aligned} \quad (7.12)$$

In the above relations, superscript k denotes summation over all layers with interfaces debonded. Using some compatibility conditions the material must

fulfill (see [105] for details), it can be shown that Eqs. (7.5) remain valid for the damaged material, so that the resolution method to find \mathbf{f}^0 is the same as in Sec. 7.1. Equation (7.5)₂ involves the mean force transmitted through the interface I_1^α of each layer. For a debonded layer, two cases must be considered. When the cracks are open, $\mathbf{t}^\alpha = 0$. When the cracks are closed, and in the framework of this exploratory study, it is supposed that the mean force is integrally transmitted, i.e. that no sliding is allowed. The solution is then given by:

$$f_{ij}^0 = \bar{f}_{ij} - (B'^{-1} : A')_{ijkl} \bar{f}_{lk} + \underbrace{B'_{ijuv}{}^{-1} L_{mukl}^{(e)\ell} \left[\frac{1}{|V|} \sum_f d_v^f n_m^f \varepsilon_{lk}^{fD} A^f - \delta_{vu} \frac{1}{|V|} \sum_k \varepsilon_{lk}^{kD} A^k h^k \right]}_{f_{ij}^{0(d)}}, \quad (7.13)$$

where superscript f refers to layers with closed cracks only. \mathbf{A}' and \mathbf{B}' are the equivalent of \mathbf{A} and \mathbf{B} in (7.6)-(7.7), but here degraded by the presence of damage:

$$A'_{ijkl} = \langle L_{ijkl}^{(e)\ell} \rangle - L_{mjkl}^{(e)\ell} (\delta_{im} - D_{im}), \quad (7.14)$$

$$B'_{ijkl} = A_{ijkl} - L_{mjkl}^{(e)\ell} (\delta_{im} - D_{im}) + L_{mjnl}^{(e)\ell} (\bar{R}_{imkn} - \bar{D}_{imkn}),$$

$$D_{ij} = \frac{1}{|V|} \sum_\beta d_i^\beta n_j^\beta A^\beta, \quad (7.15)$$

$$\bar{D}_{ijkl} = \frac{1}{|V|} \sum_\beta d_i^\beta n_j^\beta d_k^\beta n_l^\beta A^\beta / h^\beta,$$

where superscript β denotes summation over layers with open cracks. \mathbf{f}^α for a cohesive, respectively debonded layer, is then derived from (7.1), respectively (7.10), in which (7.13) is substituted for \mathbf{f}^0 . At last, the local strain field is obtained in the following form:

$$\varepsilon(\underline{\mathbf{y}}) = \mathbf{C}'(\underline{\mathbf{y}}) : \mathbf{E} + \varepsilon^{(d)}(\underline{\mathbf{y}}) + \begin{cases} \varepsilon^{\alpha D} & \text{for } \underline{\mathbf{y}} \in \text{debonded layer } \alpha, \\ \mathbf{0} & \text{elsewhere.} \end{cases} \quad (7.16)$$

The degraded elastic strain concentration tensor $\mathbf{C}'(\underline{\mathbf{y}})$ has the same form as $\mathbf{C}(\underline{\mathbf{y}})$ given by (7.8) with \mathbf{A}' and \mathbf{B}' replacing \mathbf{A} and \mathbf{B} . The field $\varepsilon^{(d)}(\underline{\mathbf{y}})$ is given by:

$$\varepsilon_{ij}^d(\underline{\mathbf{y}}) = \begin{cases} \varepsilon_{ij}^{0(d)}(\mathbf{D}, \bar{\mathbf{D}}, \{\varepsilon^{kD}\}) = Id_{ijkl} f_{lk}^{0(d)} & \text{for } \underline{\mathbf{y}} \in \text{grains,} \\ \varepsilon_{ij}^{\alpha(d)}(\mathbf{D}, \bar{\mathbf{D}}, \{\varepsilon^{kD}\}) = Id_{ijuv} f_{vm}^{0(d)} \Pi_{mu}^\alpha & \text{for } \underline{\mathbf{y}} \in \text{layer } \alpha. \end{cases} \quad (7.17)$$

At last, the overall (average) stress is obtained as follows:

$$\Sigma = \mathbf{L}' : \mathbf{E} + \Sigma^{(d)}(\mathbf{D}, \bar{\mathbf{D}}, \{\epsilon^{kD}\}), \quad \mathbf{L}' = \langle \mathbf{L}^{(e)} \rangle - \mathbf{A} : \mathbf{B}'^{-1} : \mathbf{A}', \quad (7.18)$$

$$\Sigma^{(d)}(\mathbf{D}, \bar{\mathbf{D}}, \{\epsilon^{kD}\}) = \mathbf{A} : \mathbf{f}^{0(d)} + \mathbf{L}^{(e)\ell} : \frac{1}{|V|} \sum_k \epsilon^{kD} A^k h^k. \quad (7.19)$$

In view of the above localization relations, the strain for any point $\underline{\mathbf{y}}$ in grains or layers depends on damage through the tensors \mathbf{D} and $\bar{\mathbf{D}}$ but also by the term $\epsilon^{(d)}$ involving the full set $\{\epsilon^{kD}\}$. Note that the latter dependence directly results from the term $\mathbf{f}^{0(d)}$ which, by means of (7.1) and (7.10) appears in the expression of \mathbf{f}^α and therefore in that of the strain field. This is not surprising when reported to Fig. 7.2 and relative comments concerning the transmission inside the aggregate. In particular, for a debonded layer α , one may distinguish two kinds of contribution of damage to the relative strain: a “local” one, $\epsilon^{\alpha D}$, related to the microcracks located at its own boundaries and a “nonlocal” one, $\epsilon^{\alpha(d)}$, involving the effect of the whole set of microcracks inside the SRVE.

It can be seen that \mathbf{A}' , \mathbf{B}' and therefore \mathbf{L}' are only degraded by the open cracks via the two damage tensors \mathbf{D} and $\bar{\mathbf{D}}$. This is due to the assumption of no sliding on closed crack lips. These tensors are natural candidates for macroscopic damage variables. Being tensorial by nature, they allow to account for induced anisotropy. Moreover, the moduli may be recovered with crack closure (see that $\mathbf{L}' = \mathbf{L}$ when $\beta = 0$) showing that the model is potentially capable of describing unilateral effects. At last, it is interesting to compare the damage variables emerging from the present scale transition with those resulting from micromechanical approaches for elastic cracked solids (see for instance Kachanov [30]). In the two cases, two tensorial internal variables appear necessary to describe induced anisotropy and unilateral effects: a second-order one and an extension of the latter to the fourth order, the both dimensionless and displaying information on extent and orientation of defects. The difference appears in the form of these variables and is naturally due to the difference between the damaged microstructures considered (cracks in an homogeneous elastic matrix on the one hand, cracks located at grain-matrix interfaces of a heterogeneous elastic material on the other hand). Indeed, the morphology-based modelling advanced in this chapter provides damage variables \mathbf{D} and $\bar{\mathbf{D}}$ which are not symmetric tensorial products of crack normal vectors $\underline{\mathbf{n}}^\beta$ alone, but involve the vectors $\underline{\mathbf{d}}^\beta$. In this way, such

damage variables take into account the granular character of composite microstructures considered. To conclude, one may note that the present scale transition does not make use of the hypothesis of non-interacting cracks, so that damage nonlocal effects may be identified at the microscopic level. They lead in particular to the quadratic dependence of the macroscopic stress on \mathbf{D} in the detailed forms relevant to (7.18), (7.19).

7.3. A complementary localization-homogenization procedure

The homogenized stress (7.18) conveys a full set $\{\epsilon^{kD}\}$ in addition to the damage variables \mathbf{D} and $\bar{\mathbf{D}}$. Noting L^{open} , respectively L^{closed} , the set of layers with open, respectively closed, cracks at their boundaries, one may emphasize that $\{\epsilon^{kD}\}$ includes in fact two subsets $\{\epsilon^{\beta D}; \beta \in L^{\text{open}}\}$ and $\{\epsilon^{fD}; f \in L^{\text{closed}}\}$ whose respective contributions are clearly additive in the expression of $\Sigma^{(d)}$. Indeed, remarking in (7.13) that

$$\mathbf{f}^{0(d)}(\mathbf{D}, \bar{\mathbf{D}}, \{\epsilon^{kD}\}) = \mathbf{f}^{0(d)1}(\mathbf{D}, \bar{\mathbf{D}}, \{\epsilon^{\beta D}; \beta \in L^{\text{open}}\}) \\ + \mathbf{f}^{0(d)2}(\mathbf{D}, \bar{\mathbf{D}}, \{\epsilon^{fD}; f \in L^{\text{closed}}\}),$$

one may write $\Sigma^{(d)}(\mathbf{D}, \bar{\mathbf{D}}, t\{\epsilon^{kD}\})$ as follows:

$$\Sigma^{(d)}(\mathbf{D}, \bar{\mathbf{D}}, \{\epsilon^{kD}\}) = \underbrace{\mathbf{A} : \mathbf{f}^{0(d)1} + \mathbf{L}^{(e)\ell} : \frac{1}{|V|} \sum_{\beta} \epsilon^{\beta D} A^{\beta} h^{\beta}}_{\Sigma^{(d)1}(\mathbf{D}, \bar{\mathbf{D}}, \{\epsilon^{\beta D}; \beta \in L^{\text{open}}\})} \\ + \underbrace{\mathbf{A} : \mathbf{f}^{0(d)2} + \mathbf{L}^{(e)\ell} : \frac{1}{|V|} \sum_f \epsilon^{fD} A^f h^f}_{\Sigma^{(d)2}(\mathbf{D}, \bar{\mathbf{D}}, \{\epsilon^{fD}; f \in L^{\text{closed}}\})} \quad (7.20)$$

In (7.20), $\{\epsilon^{fD}; f \in L^{\text{closed}}\}$ acquire the status of macroscopic internal variables accounting for the distortion due to the blockage of closed cracks inside the SRVE and $\Sigma^{(d)2}$ appears as the corresponding macroscopic residual stress. Let examine now the status of $\{\epsilon^{\beta D}; \beta \in L^{\text{open}}\}$. At the microscopic level, $\epsilon^{\beta D}$ represents, for a layer $\beta \in L^{\text{open}}$, the “local” contribution to its strain of the open cracks located at its own boundaries. It seems natural to think that the crack opening depends on the total strain \mathbf{E} and therefore $\epsilon^{\beta D}$

also, so that $\{\boldsymbol{\varepsilon}^{\beta D}; \beta \in L^{\text{open}}\}$ cannot *a priori* be considered as macroscopic variables independent of \mathbf{E} . This is confirmed when noting that \mathbf{L}' in (7.18) have not all the symmetries required for effective moduli suggesting that $\boldsymbol{\Sigma}^{(d)1}$ must depend, through $\{\boldsymbol{\varepsilon}^{\beta D}; \beta \in L^{\text{open}}\}$, on \mathbf{E} . Another confirmation is given by the calculation of the average free energy $\langle w \rangle_V$ showing clearly that the explicitly quadratic terms in \mathbf{E} can not give by derivation the linear part $\mathbf{L}' : \mathbf{E}$ of the stress. A non-trivial problem consists then in quantifying the relationship between each $\boldsymbol{\varepsilon}^{\beta D}$ (for an arbitrary layer $\beta \in L^{\text{open}}$) and the macroscopic strain \mathbf{E} . This is done by assuming the linearity of this relation and using thermodynamic framework as a guide. Since the stress must derive from the free energy with respect to \mathbf{E} , the linear relation $\boldsymbol{\varepsilon}^{\beta D} = \boldsymbol{\varepsilon}^{\beta D}(\mathbf{E})$ is searched in such a way that $\boldsymbol{\Sigma} = \langle \boldsymbol{\sigma} \rangle_V = \frac{\partial \langle w \rangle_V}{\partial \mathbf{E}}$. After some manipulations it follows:

$$\boldsymbol{\varepsilon}_{ij}^{\beta D} = -Id_{ij\mu\nu} d_\nu^\beta n_m^\beta / h^\beta (\mathbf{B}'^{-1} : \mathbf{A}' - \mathbf{M})_{uvkl} E_{lk} + r_{ij}^{\beta D} \quad (7.21)$$

for every layer $\beta \in L^{\text{open}}$,

$$\mathbf{M} = (\mathbf{B}' + {}^t(\mathbf{A}' + \mathbf{A}))^{-1} : ({}^t(\mathbf{A}' - \mathbf{A}) : \mathbf{B}'^{-1} : \mathbf{A}'). \quad (7.22)$$

In view of (7.21), the strain induced in a layer by the open cracks at its interfaces is controlled by \mathbf{E} , the macroscopic strain, \mathbf{D} and $\bar{\mathbf{D}}$ the damage variables (through \mathbf{A}' and \mathbf{B}') but also by the geometrical features of the layer β under consideration. The constant $\mathbf{r}^{\beta D}$ represents a residual strain induced in this layer by a residual opening of the cracks at its boundaries when $\mathbf{E} = \mathbf{0}$.

With (7.21), the homogenized stress is finally obtained as follows:

$$\boldsymbol{\Sigma} = \mathbf{L}(\mathbf{D}, \bar{\mathbf{D}}) : \mathbf{E} + \boldsymbol{\Sigma}^{(d)1}(\mathbf{D}, \bar{\mathbf{D}}, \{\mathbf{r}^{\beta D}; \beta \in L^{\text{open}}\}) + \boldsymbol{\Sigma}^{(d)2}(\mathbf{D}, \bar{\mathbf{D}}, \{\boldsymbol{\varepsilon}^{fD}; f \in L^{\text{closed}}\}), \quad (7.23)$$

where

$$\begin{aligned} \mathbf{L}(\mathbf{D}, \bar{\mathbf{D}}) &= \langle \mathbf{L}^{(e)} \rangle_V + {}^t(\mathbf{B}'^{-1} : \mathbf{A}' - \mathbf{M}) : (\mathbf{H} - {}^t(\mathbf{A}' - \mathbf{A}) \\ &\quad - (\mathbf{A}' - \mathbf{A})) : (\mathbf{B}'^{-1} : \mathbf{A}' - \mathbf{M}), \\ H_{ijkl} &= L_{mjnl}^{(e)\ell} \bar{D}_{imkn} - B_{ijkl}, \end{aligned}$$

and

$$\boldsymbol{\Sigma}^{(d)1}(\mathbf{D}, \bar{\mathbf{D}}, \{\mathbf{r}^{\beta D}; \beta \in L^{\text{open}}\}) = (\mathbf{H} - \mathbf{A} : \mathbf{B}'^{-1}) : \mathbf{L}^{(e)\ell} : \frac{1}{|V|} \sum_{\beta} \mathbf{r}^{\beta D} A^\beta h^\beta,$$

with $\Sigma^{(d)2}$ given by (7.20) and $\Sigma^{(d)1}$ corresponding to the residual stress induced by the residual opening of (open)cracks. Note that the homogenized effective moduli $\mathbf{L}(\mathbf{D}, \bar{\mathbf{D}})$ have now all the symmetries available. Considering the hypothesis of no sliding on closed crack lips, a crack is, in the present framework, necessarily open before being closed. Moreover ϵ^{fD} , for a debonded layer with closed cracks at its boundaries, does not evolve as long as the cracks remain closed. Therefore, the components of ϵ^{fD} may be calculated from those of $\epsilon^{\beta D}$ given by (7.21), i.e. from those of $\mathbf{r}^{\beta D}$, at crack closure namely precisely when the layer under consideration initially with open cracks becomes a layer with closed cracks. The crucial problem is to ensure simultaneously the homogenized energy and stress-response continuity during such crack closure transition in spite of a discontinuity of effective moduli. It is to be noted that such continuity conditions may open a way to determine the constants $\mathbf{r}^{\beta D}$, for the moment unknown, in function of damage variables \mathbf{D} and $\bar{\mathbf{D}}$. This is the aim of the current researches concerning the unilateral effect (i.e. opening/closure transition modelling) in the framework outlined herein.

7.4. Discussion

The purpose of this work was to extend the homogenization method, initially proposed by Christoffersen for elastic bonded granulates, in the presence of damage by grain-matrix debonding. This extension, realized by incorporating crack-like discontinuities with corresponding displacement jumps in a compatible way with the Christoffersen kinematical and morphological assumptions, leads to the natural emergence of two macroscopic damage tensorial variables involving granular aspects – a second-order one and a fourth-order one – in order to describe moduli degradation, induced anisotropy and unilateral effects. Moreover, the scale transition advanced accounts for initial morphology and internal organization of constituents through the presence of the fourth-order structural tensor $\bar{\mathbf{R}}$ in the homogenized expressions. In this way, the resulting micromechanical model allows to take into account, in a general 3D context, coupling effects between the primary anisotropy and the secondary, damage induced anisotropy. At last, the form of the relations obtained on micro and macroscopic levels clearly indicates some nonlocal damage effects. Besides these results, a complementary localization-homogenization procedure is proposed in order to express the local strain

induced in a layer by the open cracks at its interfaces as a function of macroscopic state variables (strain and damage) and local geometrical features of the layer concerned. Such an approach appears as a crucial step to complete the homogenized model by giving access to the effective moduli in a direct and thermodynamically consistent manner. Even if the model finally proposed is potentially capable of describing the moduli recovery by crack closure, a rigorous criterion of unilaterality is nevertheless required in order to monitor the respective parts of open and closed cracks in the total population. In the authors' opinion, the proper treatment of unilateral effect, as it is done for example by Halm and Dragon [4] and in Chapter 3 in this text, will allow to calculate $\{\epsilon^{fD}; f \in L^{\text{closed}}\}$ accounting for the frictional locking effect of closed cracks and may also provide tools to express the residual strain $\mathbf{r}^{\beta D}$ induced in a layer by the open cracks at its interfaces as a function of damage variables and geometrical features of this layer.

Note

In the first systematic studies of the “homogenization method”, see for instance P. M. Suquet, *Approach by Homogenization of some Problems in Solid Mechanics* (in: *Plastic Behavior of Anisotropic Solids*, pp. 77-117, editor: J. P. Boehler, Editions du CNRS 1985), two basic options were advanced. The first one (see Suquet *ibid.*, p. 79) was called “the mean values (or averaging) method” and the second one “the convergence method” (p. 80). The convergence approach is based on some asymptotic developments involving a small parameter, say e , related, by hypothesis, to the size of heterogeneity. The formal adequation between the heterogenous medium and the equivalent (homogenized) one is found through the analysis of mechanical fields (stress, strain, etc) corresponding to the limit $e \rightarrow 0$. This mathematically elegant approach allows for some evaluation of the first approach (averaging) as a particular approximation. Today, different averaging techniques as, e.g. self-consistent like ones are widely developed and applied. The term “homogenization” is commonly used in this context as well as for genuine convergence analyses. Nevertheless, some authors, as e.g. J. J. Telega in *Homogenization of fissured elastic solids in the presence of unilateral conditions and friction* (in: *Computational Mechanics*, 6, pp. 109-127, 1990) consider that “mathematically, the homogenization consists in a passage to a limit [...] when $e \rightarrow 0$ ”, i.e. show more favour to the convergence approach as a “true” homogeniza-

mogenization. In this Chapter we have employed the term “homogenization” in a wider sense including averaging. Our approach is obviously situated in this latter context.

Chapter 8

Adiabatic shear banding in ductile metals via anisotropic damage modelling approach

Fracture in metals and alloys may always be considered in terms of nucleation and growth of microcracks and/or microvoids until large scale separation takes place. In the case of brittle mechanisms, it is frequently assumed that weak links on the micro-level, i.e. microcracks or nuclei, are present and under the stress high enough, the crack propagates rapidly along planes of cleavage. Cleavage fracture is commonly categorized as a brittle fracture mechanism although a more complex relationship is evidenced for a number of alloys between microscopic observations taking note of cleavage and non negligible macroscopic ductility, see for example Woodward [106]. On the other extremity of a range of deterioration mechanisms there is a genuinely ductile fracture deterioration by the progressive growth and linking up of voids. The latter has been approached in these Notes in the introductory chapter (Chapter 2, Sec. 2.2) in the framework of Continuum Damage Mechanics (CDM). A phenomenon of notable importance in dynamic deformation is adiabatic shearing, which is a form of local instability spreading in the form of bands of intense deformation in impacted bodies. The work done in plastic deformation of a metal (intrinsic dissipation) is converted largely to heat, which – if not conducted away, as for high strain-rate plastic flow – leads to a high rise in temperature. In metals and alloys where the rate of thermal softening (a corresponding drop in stress) surpasses the rate of work hardening (a rise in stress), deformation is seen to concentrate in narrow soft-

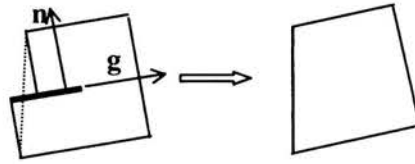
ened bands of adiabatic shear. Stemming from the pioneering work of Zener and Hollomon [107], Recht [108], extensive investigation (metallurgical and mechanical, experimental and theoretical) and literature have been devoted to the matter, see for instance references given in Longère *et al.* [29, 109]. High strength alloys and steels are primarily concerned with adiabatic shear as preponderant deformation mode in high strain rates. Sometimes, under dynamic loading, ductile fracture deterioration by void growth is observed to compete with adiabatic shear leading to complex mixed failure mechanisms.

The works by Perzyna and coworkers, see e.g. [110], attempted to incorporate the shear band formation into three-dimensional modelling regarding viscoplastic flow coupled with micro-damage process by adiabatic shear banding (ASB) embodied by specific internal variables. The aim of the present chapter is clearly situated in this perspective. Including specific anisotropy effects induced by the ASB-related damage, the model presented herein following [29] for ductile metals at large strains and high strain-rates conveys some methodological connections with the approach employed in Chapters 3-6 for quasi-brittle solids. The highly non-trivial and still arduous problem of combining finite-strain plasticity and anisotropy effects is being considered using the Mandel-Sidoroff framework, see e.g. Mandel [111], Sidoroff and Dogui [112].

8.1. The ASB-related damage variable and kinematic preliminaries

We are interested in the description of the material behaviour in the presence of ASB considered as a damage mechanism to be put forward in the framework of a 3D continuous model: within this model the deterioration at stake is to be captured by a corresponding internal variable, its evolution and its effect on elastic stiffness and viscoplastic flow. The model should be robust enough to overcome local instabilities relative to inception and growth of ASB on the mesoscale level. Another feature to be accounted for by this model is the strongly oriented character of ASB thus inducing significant mechanical anisotropy with both elasticity and plasticity being potentially affected.

In order to describe the state of the anisotropic degradation of the material caused by the presence of ASB, a 2nd order tensorial damage variable is introduced. Its components are denoted as D_{ij} and are expressed by (8.1),


 FIGURE 8.1. Equivalent homogeneous volume element ($\alpha = 1$).

where d^α and \mathbf{n}^α represent respectively the scalar intensity and the orientation of the band pattern α (see Fig. 8.1).

$$\begin{cases} D_{ij} = \sum_{\alpha} d^{\alpha} N_{ij}^{\alpha}, \\ N_{ij}^{\alpha} = n_i^{\alpha} n_j^{\alpha}. \end{cases} \quad (8.1)$$

The formal resemblance of (8.1) with the mesocracking related damage tensor \mathbf{D} (Chapters 3-6) is evident.

As discussed in the foregoing, the onset and further evolution of adiabatic shear banding are a consequence of thermal softening, respectively in the sound (i.e. undamaged) material during locally homogeneous plastic deformation, and inside bands themselves during evolving localization process. The intensity d^α includes consequently informations relative to temperature inside the band pattern α . Consider now a single band pattern ($\alpha = 1$), and introduce the adjective ‘singular’ for the processes relevant strictly to the adiabatic shear banding, and the adjective ‘regular’ for the other processes. With such a distinction, the current density d of the damage variable \mathbf{D} depends on the ‘singular’ temperature, and can thus be written as:

$$d = d(T^*, \dots), \quad (8.2)$$

where T^* represents the ‘singular’ temperature, and where the dots represent other possible arguments. Later on, an estimation of d_{\max} is given based on mechanical considerations for the case of simple shear.

The geometric consequences of the shear band pattern (Fig. 8.1) are viewed as those of a ‘super-dislocation’ (see also Pečerski [113]). By using concepts of the crystalline plasticity, a damage induced supplementary velocity gradient \mathbf{l}^d is introduced as the result of the glide velocity $\dot{\gamma}^\alpha$ caused by the band pattern α of normal \mathbf{n}^α and with orientation \mathbf{g}^α (see Fig. 8.1):

$$\mathbf{l}_{ij}^d \propto \sum_{\alpha} \dot{\gamma}^{\alpha} g_i^{\alpha} n_j^{\alpha}. \quad (8.3)$$

The partition of this damage induced velocity gradient \mathbf{l}^d gives the damage induced strain rate \mathbf{d}^d and the damage induced spin $\boldsymbol{\omega}^d$ as follows:

$$\begin{cases} D_{ij}^d \propto \sum_{\alpha} \dot{\gamma}^{\alpha} M_{ij}^{\alpha}, \\ \boldsymbol{\omega}_{ij}^d \propto \sum_{\alpha} \dot{\gamma}^{\alpha} T_{ij}^{\alpha}, \end{cases} \quad (8.4)$$

where

$$\begin{aligned} M_{ij}^{\alpha} &= (g_i^{\alpha} n_j^{\alpha})^S = \frac{1}{2}(g_i^{\alpha} n_j^{\alpha} + g_j^{\alpha} n_i^{\alpha}), \\ T_{ij}^{\alpha} &= (g_i^{\alpha} n_j^{\alpha})^{AS} = \frac{1}{2}(g_i^{\alpha} n_j^{\alpha} - g_j^{\alpha} n_i^{\alpha}). \end{aligned} \quad (8.5)$$

The kinematic variable \mathbf{d}^d allows to smooth the boundary discontinuity caused by the ASB (see Fig. 8.1). Two contributions to the inelastic evolution of the equivalent homogeneous volume element can thus be distinguished: the ‘regular’ plastic strain rate, denoted \mathbf{d}^p , and the ‘singular’ damage induced strain rate, denoted \mathbf{d}^d . The total inelastic strain rate \mathbf{d}^{dp} is defined as the sum of those two contributions:

$$d_{ij}^{dp} = d_{ij}^p + d_{ij}^d. \quad (8.6)$$

Very large strains and rotations usually occurring during the adiabatic shear banding process make the finite elastic-plastic deformation framework indispensable. Since pioneer Mandel’s works [111], many valuable contributions appeared as concerns the introduction of (initial and/or induced) anisotropy in the context of large elastic-plastic strains. Despite this, the problem remains still open, see for instance Sidoroff and Dogui [112] and Ekh and Runesson [114]. In the present approach, a spatial vision of the motion is adopted in order to preserve the physical signification of the state variables, of their derivatives and of their conjugate forces. Clearly, the Eulerian point of view is suitable to deal with plasticity whose rheology is close to fluid one in some aspects [112]. However, the Eulerian point of view is not proper to identify material symmetries.

Let C_0 be the initial undeformed configuration of the material, and C_t its deformed configuration at current time t . In order to account for finite elastic-inelastic (damage-plastic) strains, a pseudo intermediate configuration C_{inter} is introduced by elastic unloading with respect to the current configuration C_t . The deformation gradient \mathbf{F} from C_0 to C_t is conventionally

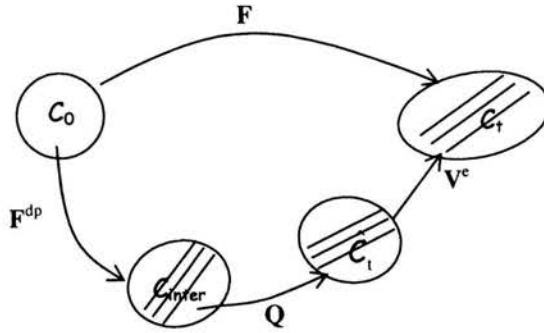


FIGURE 8.2. Intermediate configuration as pseudo material configuration.

decomposed as the product $\mathbf{F} = \mathbf{F}^e \mathbf{F}^{\text{dp}}$ ($F_{iJ} = F_{i\alpha}^e F_{\alpha J}^{\text{dp}}$), where \mathbf{F}^{dp} denotes the ‘damage-plastic’ transformation from C_0 to C_{inter} , and \mathbf{F}^e denotes the elastic transformation from C_{inter} to C_t . The Latin capital subscript indices refer to the initial configuration C_0 while the Latin lower case subscripts refer to C_t . The Greek indices are relevant to C_{inter} . Correspondingly X_R designates the reference rectangular, Cartesian coordinates of the particle which occupies x_i at time t , while its (unloaded) intermediate position is given by \hat{x}_α ($R, i, \alpha = 1, 2, 3$). In the present case, anisotropy is induced by damage (in the form of adiabatic shear bands) during the inelastic transformation \mathbf{F}^{dp} . It then seems natural to define anisotropy in the intermediate configuration C_{inter} that becomes henceforth a pseudo material configuration (see also Lubarda [115]). To ensure the double objectivity (invariance under change of frame on the current configuration C_t , and invariance under rotation of the intermediate configuration C_{inter}) of the constitutive model, derivatives in the motion of the matter with respect to the anisotropy axes \mathbf{A} are required [111]. Interference effects of the rotation of anisotropy axes \mathbf{A} with respect to the laboratory frame \mathbf{S} have then to be neutralized. Let the current configuration C_t be virtually unstressed by a pure elastic stretching $(\mathbf{V}^e)^{-1}$ to a new configuration called \hat{C}_t (Fig. 8.2). \mathbf{Q} denotes the orthogonal transformation from C_{inter} to \hat{C}_t (\mathbf{Q} describes the rotation of anisotropy axes \mathbf{A} with respect to the laboratory fixed frame \mathbf{S}), and $\mathbf{W} = \dot{\mathbf{Q}} \mathbf{Q}^T$ ($W_{ij} = \dot{Q}_{i\alpha} Q_{\alpha j}^T$) denotes the rotation rate relative to these two configurations.

The deformation gradient \mathbf{F} can be written as:

$$F_{iJ} = V_{ik}^e Q_{k\alpha} F_{\alpha J}^{\text{dp}}. \tag{8.7}$$

The velocity gradient $l_{ij} = \left(\frac{\partial v_i}{\partial x_j} \right)$ is thus expressed by:

$$l_{ij} = \dot{F}_{iK} F_{Kj}^{-1} = \overset{\nabla}{V}_{ik}^e (V_{kj}^e)^{-1} + W_{ij} + V_{im}^e \hat{l}_{mp}^{\text{dp}} (V_{pj}^e)^{-1}, \quad (8.8)$$

where

$$\overset{\nabla}{V}_{ij}^e = \dot{V}_{ij}^e - W_{ik} V_{kj}^e + V_{ip}^e W_{pj} \quad (8.9)$$

and

$$\hat{l}_{ij}^{\text{dp}} = Q_{i\alpha} l_{\alpha\beta}^{\text{dp}} (Q_{\beta j}^{\text{dp}})^T, \quad l_{\alpha\beta}^{\text{dp}} = \dot{F}_{\alpha I}^{\text{dp}} (F_{I\beta}^{\text{dp}})^{-1}. \quad (8.10)$$

Objective derivatives constructed with the orthogonal tensor \mathbf{W} , such as (8.9), will be called rotational derivatives.

The decomposition of the velocity gradient \mathbf{l} (8.8) into a symmetric part, the strain rate \mathbf{d} , and an antisymmetric part, the spin $\boldsymbol{\omega}$, yields:

$$\begin{cases} d_{ij} = d_{ij}^e + d_{ij}^{\text{dp}}, \\ \omega_{ij} = W_{ij} + \omega_{ij}^e + \omega_{ij}^{\text{dp}}. \end{cases} \quad (8.11)$$

In (8.11) \mathbf{d}^e and $\boldsymbol{\omega}^e$ represent respectively the elastic strain rate and spin, \mathbf{d}^{dp} and $\boldsymbol{\omega}^{\text{dp}}$ represent respectively the inelastic strain rate and spin. It is assumed that the class of materials considered here involves small elastic strains ($V_{ij}^e \approx \delta_{ij} + \varepsilon_{ij}$). The kinematics related quantities above are finally expressed by:

$$d_{ij}^e = \overset{\nabla}{V}_{ij}^e, \quad \omega_{ij}^e = 0, \quad d_{ij}^{\text{dp}} = \overset{\nabla}{d}_{ij}^{\text{dp}} = (\hat{l}_{ij}^{\text{dp}})^S, \quad \omega_{ij}^{\text{dp}} = \overset{\nabla}{\omega}_{ij}^{\text{dp}} = (\hat{l}_{ij}^{\text{dp}})^{\text{AS}}. \quad (8.12)$$

As a consequence, the rotation rate \mathbf{W} , needed for the rotational derivatives, becomes:

$$W_{ij} = \omega_{ij} - \omega_{ij}^{\text{dp}}. \quad (8.13)$$

As previously written by Mandel [111], constitutive relations for anisotropic elastic-plastic media need not only the definition of the strain rate but also that of the spin. An evolution equation for $\boldsymbol{\omega}^{\text{dp}}$ is indeed required to achieve the calculation of the rotational derivatives (see also Dafalias [116]).

8.2. The constitutive model

The state of the material may be described in the *current configuration* C_t employing the following variables, invariant under any rotation of the intermediate configuration C_{inter} :

- elastic left Cauchy–Green tensor: $b_{ij}^e = F_{i\alpha}^e (F_{\alpha j}^e)^T = V_{ik}^e V_{kj}^e$,
- absolute ‘regular’ temperature: T ,
- scalar isotropic strain hardening variable: p ,
- internal damage variable: $\tilde{D}_{ij} = d\tilde{N}_{ij} = Q_{i\alpha} D_{\alpha\beta} Q_{\beta j}^T$, with $\tilde{N}_{ij} = \tilde{n}_i \tilde{n}_j$ and $\tilde{n}_i = Q_{i\alpha} u_\alpha$.

The objective rotational derivative of $\tilde{\mathbf{D}}$ is obtained by neutralizing the rotation \mathbf{Q} :

$$\overset{\nabla}{\tilde{D}}_{ij} = Q_{i\alpha} \dot{D}_{\alpha\beta} Q_{\beta j}^T = \dot{\tilde{D}}_{ij} - W_{ik} \tilde{D}_{kj} + \tilde{D}_{ip} W_{pj}. \quad (8.14)$$

$D_{\alpha\beta}$ represents the damage tensor components with respect to the intermediate configuration.

The thermo-elastic response of the anisotropic medium is supposed to be described by a thermodynamic potential, namely the free energy per unit unstressed volume $\rho^p \psi(\mathbf{C}^e, T; p, \mathbf{D})$, where ρ^p represents the density in the intermediate configuration, $\mathbf{C}^e = \mathbf{F}^{eT} \mathbf{F}^e$ and $\psi(\mathbf{C}^e, T; p, \mathbf{D})$ the specific free energy. Assuming incompressible inelastic deformation ($\det \mathbf{F}^{\text{dp}} = 1$), initial and unstressed volume are equal, then $\rho_0 \psi(\mathbf{C}^e, T; p, \mathbf{D}) = \rho^p \psi(\mathbf{C}^e, T; p, \mathbf{D})$, where ρ_0 represents the initial density. Material frame indifference requirement is ensured through the invariance of the thermodynamic potential under any rotation of the intermediate configuration:

$$\rho_0 \psi(\mathbf{C}^e, T; p, \mathbf{D}) = \rho_0 \psi(\mathbf{Q} \mathbf{C}^e \mathbf{Q}^T, T; p, \mathbf{Q} \mathbf{D} \mathbf{Q}^T) = \rho_0 \psi(\mathbf{b}^e, T; p, \tilde{\mathbf{D}}).$$

The free energy per unit initial volume is further decomposed into a reversible part $\rho_0 \psi^e(\mathbf{b}^e, T; \tilde{\mathbf{D}})$, namely the elastic potential, and a stored energy part $\rho_0 \psi^p(T; p, \tilde{\mathbf{D}})$ as follows:

$$\rho_0 \psi(\mathbf{b}^e, T; p, \tilde{\mathbf{D}}) = \rho_0 \psi^e(\mathbf{b}^e, T; \tilde{\mathbf{D}}) + \rho_0 \psi^p(T; p, \tilde{\mathbf{D}}). \quad (8.15)$$

The elastic potential includes the initial isotropic linear thermo-elasticity of the sound material and damage induced anisotropic degradation effects. It is being built from the theory of isotropic scalar functions of several tensorial arguments (see Boehler [90]). The elastic degradation is described as being dependent on $\tilde{\mathbf{D}}$, thus comprising damage-induced orthotropy effects via two terms involving material constants a and b below, see also Dragon *et al.* [27]. The constants a and b and the respective terms in the energy expression

below are thus counterparts of the constants α and β and the terms concerned in the energy expression (3.4), Chapter 3. The change in notation operated here is motivated by different deterioration mechanisms underlying the corresponding models. It is assumed that possible interactions between different band clusters are not taken into account. The form (8.16) below is thus limited to the first order in $\tilde{\mathbf{D}}$:

$$\rho_0 \psi^e = \frac{\lambda}{2} e_{ii}^e e_{jj}^e + \mu e_{ij}^e e_{ji}^e - \hat{\alpha} K e_{ii}^e \Delta T - \frac{\rho_0 C}{2T_0} \Delta T^2 - a e_{kk}^e e_{ij}^e \tilde{D}_{ji} - 2b e_{ij}^e e_{jk}^e \tilde{D}_{ki}, \quad (8.16)$$

with

$$e_{ij}^e = \frac{1}{2} \ln b_{ij}^e = \ln V_{ij}^e, \quad \Delta T = T - T_0, \quad K = \frac{3\lambda + 2\mu}{3}, \quad (8.17)$$

where λ and μ represent Lamé's coefficients, K the bulk modulus, $\hat{\alpha}$ the thermal expansion coefficient, ρ_0 the initial density, C the heat capacity, a and b positive constants related to elastic energy degradation caused by adiabatic shear banding.

The stored energy reflects the competition that takes place in the material between hardening and softening. Hardening is a consequence of the micromechanisms of 'regular' plasticity, while softening is due to heating on the one hand and to current ASB related damage on the other one. During their evolution (formation and propagation), ASB modify the state of internal stresses. In this sense, one can assume that damage acts much like temperature to release stored energy. These considerations justify the choice of a multiplicative decomposition of hardening into respective heating and damage contributions. Note that in the expression (8.18) above, the introduction in the stored energy of the 2nd invariant of the damage variable $\tilde{\mathbf{D}}$ allows to produce some band interaction effects:

$$\rho_0 \psi^p = R_\infty \left[p + \frac{1}{k} \exp(-\hat{k}p) \right] \exp(-\gamma T) \exp\left(-d_1 \tilde{D}_{ii} - \frac{d_2}{2} \tilde{D}_{ij} \tilde{D}_{ji}\right), \quad (8.18)$$

where R_∞ represents the saturation stress, \hat{k} the plastic hardening parameter linked to the initial hardening modulus, γ the thermal softening scalar parameter, d_1 and d_2 the damage (ASB) related softening constants.

A model consistent with irreversible thermodynamic framework should satisfy the Clausius-Duhem dissipation inequality. The latter is written below

in the current configuration:

$$D_{\text{int}} = \sigma_{ij} d_{ji} - \rho \left(\dot{\psi} + s\dot{T} \right) \geq 0, \quad (8.19)$$

where σ represents the thermo-elastic (reversible) Cauchy stress tensor, ρ is the current density, and s is the entropy.

The invariance of $\dot{\psi}$ requires objective derivatives for the tensors. To avoid surplus contribution to dissipated energy, rotational derivatives are used following Dogui and Sidoroff [117]:

$$\dot{\psi} = \frac{\partial \psi}{\partial b_{ij}^e} \overset{\nabla}{b}_{ji}^e + \frac{\partial \psi}{\partial T} \dot{T} + \frac{\partial \psi}{\partial p} \dot{p} + \frac{\partial \psi}{\partial \tilde{D}_{ij}} \overset{\nabla}{\tilde{D}}_{ji}. \quad (8.20)$$

Derivation of \mathbf{e}^e yields an equality between the rotational derivative $\overset{\nabla}{\mathbf{e}}^e$ and the elastic strain rate \mathbf{d}^e :

$$\overset{\nabla}{e}_{ij}^e = d_{ij}^e = \dot{e}_{ij}^e - W_{ik} e_{kj}^e + e_{ip}^e W_{pj}. \quad (8.21)$$

The Gibbs relation and the Clausius-Duhem inequality are finally written as:

$$\begin{cases} \rho \dot{\psi} = -\rho s \dot{T} + \sigma_{ij} d_{ji}^e + R \dot{p} - \tilde{K}_{ij} \overset{\nabla}{\tilde{D}}_{ji}, \\ D_{\text{int}} = \sigma_{ij} d_{ji}^{\text{dp}} - R \dot{p} + \tilde{K}_{ij} \overset{\nabla}{\tilde{D}}_{ji} \geq 0, \end{cases} \quad (8.22)$$

where R represents the isotropic hardening conjugate force, and $\tilde{\mathbf{K}}$ the damage conjugate force.

Conjugate forces are derived from the thermodynamic potential:

$$\begin{aligned} \tau_{ij} = J \sigma_{ij} = \rho_0 \frac{\partial \psi}{\partial e_{ij}^e} &= \lambda e_{kk}^e \delta_{ij} + 2\mu e_{ij}^e - \hat{\alpha} K \Delta T \delta_{ij} \\ &- a \left(e_{mn}^e \tilde{D}_{nm} \delta_{ij} + e_{kk}^e \tilde{D}_{ij} \right) - 2b \left(e_{ik}^e \tilde{D}_{kj} + \tilde{D}_{ik} e_{kj}^e \right), \end{aligned} \quad (8.23)$$

$$\begin{aligned} r = JR = \rho_0 \frac{\partial \psi}{\partial p} \\ = R_{\infty} \left[1 - \exp(-\hat{k}p) \right] \exp(-\gamma T) \exp \left(-d_1 \tilde{D}_{kk} - \frac{d_2}{2} \tilde{D}_{kl} \tilde{D}_{lk} \right), \end{aligned} \quad (8.24)$$

$$\begin{aligned} \tilde{k}_{ij} = J \tilde{K}_{ij} = -\rho_0 \frac{\partial \psi}{\partial \tilde{D}_{ij}} &= a e_{kk}^e e_{ij}^e + 2b e_{ik}^e e_{kj}^e + R_{\infty} \left[p + \frac{1}{\hat{k}} \exp(-\hat{k}p) \right] \\ &\cdot \exp(-\gamma T) \exp \left(-d_1 \tilde{D}_{kk} - \frac{d_2}{2} \tilde{D}_{kl} \tilde{D}_{lk} \right) \left[d_1 \delta_{ij} + d_2 \tilde{D}_{ij} \right], \end{aligned} \quad (8.25)$$

$$\rho_0 s = -\rho_0 \frac{\partial \psi}{\partial T} = \hat{\alpha} K e_{kk}^e + \frac{\rho C}{T_0} \Delta T + \gamma R_\infty \left[p + \frac{1}{\hat{k}} \exp(-\hat{k}p) \right] \exp(-\gamma T) \cdot \exp\left(-d_1 \tilde{D}_{kk} - \frac{d_2}{2} \tilde{D}_{kl} \tilde{D}_{lk}\right), \quad (8.26)$$

where $\boldsymbol{\tau}$ represents the thermo-elastic Kirchhoff stress tensor, and J the Jacobian (determinant) of \mathbf{F} .

Isotropic heating and anisotropic damage contribute to reduce the stress level $\tau_{ij}(\mathbf{e}^e, T; \tilde{\mathbf{D}})$ according to (8.23). Positive constants a and b contribute both to reduce Young's modulus, while b is alone responsible for the decrease of the shear modulus (see also Sec. 8.3). Without heating and damage (isothermal conditions in quasi-static loading), the conjugate force $r(T; p, \tilde{\mathbf{D}})$ in (8.24), relative to isotropic hardening, tends to the saturation stress $R_\infty \exp(-\gamma T_0)$. This force increases during pure hardening but decreases with heating and damage, describing the competition between hardening and softening. The damage conjugate force $\tilde{\mathbf{k}}(\mathbf{e}^e, T; p, \tilde{\mathbf{D}})$ – the energy release rate with respect to $\tilde{\mathbf{D}}$ – given by (8.25) includes a first contribution from the reversible part of the free energy, and a second one from the stored energy. The corresponding terms represent respectively elastic and stored energy release rates. It is noteworthy that both contributions to the damage conjugate force exist before damage inception. This means that a finite supply of energy is necessary to activate the damage process ('constrained equilibrium' configuration for the damage internal variable vs. its conjugate force according to the terminology of Maugin [118]).

The objective formulation of the incremental constitutive model can be written in a compact form as follows:

$$\begin{Bmatrix} +\frac{\nabla}{\tau_{ij}} \\ +\dot{r} \\ -\tilde{k}_{ij} \\ -\rho_0 \dot{s} \end{Bmatrix} = \begin{bmatrix} C_{ijkl} & 0 & E_{ijkl} & J_{ij} \\ 0 & Q & A_{kl} & S \\ E_{ijkl} & A_{ij} & L_{ijkl} & V_{ij} \\ J_{kl} & S & V_{kl} & X \end{bmatrix} \begin{Bmatrix} d_{kl}^e \\ \dot{p} \\ \frac{\nabla}{\tilde{D}_{kl}} \\ \dot{T} \end{Bmatrix}, \quad (8.27)$$

with

$$C_{ijkl} = \rho_0 \frac{\partial^2 \psi}{\partial e_{ij}^e \partial e_{kl}^e}, \quad E_{ijkl} = \rho_0 \frac{\partial^2 \psi}{\partial e_{ij}^e \partial \tilde{D}_{kl}}, \quad J_{ij} = \rho_0 \frac{\partial^2 \psi}{\partial e_{ij}^e \partial T}, \quad Q = \rho_0 \frac{\partial^2 \psi}{\partial p^2},$$

and

$$S = \rho_0 \frac{\partial^2 \psi}{\partial p \partial T}, \quad A_{ij} = \rho_0 \frac{\partial^2 \psi}{\partial p \partial \tilde{D}_{ij}}, \quad L_{ijkl} = \rho_0 \frac{\partial^2 \psi}{\partial \tilde{D}_{ij} \partial \tilde{D}_{kl}},$$

$$V_{ij} = \rho_0 \frac{\partial^2 \psi}{\partial \tilde{D}_{ij} \partial T}, \quad X = \rho_0 \frac{\partial^2 \psi}{\partial T^2}.$$

The dissipation (8.22)₂ can be decomposed into a ‘regular’ part directly linked to plasticity and a ‘singular’ part resulting from band formation $D_{\text{int}} = D_{\text{reg}} + D_{\text{sing}}$, where:

$$D_{\text{reg}} = \sigma_{ij} d_{ji}^p - R\dot{p}, \quad D_{\text{sing}} = \sigma_{ij} d_{ji}^d + F_{ij} \overset{\nabla}{\tilde{D}}_{ji}. \quad (8.28)$$

The effects of ‘singular’ heating localized inside the band cluster are included, by definition of the damage variable (8.1)-(8.2), in the scalar damage density d^α (8.2), evolving with the ongoing deterioration. ‘Regular’ heating caused by plasticity outside the bands is then expressed by the common relation established with the adiabaticity assumption:

$$\rho C \dot{T} = \sigma_{ij} d_{ji}^p - R\dot{p}. \quad (8.29)$$

One may distinguish three stages during the deformation progress: before the onset of localization, ‘regular’ plasticity is the only dissipative mechanism ; just after the onset of localization, both mechanisms namely ‘regular’ plasticity and ‘singular’ damage coexist; when localization advances, ASB damage process becomes progressively the prevalent dissipative mechanism. A single yield function that includes both plasticity and damage effects appeared to be suitable to favour such a chronology in the evolution of ‘regular’ and ‘singular’ variables. The following extended form of the plasticity and damage loading function F is postulated:

$$F(\tau_{ij}, r, \tilde{k}_{ij}) = \hat{J}_2^s(\tau_{ij}, \tilde{k}_{ij}) - (R_0 + r). \quad (8.30)$$

The generalized 2nd invariant $\hat{J}_2^s(\tau, \tilde{\mathbf{k}})$ incorporates the damage conjugate force $\tilde{\mathbf{k}}(\tilde{\mathbf{D}}, \dots)$:

$$\hat{J}_2^s(\tau_{ij}, \tilde{k}_{ij}) = \sqrt{\frac{3}{2} s_{ij} P_{ijkl}(\tilde{k}_{mn}) s_{kl}}, \quad (8.31)$$

where \mathbf{s} represents the deviatoric part of the Kirchhoff stress tensor, and $\mathbf{P}(\tilde{\mathbf{k}})$ the 4th order tensor inducing anisotropy in the plastic flow:

$$P_{ijkl} = \frac{1}{2} (\delta_{ik} \delta_{jl} + \delta_{il} \delta_{jk}) + 2 \sum_{q=2}^N \eta_q \left(\tilde{k}_{mn}^+ \tilde{N}_{nm} \right)^q \tilde{M}_{ij} \tilde{M}_{kl}. \quad (8.32)$$

The tensor $\mathbf{P}(\tilde{\mathbf{k}})$ includes a first term relative to conventional plasticity without damage and a second one relative to damage induced effects on the plastic flow. In order to preserve the continuity of stress at the onset of damage, the damage driving force $\tilde{\mathbf{k}}$ intervenes via the expression $\text{tr}(\tilde{\mathbf{k}}^+\tilde{\mathbf{N}})$, the latter representing the difference between the current value $\text{tr}(\tilde{\mathbf{k}}\tilde{\mathbf{N}})$ and the corresponding one at the incipience of damage $k_{\text{inc}} = \text{tr}(\tilde{\mathbf{k}}\tilde{\mathbf{N}})_{\text{inc}}$:

$$\tilde{k}_{ij}^+\tilde{N}_{ji} = \left\langle \tilde{k}_{ij}\tilde{N}_{ji} - k_{\text{inc}} \right\rangle, \quad (8.33)$$

the bracket $\langle \cdot \rangle$ defining the ramp function. To determine k_{inc} an auxiliary analysis based on a perturbation method will be conducted for a particular loading path and generalized further (see below).

The function R_0 in (8.30), which represents the radius of the Huber–Mises cylinder without hardening in the stress space, must account for heating and damage softening. A form similar to that of the hardening conjugate force (8.24) is adopted:

$$R_0 = R_i \exp(-\gamma T) \exp\left(-d_1 \tilde{D}_{kk} - \frac{d_2}{2} \tilde{D}_{mn} \tilde{D}_{nm}\right), \quad (8.34)$$

where R_i represents an internal stress, γ is a thermal softening parameter, d_1 and d_2 are damage (ASB) softening parameters.

The inelasticity criterion $F = 0$ is assumed. The viscoplastic flow and (viscous) damage growth domain is thus $F \geq 0$. The existence of a viscoplastic potential of Perzyna's type [119] is assumed. On the other hand, as time dependent shear banding (damage mechanism considered here) is an evident consequence of thermo-viscoplastic flow, the viscous damage potential is chosen in a form close to that of plasticity:

$$\phi_p^c = \frac{Y}{n+1} \left\langle \frac{F}{Y} \right\rangle^{n+1}, \quad \phi_d^c = \frac{Z}{m+1} \left\langle \frac{F}{Z} \right\rangle^{m+1}, \quad (8.35)$$

where F represents the yield function, Y and n viscous parameters relative to 'regular' plasticity, Z and m viscous parameters relative to 'singular' damage.

Evolution laws are consequently derived from the normality rule:

$$\begin{aligned} d_{ij}^{\text{dp}} &= d_{ij}^{\text{p}} + d_{ij}^{\text{d}} = \frac{\partial \phi_p^c}{\partial \tau_{ij}} = \Lambda^{\text{p}} \frac{\partial F}{\partial \tau_{ij}}, \\ -\dot{p} &= \frac{\partial \phi_p^c}{\partial r} = \Lambda^{\text{p}} \frac{\partial F}{\partial r}, \quad \tilde{D}_{ij}^{\text{d}} = \frac{\partial \phi_d^c}{\partial \tilde{k}_{ij}} = \Lambda^{\text{d}} \frac{\partial F}{\partial \tilde{k}_{ij}}, \end{aligned} \quad (8.36)$$

the viscoplasticity and viscous damage respective multipliers being expressed by:

$$\Lambda^p = \left\langle \frac{\partial \phi_p^c}{\partial F} \right\rangle = \left\langle \frac{F}{Y} \right\rangle^n, \quad \Lambda^d = \left\langle \frac{\partial \phi_d^c}{\partial F} \right\rangle = \left\langle \frac{F}{Z} \right\rangle^m. \quad (8.37)$$

The corresponding fluxes can finally be written as follows:

$$\begin{cases} d_{ij}^p = \frac{3}{2} \Lambda^p \frac{s_{ij}}{\hat{J}_2^s}, \\ d_{ij}^d = 3 \Lambda^p \frac{\sum_{q=2}^N \eta_q \left(\tilde{k}_{mn}^+ \tilde{N}_{nm} \right)^q s_{kl} \tilde{M}_{kl}}{\hat{J}_2^s} M_{ij}, \\ \dot{p} = \Lambda^p, \\ \tilde{D}_{ij}^\nabla = \frac{3}{2} \Lambda^d \frac{\sum_{q=2}^N q \eta_q \left(\tilde{k}_{mn}^+ \tilde{N}_{nm} \right)^{q-1} \left(s_{kl} \tilde{M}_{kl} \right)^2}{\hat{J}_2^s} \tilde{N}_{ij}. \end{cases} \quad (8.38)$$

The evolution laws (8.38) verify the collinearity of the ‘regular’ plastic strain rate \mathbf{d}^p with the deviatoric part \mathbf{s} of the Kirchhoff stress tensor, the collinearity of the ‘singular’ damage induced strain rate \mathbf{d}^d with the orientation tensor $\tilde{\mathbf{M}}$, according to (8.4), and finally the collinearity of the damage rate $\tilde{\mathbf{D}}^\nabla$ with the orientation tensor $\tilde{\mathbf{N}}$ for conservative damage growth configuration considered here, according to (8.1). On the other hand, the form of the polynomial in $\text{tr}(\tilde{\mathbf{k}}^+ \tilde{\mathbf{N}})$, starting with the exponent $q = 2$ (see (8.38)₂ and (8.38)₄), ensures the concomitance of the damage induced rates \mathbf{d}^d and $\tilde{\mathbf{D}}^\nabla$. The adiabatic shear banding process which generates the damage induced strain rate \mathbf{d}^d modifies the initial direction of the inelastic strain rate \mathbf{d}^{dp} . The damage conjugate force $\tilde{\mathbf{k}}$ is actually the preponderant driving force of the damage induced strain rate \mathbf{d}^d , while the damage conjugate force $\tilde{\mathbf{k}}$ and the resolved shear stress $\tau_{\text{res}} = \text{tr}(\mathbf{s} \tilde{\mathbf{M}})$ keep approximately the same weight in the expression governing the magnitude of the damage rate $\tilde{\mathbf{D}}^\nabla$, recalling that shearing is at the very origin of the damage process.

In the absence of damage, the ‘regular’ structure of matter can be supposed approximately statistically isotropic, what implies that $\boldsymbol{\omega}^p = \mathbf{0}$, see Mandel [120]. The rate \mathbf{W} is in this case equal to the spin $\boldsymbol{\omega}$: rotational derivatives are then simply Zaremba–Jaumann derivatives. The presence of damage generates the spin $\boldsymbol{\omega}^d$. Assuming that the effects of the distortions

caused by the presence of ASB are concentrated in their close vicinity, 'regular' matter is supposed to be globally weakly affected. In this sense, the 'regular' plastic spin ω^P can be neglected with respect to the 'singular' damage induced spin ω^d . The rotation rate (8.13) reduces to:

$$W_{ij} = \omega_{ij} - \omega_{ij}^D. \quad (8.39)$$

The detailed expression of the damage induced strain rate \mathbf{d}^d defined by (8.4)₁ is given by (8.38)₂; it allows now to specify the form of the damage induced spin ω^d (8.4)₂ as follows:

$$\omega_{ij}^d = 3\Lambda^p \frac{\sum_{r=2}^N \eta_r (\tilde{k}_{pq}^+ \tilde{N}_{qp})^r s_{kl} M_{kl}}{\hat{J}_2^s} T_{ij}. \quad (8.40)$$

As stressed before, material behaviour, described via the incremental law (8.27), requires objective rotational derivatives. The above evaluation of the damage induced spin has been obtained from the analogy of damage induced viscoplastic deformation with finite plastic distortion in crystals, thus completing the constitutive relations.

The above constitutive model is now completed by a damage incipience criterion based on a simplified analysis of material instability using the linear perturbation method in order to determine $k_{inc} = \text{tr}(\tilde{\mathbf{k}}\tilde{\mathbf{N}})_{inc}$ (8.33), which activates the damage-related rates \mathbf{d}^d and $\tilde{\mathbf{D}}^\nabla$.

The method is in general applied in the case of simple shear under constant velocity boundary conditions. Assuming negligible elastic effects, laminar viscoplastic flow and adiabatic conditions, the problem can be reduced to a one-dimensional formulation, see for instance Bai [121], Clifton *et al.* [122], Molinari [123], and Shawki and Clifton [124]. Admitting analytical solutions, the linear perturbation method provides in this case a criterion for the onset of instability, which is interpreted as the incipience of the adiabatic shear banding process. Nevertheless, instability does not imply rigorously localization [123]. This means that the use of the method gives a 'lower' bound of the deformation localization incipience. An auxiliary simplified analysis performed and not detailed here is intended to help to establish damage incipience threshold from mechanical considerations. Instead of rigorous instability search (the above-mentioned 'lower' bound for localization), the aim is to find a more realistic ('upper' bound) evaluation for localization incipience. The hypotheses taken further favour delaying the strong localization onset with respect to the supposed instability onset.

In addition to the current assumptions mentioned above, a supplementary simplification is made concerning the contribution of R_0 (8.34) to the thermal softening. By neglecting the latter ($\frac{\partial R_0}{\partial T} = 0$), the aforementioned delayed estimation (an ‘upper’ bound for the instability onset) is reached without loosing the mechanical consistency. It is noteworthy that this simplification yields closed-form results. On the other hand, the extension of the one-dimensional case to a three-dimensional formulation is obtained by introducing the resolved shear stress $\tau_{\text{res}} = \text{tr}(\mathbf{s}\tilde{\mathbf{M}})$ as the projection of the deviatoric tensor \mathbf{s} on the band cluster plane and along the glide direction. In this case, the perturbation analysis leads to the following instability condition:

$$G\left(\tau_{ij}, r, \dot{p}; \frac{\partial r}{\partial p}, \frac{\partial r}{\partial T}\right) = \sqrt{3\left(s_{ij}\tilde{M}_{ji}\right)^2} - \left(r - \frac{Y\dot{p}^{\frac{1}{n}}}{n} + \rho_0 C \frac{\frac{\partial r}{\partial p}}{\left(-\frac{\partial r}{\partial T}\right)}\right) > 0, \quad (8.41)$$

which relates the resolved shear stress τ_{res} to the isotropic conjugate force r , the strain rate-induced overstress $Y\dot{p}^{\frac{1}{n}}$, and the ratio of the plastic hardening $\frac{\partial r}{\partial p}$ to the thermal softening $\frac{\partial r}{\partial T}$. In the present simplified analysis, the damage process is actually assumed to run as soon as $G(\tau_{ij}, r, \dot{p}; \frac{\partial r}{\partial p}, \frac{\partial r}{\partial T}) = 0$. This latter condition must be interpreted as the auxiliary indicator for the damage process incipience leading to the determination of the damage conjugate force threshold $k_{\text{inc}} = \text{tr}(\tilde{\mathbf{k}}\tilde{\mathbf{N}})_{\text{inc}}$ (8.33).

It is noteworthy that the criterion (8.41) has been obtained from an analysis based on the linear perturbation method (which has not been detailed here) rather than from an arbitrary purely phenomenological damage incipience criterion.

8.3. Evaluation and application of the model

The three-dimensional constitutive model developed in Sec. 8.2 is tested on a volume element (material point) loaded in simple shear in the context of adiabatic dynamic process. The time integration procedure is purely explicit and the time increment is imposed at the beginning of the analysis. The simple shear loading is applied via the velocity gradient l_{12} (Fig. 8.3(b)) and the damage process (strong deformation localization) is supposed to occur inside the material through the development of a single shear band pattern of normal vector \mathbf{n} collinear with x_2 axis (Fig. 8.3(a)).

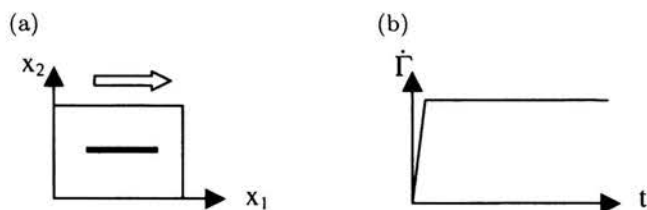


FIGURE 8.3. (a) Volume element containing a band. (b) Nominal shear strain rate history.

The nominal deformation gradient \mathbf{F} , the nominal velocity gradient \mathbf{l} , and the damage variable $\tilde{\mathbf{D}}$ are given by:

$$[\mathbf{F}] = \begin{bmatrix} 1 & \gamma & 0 \\ 0 & 1 & 0 \\ 0 & 0 & 1 \end{bmatrix}, \quad [\mathbf{l}] = \dot{\Gamma} \begin{bmatrix} 0 & 1 & 0 \\ 0 & 0 & 0 \\ 0 & 0 & 0 \end{bmatrix}, \quad [D] = d \begin{bmatrix} 0 & 0 & 0 \\ 0 & 1 & 0 \\ 0 & 0 & 0 \end{bmatrix},$$

where $\dot{\Gamma}$ represents the nominal shear strain rate, and Γ the nominal shear strain ($\Gamma = \dot{\Gamma}t$).

In order to illustrate qualitatively the model capabilities, the well-known experimental data obtained by Marchand and Duffy [125] have been chosen as general reference. Model constants (Table 8.1) have been identified from their experimental data (Fig. 8.4). Consequently, the curve in Fig. 8.5 should not be considered as genuine model validation; it simply reproduces the experimental curve of Fig. 8.4. Following simulations have been performed for $T_0 = 20^\circ\text{C}$ and $\dot{\Gamma} = 1600\text{s}^{-1}$. The value of nominal shear strain at the damage incipience (strong deformation localization onset) is close to 39%.

TABLE 8.1. Material constants of the constitutive model.

ρ_0 [kg/m ³]	C [J/kg.K]	E [MPa]	ν	α [K ⁻¹]	a [MPa]
7800	500	200e+3	0.33	1e-6	0
b [MPa]	R_i [MPa]	R_∞ [MPa]	\hat{k}	γ [°C ⁻¹]	d_1
15e+3	510	400	20	1.5e-3	0.05
d_2	$\eta_2(N=2)$ [MPa ⁻²]	Y [MPa s ^{1/n}]	n	Z [MPa s ^{1/m}]	m
0.05	0.12	100	10	19	2

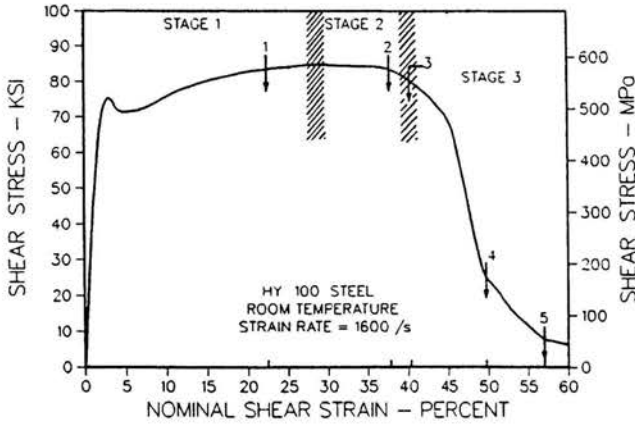


FIGURE 8.4. Experimental stress-strain curve (after Marchand and Duffy, [5]).

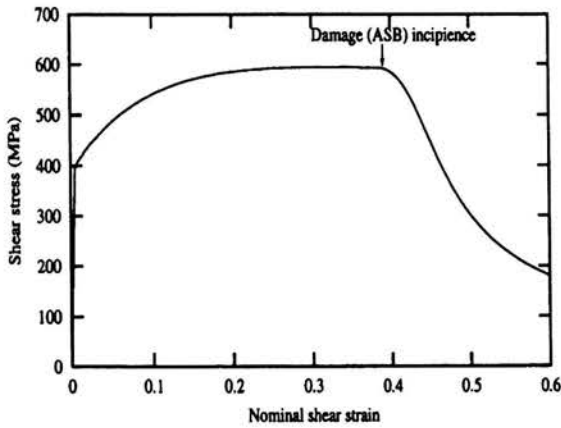
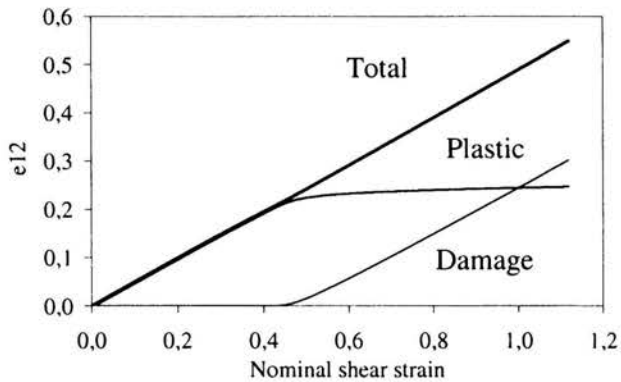
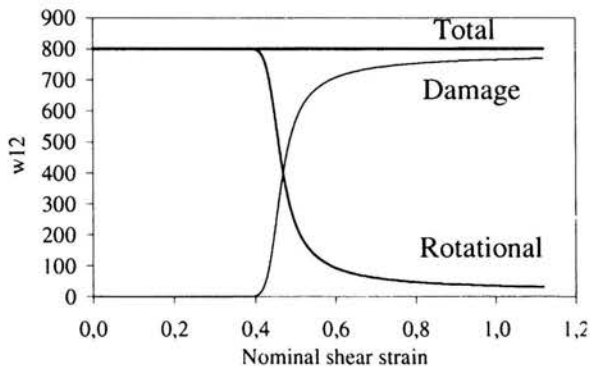


FIGURE 8.5. Shear stress τ_{12} vs. nominal shear strain Γ reproduced with the 3D model.

Various contributions to the calculated strain component e_{12} are plotted versus the nominal shear strain Γ in Fig. 8.6. After the onset of damage, the damage-related strain contribution increases while both elastic strain and plastic 'regular' rate decrease: as the deformation concentrates more and more inside the bands, the mechanism of damage replaces progressively the mechanism of 'regular' plasticity.

Various contributions to the calculated spin component ω_{12} are plotted versus the nominal shear strain Γ in Fig. 8.7. As mentioned above, the rota-

FIGURE 8.6. Strain e_{12} vs. nominal shear strain Γ .FIGURE 8.7. Spin w_{12} vs. nominal shear strain Γ .

tion rate \mathbf{W} represents, in the absence of damage, the spin $\boldsymbol{\omega}$; the objective derivative is thus simply the Zaremba–Jaumann derivative. After the onset of damage, Fig. 8.7 shows how the increase of damage-induced spin $\boldsymbol{\omega}^d$ leads to the decrease of the rotation rate \mathbf{W} .

Components of the thermo-elastic Kirchhoff stress tensor $\boldsymbol{\tau}$ (called S_{ij}) are plotted versus the nominal shear strain Γ in Fig. 8.8. The various stress contributions to the generalized 2nd invariant \hat{J}_2^s (called J_2) are detailed in Fig. 8.9. It is noteworthy that, while the shear stress τ_{12} decreases strongly, the isotropic hardening conjugate force r remains significant. This preserves a non vanishing strength of the material outside the bands.

The first invariant (density d) of the damage variable \mathbf{D} is given versus the nominal shear strain Γ in Fig. 8.10. At the end of the calculations, the

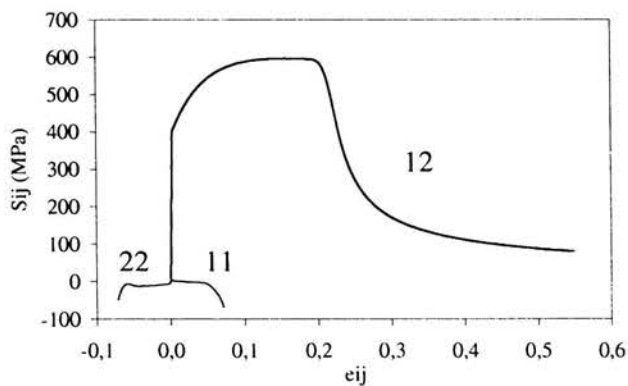
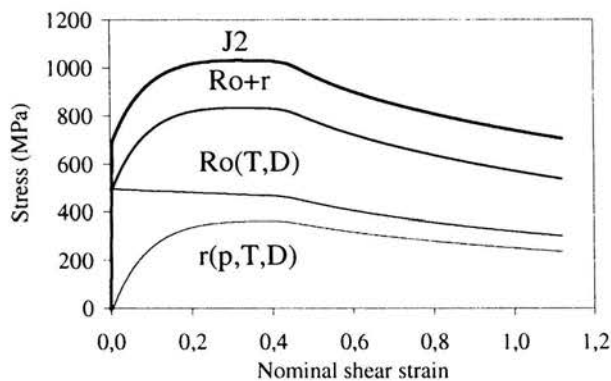
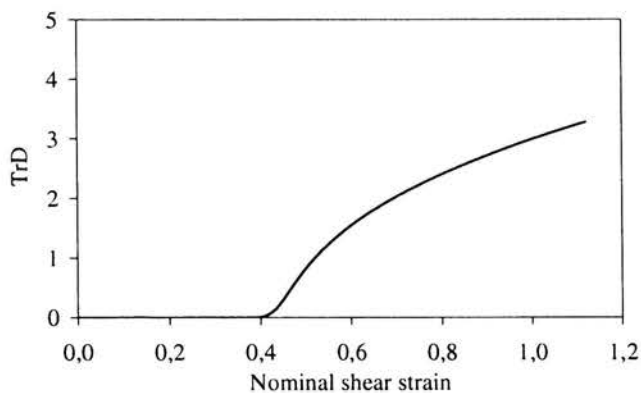


FIGURE 8.8. Stress vs. strain curves.

FIGURE 8.9. \hat{J}_2^s contributions vs. shear strain Γ .FIGURE 8.10. Damage density vs. nominal shear strain Γ .

value of d is about 3. Interpretation of this result needs returning on the definition (8.2) of the density d of the damage variable \mathbf{D} : $d = d(T^*, \dots)$. In the case of simple shear, neglecting second order terms (resulting from complete time integration), the thermo-elastic shear stress (8.23) is approximately:

$$\tau_{12} = 2\mu e_{12}^e - 2be_{12}^e \tilde{D}_{22} = 2(\mu - b\tilde{D}_{22}) e_{12}^e, \quad (8.42)$$

where

$$\tilde{D}_{22} = d\tilde{n}_2\tilde{n}_2, \quad \tilde{n} \approx (0, 1, 0). \quad (8.43)$$

According to (8.42) and (8.43), with the notation employed in (8.27), one can write:

$$C_{1212} = \mu - bd, \quad (8.44)$$

where C_{1212} represents the current 'global' shear modulus and μ its initial value.

As the deformation is accommodated by ASB at some advanced stage of localization, the current 'global' shear modulus is close to the shear modulus of the band material. At high temperature, especially inside the bands, the shear modulus is strongly affected. In the guise of highly overestimating evaluation of an upper bound for $d = d(T^*)$, we can state first that temperature inside the band is bounded by the melting point. Consequently the shear modulus is bounded by its value at the melting temperature. If $\mu(T_m) \approx 0$, the upper bound d_{\max} can be crudely approximated from (8.44) by:

$$d_{\max} \approx \frac{\mu}{b}. \quad (8.45)$$

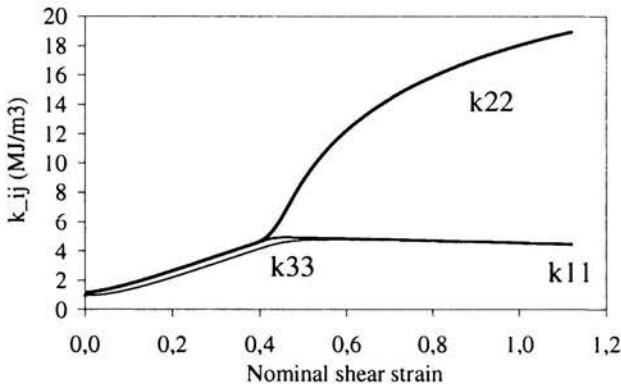


FIGURE 8.11. Damage force $\tilde{\mathbf{k}}$ vs. nominal shear strain Γ .

In the present numerical example, the value of b is chosen as 15 GPa (Table 8.1), which gives an upper bound for d_{\max} close to 5. The value close to 3 attained for nominal shear strain of about 1.2 is well below this limit. If prolonged further, the curve in Fig. 8.10 would ultimately approach the upper bound limit.

The components of the damage force tensor $\tilde{\mathbf{k}}$ (called k_{ij}) are plotted versus the nominal shear strain Γ in Fig. 8.11. The damage conjugate force increases with the nominal shear strain. At the onset of damage, the component \tilde{k}_{22} diverges from \tilde{k}_{11} and \tilde{k}_{33} to increase more strongly in the damage process.

Different loading conditions have been imposed in shear to test the model capabilities. The following effects are illustrated in Figs. 8.12 and 8.13:

- nominal shear strain rate $\dot{\Gamma}$ effect on stress-nominal strain response,
- initial temperature T_0 effect on stress-nominal strain response.

Figure 8.12 shows that instability appears earlier when the nominal shear strain rate is higher. This agrees with experimental evidence. Concurrently the influence of the nominal shear strain rate on stress increase is stronger after the onset of damage.

Figure 8.13 shows that instability appears earlier when the initial temperature is lower. The global experimental trend is respected but numerical values of nominal shear strain Γ at the onset of localization do not agree exactly with experimental ones [125]. The influence of the nominal shear strain rate on stress is higher before the onset of damage.

The final objective of the present chapter is clearly the simulation of penetration engineering problems by means of an industrial finite element calculation code, namely LS-DYNA. The necessary step consists thus in the numerical implementation of the constitutive model *in this context*. As stated above, this context imposes constraints relative to the features of the boundary value problem to treat, the finite element code to use, the calculation duration to respect, and obviously the accuracy (versus experimental evidence) to reach. The implementation of a ‘user material’ should not interfere with a numerical environment affected by the penetration problem related-boundary conditions, concerning for instance surface interaction, rezoning in the case of erosion, and others, which are already costly in calculation duration. For instance, the use of the constitutive model should not imply a decrease in the element size (which obviously means an increase in the

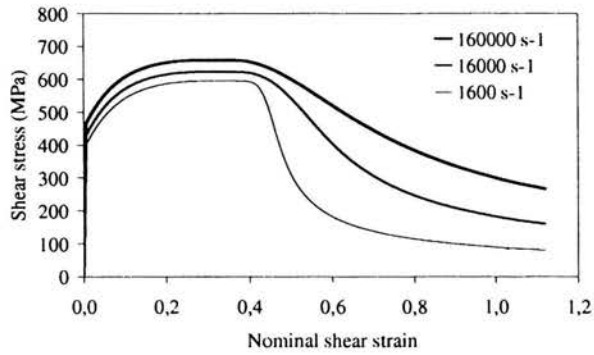


FIGURE 8.12. Shear stress vs. nominal shear strain Γ , $T_0 = 20^\circ\text{C}$.

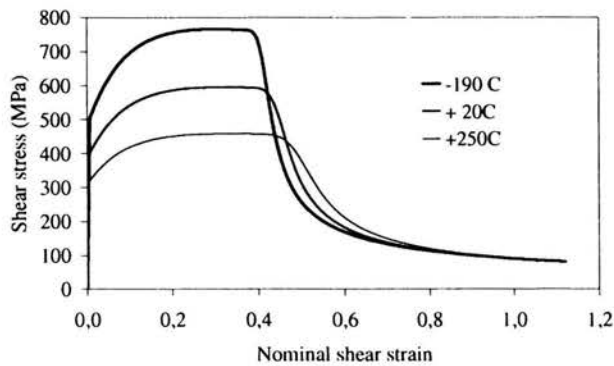


FIGURE 8.13. Shear stress vs. nominal shear strain Γ , $\dot{\Gamma} = 1600\text{ s}^{-1}$.

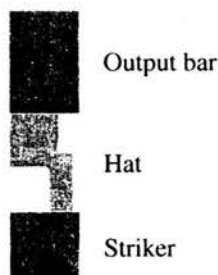


FIGURE 8.14. Partial view of the geometry (half).

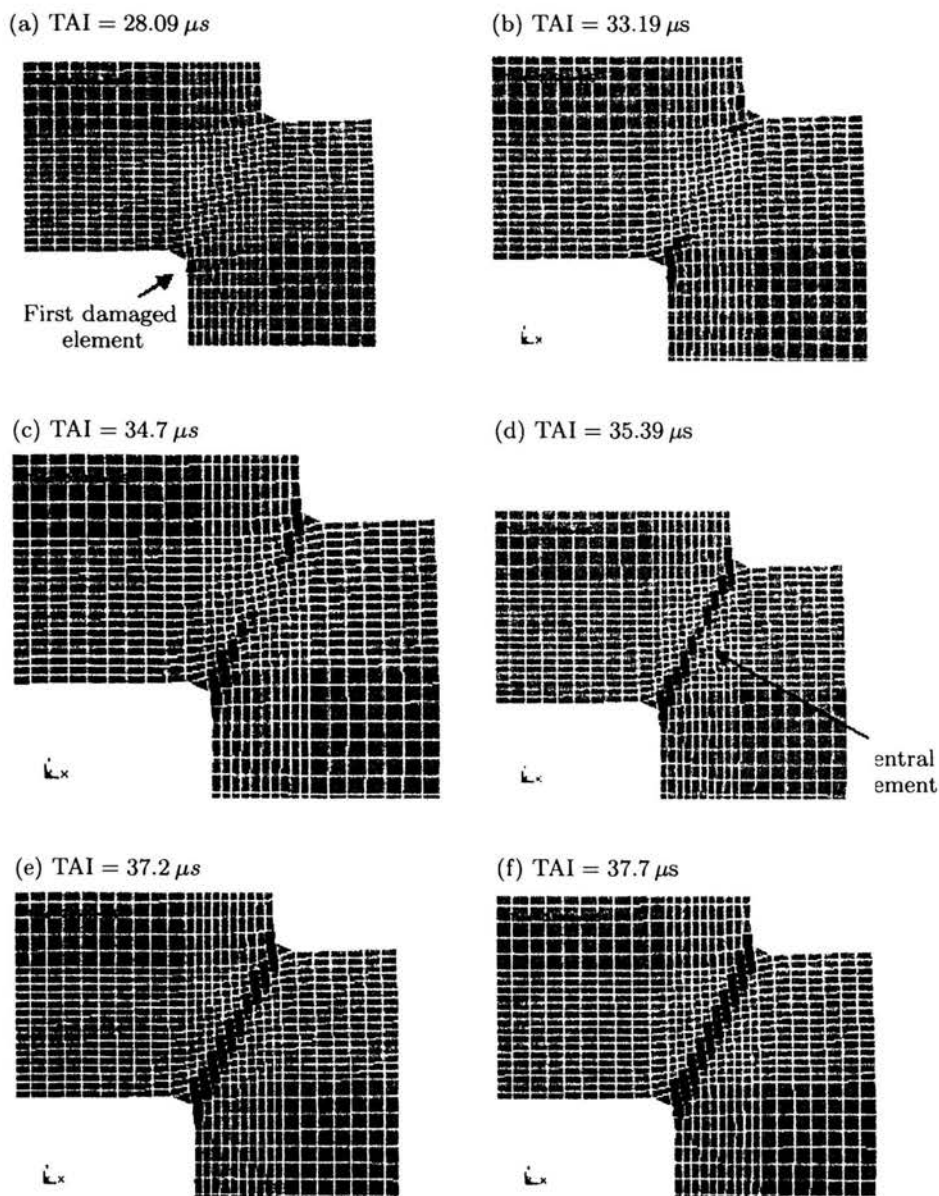
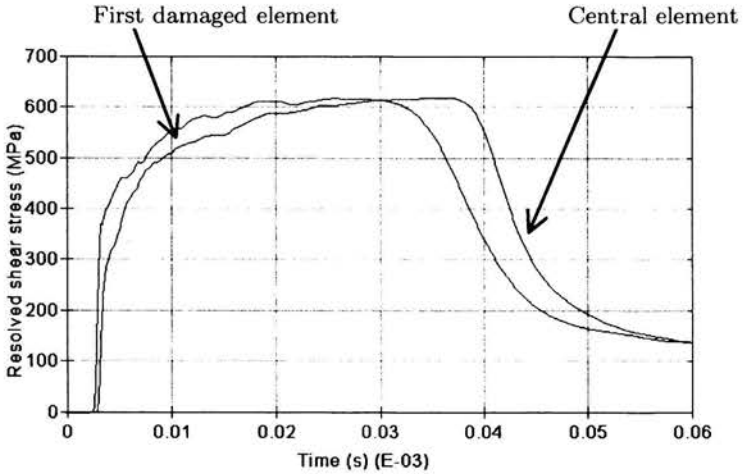
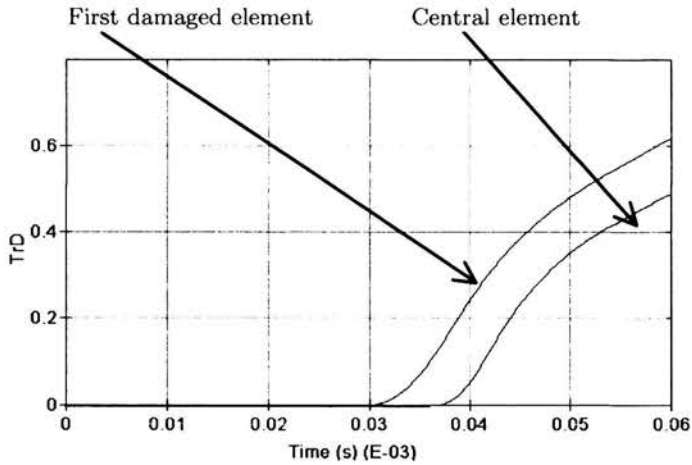


FIGURE 8.15. Adiabatic shear (damage) kinetics in the hat specimen – numerical simulation; after Longère *et al.* [127].

FIGURE 8.16. Resolved shear stress $\tau_{res} = \text{tr}(sM)$ history.FIGURE 8.17. Damage $\text{tr}D$ history.

number of elements) in order to ensure the calculation convergence. With this aim in view, a crucial choice regards the numerical integration algorithm of the evolution equations. This choice is here strongly affected by the code facilities for using a great number of history variables. In the implementation accomplished, the integration algorithm is fully explicit combined with a sampling procedure which reduces, if necessary, the local time step set by the code, Kulkarni *et al.* [126].

The following simulation based on the calculations with the code LS-DYNA tends to represent the loading of a plate hat specimen in a tungsten alloy Hopkinson bars-like device (Fig. 8.14). Only half the device is meshed with adequate boundary conditions. The initial velocity of the striker bar is 15 m/s. An initial gap exists between the lower pressure bar and the specimen, thus the time to impact is 1.4 μ s. The constitutive model has been implemented as 'user material'. Model constants are those of Table 8.1. Figure 8.15 shows the evolution of the adiabatic shearing (damage process) in the specimen at different times after impact (TAI). ASB initiate from the corners and meet progressively. In real tests, fracture would appear furthermore.

According to Fig. 8.16, the model is able to describe the local stress drop caused by the formation and evolution of ASB in a realistic manner.

Remarks

It is hoped that this text, synthesizing the 2002 AMAS course given by the first author, has allowed for deeper insight into several 'modelling challenges' and advances of the contemporary nonlinear mechanics of deteriorating materials. The present notes have attempted to introduce some basic concepts and related issues of constitutive modelling involving damage (Chapter 2) and to review, in an extensive manner, selected developments of the authors' team in the field of anisotropic damage for quasi-brittle and ductile engineering materials (Chapters 3-8).

The deterioration process by multiple mesocrack growth, coupled with additional dissipative mechanisms, notably frictional sliding related plasticity for closed equivalent crack systems, has been of primary focus in Chapters 3-6. The pivotal issues of the control of mesocrack closure/opening and of related 'unilateral' phenomena have been addressed employing rigorous tools of multilinear elasticity. These issues are still debated in the research community, see e.g. the recent works [85, 86]. The methodology applied herein exploits the traditional framework of internal variable formalism for irreversible damage and friction phenomena. However, both, they are treated in a non-classical manner (pseudo-standard phenomenological modelling) and a strong connection to micromechanical analyses is maintained. A specific micromechanical approach is outlined in Chapter 7.

The particular deterioration mechanism regarding ductile metals, namely adiabatic shear banding is considered in Chapter 8. The modelling methodology, put forward in the finite strain elastic-viscoplastic framework, has had to face the difficulties inherent to the Eulerian formulation to cope with deterioration related anisotropy effects combined with objectivity requirements. A coherent model has been formulated and promising numerical results concerning an impacted structure illustrated.

Computational efficiency and reasonably manageable identification of material parameters for the constitutive models presented have been issues of strong concern herein. It is believed that conjunction of multiple methodological tools for damage related constitutive modelling, as shown in the present notes, can provide a conceptual impetus for Continuum Damage Mechanics to be employed to a larger extent to treat complex problems of structural reliability, as postulated recently by Krajcinovic in [2].

Bibliography

1. D. KRAJČINOVIC, *Damage Mechanics*, North-Holland-Elsevier, Amsterdam 1996.
2. D. KRAJČINOVIC, Damage Mechanics: accomplishments, trends and needs, *International Journal of Solids and Structures*, Vol.37, pp.267-277, 2000.
3. A. DRAGON, F. CORMERY, T. DESOYER, and D. HALM, Localised failure analysis using damage models, in: *Localisation and Bifurcation Theory for Soils and Rocks*, (R. Chambon, J. Desrues and J. Vardoulakis, Eds.), pp.127-140, A.A. Balkema, Rotterdam 1994.
4. D. HALM and A. DRAGON, A model for anisotropic damage by mesocrack growth ; unilateral effect, *International Journal of Damage Mechanics*, Vol.5, pp.384-402, 1996.
5. D. HALM and A. DRAGON, An anisotropic model of damage and frictional sliding for brittle materials, *European Journal of Mechanics, A) Solids*, Vol.17, No 3, pp.439-460, 1998.
6. A. BURR, F. HILD, and F.A. LECKIE, Continuum description of damage in ceramic-matrix composites, *European Journal of Mechanics, A) Solids*, Vol.16, No.1, pp.53-78, 1997.
7. C. DENOUEL and F. HILD, A damage model for the dynamic fragmentation of brittle solids, *Computer Methods in Applied Mechanics and Engineering*, Vol.183, pp.247-258, 2000.
8. P. LADEVEZE and J. LEMAITRE, Damage effective stress in quasi-unilateral conditions, in: *16 th IUTAM Congress, Lyngby, Denmark 1984*.
9. P. LADEVEZE, About a damage mechanics approach, in: *Mechanics and Mechanisms of Damage in Composites and Multimaterials* (D. Baptiste, Ed.), pp.119-142, MEP, London 1991.
10. J. LEMAITRE, *A Course on Damage Mechanics*, Springer, Berlin 1992.

11. J. MAZARS, A model of a unilateral elastic damageable material and its application to concrete, in: *Fracture Toughness and Fracture Energy of Concrete* (F.H. Wittman, Ed.), pp.61-71, Elsevier, Amsterdam 1986.
12. J.C. SIMO and J.W. JU, Strain and stress based continuum damage models – I. Formulation, *International Journal of Solids and Structures*, Vol.23, No 7, pp.821-840, 1987.
13. S. YAZDANI and H.L. SCHREYER, An anisotropic damage model with dilatation for concrete, *Mechanics of Materials*, Vol.7, No 3, pp.231-244, 1988.
14. J.-L. CHABOCHE, Damage induced anisotropy: on the difficulties associated with the active / passive unilateral condition, *International Journal of Damage Mechanics*, Vol.1, No.2, pp.148-171, 1992.
15. V.A. LUBARDA and D. KRAJGINOVIC, Some fundamental issues in rate theory of damage-elastoplasticity, *International Journal of Plasticity*, Vol.11, pp.763-797, 1995.
16. G. PECQUEUR, Etude expérimentale et modélisation du comportement d'une craie et d'un grès en torsion, *Ph.D. Thesis*, University Lille-I, France 1995.
17. J.B. WALSH, The effect of cracks on the compressibility of rocks, *Journal of Geophysical Research*, Vol.70, pp.399-411, 1965.
18. M. KACHANOV, A microcrack model of rock inelasticity, Part I: Frictional sliding on microcracks, *Mechanics of Materials*, Vol.1, pp.19-27, 1982.
19. H. HORII and S. NEMAT-NASSER, Overall moduli of solids with microcracks: load-induced anisotropy, *Journal of the Mechanics and Physics of Solids*, Vol.31, No.2, pp.155-171, 1983.
20. S. ANDRIEUX, Y. BAMBERGER, and J.-J. MARIGO, Un modèle de matériau microfissuré pour les bétons et les roches, *Journal de Mécanique théorique et appliquée*, Vol.5, No 3, pp.471-513, 1986.
21. S. NEMAT-NASSER and M. OBATA, A microcrack model of dilatancy in brittle materials, *Journal of Applied Mechanics (Transactions of the ASME)*, Vol.55, pp.24-35, 1988.
22. J.W. JU, On two-dimensional self-consistent micromechanical damage models for brittle solids, *International Journal of Solids and Structures*, Vol.27, No 2, pp.227-258, 1991.
23. D. KRAJGINOVIC, M. BASISTA, and D. SUMARAC, Basic principles, in: *Damage Mechanics of Composite Materials*, (R. Talreja, Ed), pp.1-51, Elsevier, Amsterdam 1994.

24. L. GAMBAROTTA and S. LAGOMARSINO, A microcrack damage model for brittle materials, *International Journal of Solids and Structures*, Vol.30, No.2, pp.177-198, 1993.
25. C. FOND and Y. BERTHAUD, Extensions of the pseudo-tractions technique for friction in cracks, circular cavities and external boundaries ; effect of the interactions on the homogenized stiffness, *International Journal of Fracture*, Vol.74, pp.1-28, 1995.
26. B.R. LAWN and D.B. MARSHALL, Nonlinear stress-strain curves for solids containing closed-cracks with friction, *Journal of the Mechanics and Physics of Solids*, Vol.46, No.1, pp.85-113, 1998.
27. A. DRAGON, D. HALM and T. DESOYER, Anisotropic damage in quasi-brittle solids: modelling, computational issues and applications, *Computer Methods in Applied Mechanics and Engineering*, Vol.183, pp.331-352, 2000.
28. C. NADOT-MARTIN, N. LESUR, D. HALM, H. TRUMEL, and A. DRAGON, A non-classical micro-macro transition towards the anisotropic damage behaviour of particulate composites, *Journal de Physique IV France*, Vol.105, pp.55-62, 2003.
29. P. LONGERE, A. DRAGON, H. TRUMEL, T. DE RESSEGUIER, X. DEPRINCE, and E. PETITPAS, Modelling adiabatic shear banding via damage mechanics approach, *Archives of Mechanics*, Vol.55, No.1, pp.3-38, 2003.
30. M. KACHANOV, Micromechanical modelling of quasi-brittle materials behavior, *Applied Mechanics Reviews*, Vol.45, No.8, pp.304-335, 1992.
31. M. ORTIZ, An analytical study of the localized failure modes of concrete, *Mechanics of Materials*, Vol.6, pp.159-174, 1997.
32. R. BILLARDON and I. DOGHRI, Localization bifurcation analysis for damage softening elastoplastic materials, in: *Cracking and Damage. Strain Localization and Size Effects* (J. Mazars and Z. B. Bazant, Eds.), pp.295-307, Elsevier, London 1989.
33. T. DESOYER and F. CORMERY, On uniqueness and localization in elastic-damage materials, *International Journal of Solids and Structures*, Vol.31, No.5, pp.733-744, 1994.
34. J.-J. MARIGO, Formulation d'une loi d'endommagement d'un matériau élastique, *Comptes rendus de l'Académie des Sciences (Paris)*, Vol.292 (II), No.19, pp.1309-1312, 1981.
35. G. ROUSSELIER, Finite deformation constitutive relations including ductile fracture damage, in: *Three-Dimensional Constitutive Relations and Ductile Fracture* (S. Nemat-Nasser, Ed.), pp.331-354, North Holland Publ. Comp., Amsterdam 1981.

36. M. KACHANOV, Continuum model of medium with cracks, *Journal of the Engineering Mechanics Division (ASCE)*, Vol.106, No.EM5, pp.1039-1051, 1980.
37. J. LEMAITRE and J.-L. CHABOCHE, Aspect phénoménologique de la rupture par endommagement, *Journal de Mécanique Appliquée*, Vol.2, No.3, pp.317-365, 1978.
38. J.-J. MARIGO, Etude numérique de l'endommagement, *EDF - Bulletin de la Direction des Etudes et Recherches, Série C-Mathématiques, Informatique*, No.2, pp.27-48, 1982.
39. J.R. RICE, The localization of plastic deformation, in: *Theoretical and Applied Mechanics* (W. T. Koiter, Ed.), pp.207-220, North-Holland Publ. Comp., Amsterdam 1976.
40. G. BORRE and G. MAIER, On linear versus non-linear flow rules in strain localization analysis, *Meccanica*, Vol.24, pp.36-41, 1989.
41. N.S. OTTOSEN and K. RUNESSON, Properties of discontinuous bifurcation solutions in elastoplasticity, *International Journal of Solids and Structures*, Vol.27, pp.401-421, 1991.
42. R. HILL, A general theory of uniqueness and stability un elastic-plastic solids, *Journal of the Mechanics and Physics of Solids*, Vol.6, pp.236-249, 1958.
43. B. RANIECKI and O.T. BRUHNS, Bounds to bifurcation stresses in solids with non-associated plastic flow law at finite strain, *Journal of the Mechanics and Physics of Solids*, Vol.29, No.2, pp.153-172, 1981.
44. M. KACHANOV, Elastic solids with many cracks and related problems, *Advances in Applied Mechanics*, Vol.30, pp.259-445, 1994.
45. J.W. JU, Isotropic and anisotropic damage variables in continuum damage mechanics, *Journal of Applied Mechanics (Transactions of the ASME)*, Vol.116, No.12, pp.2764-2770, 1990.
46. E. LORENTZ and S. ANDRIEUX, A variational formulation for nonlocal damage models, *International Journal of Plasticity*, Vol.15, pp.119-138, 1999.
47. G. PIJAUDIER-CABOT and R. DE BORST, Enriched damage models for continuum failure analyses, in: *Continuum Thermodynamics (P. Germain's Anniv. Volume)*, (G.A. Maugin, R. Drouot and F. Sidoroff Eds.), pp.355-366, Kluwer Acad. Publ., Dordrecht 2000.
48. A. DRAGON, Plasticity and ductile fracture damage: study of void growth in metals, *Engineering Fracture Mechanics*, Vol.21, No.4, pp.875-885, 1985.

49. A.L. GURSON, Continuum theory of ductile rupture by void nucleation and growth: Part I – Yield criteria and flow rules for porous ductile media, *Journal of Engineering Materials and Technology (Transactions of the ASME)*, Vol.99, pp.2-15, 1977.
50. B. BUDIANSKY, J.W. HUTCHINSON, and S. SLUTSKY, Void growth and collapse in viscous solids, in: *Mechanics of Solids, the Rodney Hill 60th Anniversary Volume* (H. G. Hopkins and M. j. Sewell, Eds.), pp.13-45, Pergamon Press, Oxford 1982.
51. J.-B. LEBLOND, G. PERRIN, and J.DEVAUX, An improved Gurson-type model for hardenable ductile metals, *European Journal of Mechanics, A) Solids*, Vol.14, No.4, pp.499-527, 1995.
52. F.A. MCCLINTOCK, A criterion for ductile fracture by growth of holes, *Journal of Applied Mechanics (Transactions of the ASME)*, Vol.35, pp.363-371, 1968.
53. J.R. RICE and D.M. TRACEY, On the ductile enlargement of voids in triaxial stress fields, *Journal of the Mechanics and Physics of Solids*, Vol.17, pp.201-217, 1969.
54. G. ROUSSELIER, New results with simple continuum damage mechanics models, in: *Continuous Damage and Fracture* (A. Benallal, Ed.), pp.293-303, Elsevier, Paris 2000.
55. K. SIRUGUET, Rupture ductile à basse triaxialité: effet des inclusions sur la croissance et la coalescence des cavités, *Ph.D. Thesis*, University Paris – VI, 1999.
56. V. TVERGAARD and A. NEEDLEMAN, Analysis of the cup-cone fracture in a round tensile bar, *Acta Metallurgica*, Vol.32, pp.157-169, 1984.
57. A. NEEDLEMAN and V. TVERGAARD, Analyses of plastic flow localization in metals, *Applied Mechanics Reviews*, Vol.45, No.2, pp.S3-S18, 1992.
58. G.-C. LI, X.-W. LING, and H. SHEN, On the mechanism of void growth and the effect of straining mode in ductile materials, *International Journal of Plasticity*, Vol.16, pp.39-57, 2000.
59. E.C. AIFANTIS, On the microstructural origin of certain inelastic models, *Journal of Engineering Materials and Technology (Transactions of the ASME)*, Vol.106, pp.326-334, 1984.
60. R. DE BORST, A generalization of J_2 -flow theory for polar continua, *Computer Methods in Applied Mechanics and Engineering*, Vol.103, pp.347-362, 1993.
61. N.A. FLECK, G.M. MULLER, F. ASHBY, and J.W. HUTCHINSON, Strain gradient plasticity: theory and experiment, *Acta Metallurgica et Materialia*, Vol.42, pp.475-487, 1994.

62. G. PIJAUDIER-CABOT AND Z.P. BAZANT, Nonlocal damage theory, *Journal of the Engineering Mechanics (ASCE)*, Vol.113, pp.1512-1533, 1987.
63. J.-B. LEBLOND, G. PERRIN, and J. DEVAUX, Bifurcation effects in ductile metals with nonlocal damage, *Journal of Applied Mechanics (Transactions of the ASME)*, Vol.61, pp.236-242, 1994.
64. Z. MROZ and A. SEWERYN, Damage evolution rule for multiaxial variable loading, in: *Damage Mechanics in Engineering Materials* (G.Z. Voyiadjis, J.-W. Ju and J.-L. Chaboche, Eds.), pp.145-162, Elsevier, Amsterdam 1998.
65. R. DE BORST, M.G.D. GEERS, R.H.J. PEERLINGS, and A. BENALLAL, Some remarks on gradient and nonlocal damage theories, in: *Damage Mechanics in Engineering Materials* (G. Z. Voyiadjis, J.-W. Ju and J.-L. Chaboche, Eds.), pp.223-236, Elsevier, Amsterdam 1998.
66. V. TVERGAARD and A. NEEDLEMAN, Nonlocal effects on localization in a void-sheet, *International Journal of Solids and Structures*, Vol.34, No.18, pp.2221-2238, 1997.
67. J. OLIVER, On the discrete constitutive models induced by strong discontinuity kinematics and continuum constitutive equations, *International Journal of Solids and Structures*, Vol.37, pp.7207-7229, 2000.
68. N. HANSEN and H. SCHREYER, Damage deactivation, *Journal of Applied Mechanics (Transactions of the ASME)*, Vol.62, pp.450-458, 1995.
69. Z. WESOŁOWSKI, Elastic material with different elastic constants in two regions of variability of deformation, *Archives of Mechanics*, Vol.4, No.21, pp.449-468, 1969.
70. A. CURNIER, Q. HE, and P. ZYSSET, Conewise linear elastic materials, *Journal of Elasticity*, Vol.37, pp.1-38, 1995.
71. J.-L. CHABOCHE, Une nouvelle condition unilatérale pour décrire le comportement des matériaux avec dommage anisotrope, *Comptes Rendus de l'Académie des Sciences (Paris)*, Vol.314 (II), pp.1395-1401, 1992.
72. B. HALPHEN and NGUYEN QUOC SON, Sur les matériaux standards généralisés, *Journal de Mécanique*, Vol.14, No.1, pp.39-63, 1975.
73. P.-B. BADEL, Contributions à la simulation numérique de structures en béton armée, *Ph.D. Thesis*, University Paris-VI, 2001.
74. G. PECQUEUR, A. MIKOLAJCZAK, J.M. SIWAK, and A. DRAGON, Validation of an anisotropic damage model under torsional loading, in: *Prediction and Performance in Rock Mechanics and Rock Engineering – Eurock'96*, Vol.1 (G. Barla, Ed.), pp.19-24, A.A. Balkema, Rotterdam 1996.

75. R. MICHALOWSKI and Z. MROZ, Associated and non-associated sliding rules in contact friction problems, *Archives of Mechanics*, Vol.30, No.3, pp.259-276, 1978.
76. H. HORII and S. NEMAT-NASSER, Compression-induced microcrack growth in brittle solids: axial splitting and shear failure, *Journal of Geophysical Research*, Vol.90, No.B4, pp.3105-3125, 1985.
77. M. BARQUINS, C. CHAKER, and P. PETIT, Influence du frottement sur le branchement de fissures à partir de défauts obliques soumis à une compression uniaxiale, *Comptes Rendus de l'Académie des Sciences (Paris)*, Vol.324 (IIb), pp.29-36, 1997.
78. F. CORMERY, Contribution à la modélisation de l'endommagement par mésofissuration et du phénomène de localisation associé, *Ph.D. Thesis*, University Poitiers and ENSMA, 1994.
79. M. ORTIZ and E.P. POPOV, Accuracy and stability of integration algorithms for elastoplastic constitutive relations, *International Journal for Numerical Methods in Engineering*, Vol.21, pp.1561-1576, 1985.
80. D.V. PHAM, Suivi numérique des bandes de localisation dans les structures endommageables (endommagement par mesofissuration, anisotropie induite). Applications en géomécanique, *Ph.D. Thesis*, University Poitiers and ENSMA, 1994.
81. D. HALM, P. BADEL, and A. DRAGON, Computational issues and applications for 3D anisotropic damage modelling: coupling effects of damage and frictional sliding, *Revue européenne des éléments finis*, Vol.10, No.2-3-4, pp.243-258, 2001.
82. A. ONAISI, Mécanismes de rupture d'un bloc percé en mécanique des roches en relation avec la rupture en parois d'un forage pétrolier, *Ph.D. Thesis*, Ecole Centrale des Arts et Manufactures (Paris), 1989.
83. A. DRAGON, Modélisation de l'endommagement des matériaux rocheux, in: *Lois incrémentales, viscoplasticité, endommagement. Modèles de comportement des sols et des roches (2). Traité MIM - Mécanique et Ingénierie des Matériaux*, pp.99-139, Hermes-Lavoisier, Paris 2002.
84. S. PASCAL, Comportement mécanique de composites mortier-polymère, *Ph.D. Thesis*, Ecole Centrale des Arts et Manufactures (Paris), 2002.
85. F. CORMERY and H. WELEMANE, A critical review of some damage models with unilateral effect, *Mechanics Research Communications*, Vol.29, pp.391-395, 2002.

86. H. WELEMANE, Une modélisation des matériaux microfissurés. Application aux roches et aux bétons, *Ph.D. Thesis*, Université des Sciences et Technologies de Lille, 2002.
87. E.T. ONAT and F.A. LECKIE, Representation of mechanical behaviour in the presence of changing internal structure, *Journal of Applied Mechanics (Transactions of the ASME)*, Vol.55, pp.1-10, 1988.
88. V.A. LUBARDA and D. KRAJČINOVIC, Damage tensors and the crack density distribution, *International Journal of Solids and Structures*, Vol.30, No.20, pp.2859-2877, 1993.
89. C. MAUGE and M. KACHANOV, Effective elastic properties of an anisotropic material with arbitrarily oriented interacting cracks, *Journal of the Mechanics and Physics of Solids*, Vol.42, pp.561-584, 1994.
90. J.P. BOEHLER, Lois de comportement anisotrope des milieux continus, *Journal de Mécanique*, Vol.17, pp.153-190, 1978.
91. R. TALREJA, Internal variable damage mechanics of composite materials, in: *Yielding, damage and failure of anisotropic solids*, (J.P. Boehler, Ed.) pp.509-533, Mechanical Engineering Publications, London 1990.
92. P. LADEVEZE, Inelastic strain and damage, in: *Damage Mechanics of Composite Materials*, (R. Talreja, Ed.), Composite Materials Series 9, Elsevier, pp.117-138, Amsterdam 1994.
93. K. KANATANI, Distribution of directional data and fabric tensors, *International Journal of Engineering Sciences*, Vol.22, pp.149-164, 1984.
94. A.J.M. SPENCER, Constitutive theory for strongly anisotropic solids, in: *Continuum theory of the mechanics of fiber-reinforced composites*, (A.J.M. Spencer, Ed.), pp.1-32, Springer, Wien 1984.
95. A. MATZENMILLER and J.L. SACKMAN, On damage induced anisotropy for fiber composites, *International Journal of Damage Mechanics*, Vol.3, pp.71-86, 1994.
96. S.C. COWIN, The relationship between the elasticity tensor and the fabric tensor, *Mechanics of Materials*, Vol.4, pp.137-147, 1985.
97. M.W. BIEGLER and M.M. MEHRABADI, An energy-based constitutive model for anisotropic solids subject to damage, *Mechanics of Materials*, Vol.19, pp.151-164, 1995.
98. D. HALM, A. DRAGON, and Y. CHARLES, A modular damage model for quasi-brittle solids - interaction between initial and induced anisotropy, *Archives of Applied Mechanics*, Vol.72, pp.498-510, 2002.

99. B. AUDOIN and C. BASTE, Ultrasonic evaluation of stiffness tensor changes and associated anisotropic damage in a ceramic matrix composite, *Journal of Applied Mechanics (Transactions of the ASME)*, Vol.61, pp.309-316, 1994.
100. X. AUBARD, Phenomenological approach to the mechanical behaviour of the two 2D SiC-SiC composites at room temperature, in: *Developpements in the science and technology of composite materials, Proc. ECCM5*, (A.R. Bunsell et al., Eds.), pp.741-746, Bordeaux 1992.
101. M. BORNERT, C. STOLZ, and A. ZAOUI, Morphologically representative pattern-based bounding in elasticity, *Journal of the Mechanics and Physics of Solids*, Vol.44, pp.307-331, 1996.
102. C. MARTIN, A. DRAGON, and H. TRUMEL, A viscoelastic homogenization for a class of filled elastomers, *Mechanics Research Communications*, Vol.26, No.3, pp.327-334, 1999.
103. J. CHRISTOFFERSEN, Bonded granulates, *Journal of the Mechanics and Physics of Solids*, Vol.31, pp.55-83, 1983.
104. C. NADOT-MARTIN, H. TRUMEL, and A. DRAGON, Morphology-based homogenization for viscoelastic particulate composites: Part I: Viscoelasticity sole, *European Journal of Mechanics, A) Solids*, Vol.22, pp.89-106, 2003.
105. C. MARTIN, Contribution à l'homogénéisation du comportement viscoélastique et de la détérioration d'une classe d'élastomères fortement chargés, *Ph.D. Thesis*, University Poitiers and ENSMA, 1999.
106. R.L. WOODWARD, Material failure at high strain rates, in: *High-Velocity Impact Dynamics* (J.A. Zukas, Ed.), pp.65-125, Wiley, New York 1990.
107. C. ZENER and J.H. HOLLomon, Effect of strain rate upon plastic flow of steel, *Journal of Applied Physics*, Vol.15, pp.22-32, 1944.
108. R.F. RECHT, Catastrophic thermoplastic shear, *Journal of Applied Mechanics (Transactions of the ASME)*, Vol.31E, pp.189-193, 1964.
109. P. LONGÈRE, A. DRAGON, H. TRUMEL, T. DE RESSEGUIER, X. DEPRINCE, and E. PETITPAS, A 3D constitutive model involving adiabatic shear banding in the context of finite damage elastoplasticity, in: *Computational Plasticity VII, Fundamentals and Applications* (D.R.J. Owen, E. Onate and B. Suarez, Eds.), CD-ROM edition, paper no.99, CIMNE, Barcelona 2003.
110. P. PERZYNA, Influence of anisotropic effects on the micro-damage process in dissipative solids, in: *Yielding, Damage and Failure of Anisotropic Solids* (J.-P. Boehler, Ed.), pp.483-507, Mechanical Engineering Publications, London 1990.

111. J. MANDEL, Equations constitutives et directeurs dans les milieux plastiques et viscoplastiques, *International Journal of Solids and Structures*, Vol.9, pp.725-740, 1973.
112. F. SIDOROFF and A. DOGUI, Some issues about anisotropic elastic-plastic models at finite strain, *International Journal of Solids and Structures*, Vol.38, pp.9569-9578, 2001.
113. R. PECHERSKI, Macroscopic effects of micro-shear banding in plasticity of metals, *Acta Mechanica*, Vol.131, pp.203-224, 1998.
114. M. EKH and K. RUNESSON, Modelling and numerical issues in hyperelastoplasticity with anisotropy, *International Journal of Solids and Structures*, Vol.38, pp.9461-9478, 2001.
115. V.A. LUBARDA, An analysis of large-strain damage elastoplasticity, *International Journal of Solids and Structures*, Vol.31, pp.2951-2964, 1994.
116. Y.F. DAFALIAS, A missing link in the macroscopic constitutive formulation of large plastic deformations, in: *Plasticity Today* (A. Sawczuk and G. Bianchi, Eds.), Elsevier, London 1985.
117. A. DOGUI and F. SIDOROFF, Quelques remarques sur la plasticité anisotrope en grandes déformations, *Comptes Rendus de l'Académie des Sciences (Paris)*, Vol.299 (II), No.18, pp.1225-1228, 1984.
118. G.A. MAUGIN, *The Thermomechanics of Nonlinear Irreversible Behaviours. An Introduction*, World Scientific, Singapore, New Jersey 1999.
119. P. PERZYNA, Fundamental problems in viscoplasticity, *Advances in Applied Mechanics*, Vol.9, pp.243-377, 1966.
120. J. MANDEL, Relations de comportement pour un solide élastoplastique anisotrope en transformation finie in: *Comportement plastique des solides anisotropes, Colloque internat. CNRS no.319* (J.-P. Boehler, Ed.), pp.197-210, Editions CNRS, Paris 1981.
121. Y.L. BAI, Thermoplastic instability in simple shear, *Journal of the Mechanics and Physics of Solids*, Vol.36, No.4, pp.195-207, 1982.
122. R.J. CLIFTON, J. DUFFY, K.A. HARTLEY, and T.G. SHAWKI, On critical conditions for shear band formation at high strain rates, *Scripta Metallurgica*, Vol.18, pp.443-448, 1984.
123. A. MOLINARI, Instabilité thermoviscoplastique en cisaillement simple, *Journal de Mécanique théorique et appliquée*, Vol.4, pp.659-684, 1985.
124. T.G. SHAWKI and R.J. CLIFTON, Shear band formation in thermal viscoplastic materials, *Mechanics of Materials*, Vol.8, pp.13-43, 1989.

125. A. MARCHAND and J. DUFFY, An experimental study of the formation process of adiabatic shear bands in a structural steel, *Journal of the Mechanics and Physics of Solids*, Vol.36, No.3, pp.251-283, 1988.
126. M. KULKARNI, T. BELYTSHKO, and A. BAYLISS, Stability and error analysis for time integrators applied to strain-softening materials, *Computer Methods in Applied Mechanics and Engineering*, Vol.124, pp.335-363, 1995.
127. P. LONGERE, A. DRAGON, H. TRUMEL, T. DE RESSEGUIER, X. DEPRINCE, and E. PETITPAS, Forthcoming paper, 2003.